Geochemical Variations in Glauconitic Minerals: Applications as a Potassium Fertiliser Resource

---

A THESIS SUBMITTED IN PARTIAL
FULFILMENT OF THE REQUIREMENT FOR
THE DEGREE OF

Master of Science

AT THE DEPARTMENT OF GEOLOGICAL
SCIENCES, UNVIVERSITY OF CANTERBURY

by Joshua Ballantyne Smaill

University of Canterbury

2015

Frontispiece

The precipitation of glauconitic minerals is unique and fascinating. Here, a benthic foraminifera has been infilled by glaucony crystallites which have retained the morphology of the host grain.

Abstract

Nutrients for plant growth are often limited in soil systems and additions are required in the form of fertiliser. Potassium is an essential macro-nutrient for plants and demands for K are expected to increase in the future. Glaucony is an abundant marine mineral which may provide an alternative K-rich fertiliser resource. The South Island of New Zealand contains deposits of glaucony-rich rocks which were deposited in the Early- to Mid-Cenozoic during periods of low sedimentation to the seafloor. Here, the geochemistry of glaucony from the Waitaki Basin (Otago), the Waipara Greensand (North Canterbury) and the Stoney Creek Limestone (Karamea) was examined using spatially resolved geochemical analysis and dissolution experiments. Grain-by-grain analysis using Laser Ablation Induction Coupled Plasma Mass Spectrscopy (LA-ICP-MS) and Scanning Electron Microscopy with Energy Dispersive Spectroscopy (SEM + EDS) revealed that glaucony from all deposits were of the mature type and were enriched in K. Glaucony derived from growth inside faecal pellets was found to contain elevated K and Fe concentrations compared to bioclast hosted glaucony. These variations can be explained by the physical properties of host grains and sea-floor redox conditions at the time of precipitation, both of which increased ionic mobility into the zone of glauconitisation. Solubility analysis showed that K^+ was released from glaucony more rapidly than any other element. Additionally, decreasing the pH and introducing an oxidising agent (i.e, birnessite which is ubiquitous in soil environments) accelerated K^+ release 13-fold. Trace metals including Cr, Zn, Cu and Ni were present in the solid phase analysis, however further investigation revealed that these elements were released into solution in low concentrations and may present a source of micro-nutrients, not a soil contaminant. These results suggest that glaucony may offer a source of slow releasing K fertiliser, and the South Island of New Zealand is ideally situated as a place to consider using glaucony as a locally sourced, environmentally sustainable K resource for agriculture.

Acknowledgments

Doctor Catherine Reid and Dr Chris Oze have been the best team of supervisors I could have asked for. Catherines' guidance in the field, constructive criticism of this manuscript and oversight of where my research needed to go has been invaluable and I appreciate all of the time she has given me. Chris has become a mentor for me throughout my time at Canterbury University. His ability to distill complex information into simple ideas and then relate these ideas to the big picture has been crucial for this project and for my development as a scientist. Catherine and Chris are experts in their field, but more importantly they were always approachable and willing to make time for me. It has been a privilege to have worked with them both throughout my undergraduate degree and my MSc.

I am grateful to the many technicians who helped me gather data. Mike Palin, Claudine Stirling and Malcolm Reid were of great assistance at the Otago Community Trust Center for Trace Element Analysis, University of Otago. Mike Palin went out of his way to help me and spent a great amount of his own time explaining how to process the data we gathered using LA-ICP-MS. Geoffrey Smith and Keith Gordon also spent significant amounts of their time showing me how to operate the Raman microscope in the Chemistry Department at the University of Otago.

From the University of Canterbury, Stephen Brown was of great assistance for X-Ray Diffraction analysis. He was always happy to answer any questions I had and I have learnt a lot from Stephen. Mike Flaws helped with the acquisition of major element concentrations using equipment in the Mechanical Engineering Department, Robert Stainthorpe ran samples for dissolution analysis, Kerry Swanson helped obtain SEM photomicrographs and Rob Spiers cut thin sections and polished grain mounts.

I would like to thank Peter Curry for allowing access to the Oparara Quarry, Karamea, and the farm owners of Ross Farm, Oamaru, for allowing me to sample rocks from their farm.

Finally, thanks to my family and friends who have made this thesis possible. My parents have always encouraged me to continue doing what I enjoy and I will be forever grateful for the opportunities they have provided for me. I was incredibly lucky to share an office with some of my best friends. Jo, Fraser and Emma were always considerate and constructive and I have learnt a lot from them all.

Contents

List of Figures

List of Tables

1 Introduction

Potassium is an essential macro-nutrient for plant growth and is involved in important biochemical processes in plants (McLaren and Cameron, 1990; Karimi et al., 2012; Zorb et al., 2014). In certain soil systems K is limited and the addition of fertiliser becomes necessary to avoid K deficiency in plants. The demand for K fertiliser is currently satisfied by mineral salts bearing high elemental concentrations of K (Fixen and Johnston, 2011); however, the global requirement for K is expected to increase in the short-term future and alternative sources of K are desirable (Heffer and Prud, 2014). Investigations into K-rich minerals may provide alternative fertiliser resources to benefit the agricultural industry.

Glaucony is an abundant, K- and Fe-rich mineral present in many marine rocks. Deposits of glauconitic minerals are found in many countries including North America (Dooley, 1998), India (Banerjee et al., 2012b), Australia (Doepel, 2013) and New Zealand (Seed, 1964; Merchant, 2012). Glaucony forms during periods of low sedimentation to the seafloor, and common environments for precipitation are on the inner-shelf to shelf-break in water depths between 50-500 m (Odin and Fullagar, 1988; Amorosi et al., 2007). The precipitation of glaucony involves crystallites infilling host grains which are often faecal pellets or bioclast tests (Banerjee et al., 2012a; Amorosi et al., 2007). Over time, glaucony matures both chemically and structurally as K increases in concentration as the interlayer cation (McRae, 1972; Odin and Matter, 1981). The high K content and Cation Exchange Capacity (CEC) associated with the clay mineral structure makes glaucony appealing as a source of K and as a soil conditioner for agricultural systems.

Glauconitic minerals have been used as a K fertiliser in the past, and agricultural land containing indigenous glaucony is usually very fertile (McRae, 1972). Historical accounts of using 'greensands' (rocks containing >50% glaucony) to enhance crop productivity date back to the 1760's, when agricultural land in the northeast of North America showed long term improvements following additions of glauconitic marls (Cook, 1868). Glaucony is not commonly used in modern agriculture; however, it has been considered as an alternative form of potash (K_2O derived from minerals) in many areas. The South Island of New Zealand contains significant deposits of glauconitic minerals which potentially offer a source of K to the agricultural industry, on which the New Zealand economy is largely dependent upon.

Glaucony deposits from the South Island have been the focus of chemical (Seed, 1964; McConchie and Lewis, 1980) and stratigraphic research (Kapoutsos, 2005); however, no

investigation into the application of glaucony as a beneficial mineral to the agricultural industry has been conducted using these deposits. The key aims of this research are to assess the geochemical variations between different deposits of glaucony and determine the solubility of glaucony, both in terms of whether different deposits release elements in different ways and whether there are concerns related to harmful trace elements being released into soil systems. The hypothesis guiding this research is that glaucony will release sufficient K^+ into solution and provide a feasible alternative fertiliser resource. To resolve this hypothesis, three key questions are used as a guide. 1) How much K_2O is present in glauconitic minerals and what causes elemental variations? 2) Do different deposits of glaucony release elements in different ways? 3) If so, how much K^+ is released and what are the key factors influencing the solubility of glaucony?

Table 1 – Approaches taken to achieve research aims

Research question/aim	Approach taken
Evaluate variations in major, trace and rare earth elements between outcrops	Collect and prepare samples for analysis using LA-ICP-MS (trace and rare earths') and SEM+EDS (major elements)
Assess the influence of host grain material on glaucony maturation	Intepret host grains based on morphological features under the binocular microscope and measure elemental concentrations on a grain by grain basis
Ascertain the mass of elements released from glaucony over time	Measure the concentration of elements released from glaucony using ICP-MS at set time periods, and predict the masses of elements released using linear equations and mass balance calculations
Assess the influence that strong oxidising agents and pH have on the solubility of glaucony	Add birnissite to a solution dissolving glaucony at acidic and basic pH, and measure elements released
Determine whether different deposits of glaucony have distinct release characteristics	Measure elements released during lexiviation testing for a carbonate hosted deposit and a siliciclastic hosted deposit
Estimate the palaeoredox conditions at the time of glaucony precipitation for different outcrops	Measure redox sensitive Rare Earth Element (REE) concentrations to determine the fractionation behaviour in different outcrops
Evaluate the application of Raman spectroscopy and X-Ray Diffraction (XRD) analysis for determining glaucony maturity	Collect Raman spectra for ∼100 grains of glaucony and conduct principal co-ordinate analysis on data. Assess the crystal structure of glaucony using XRD.

This thesis is split into six chapters as outlined below.

1. **Introduction**: This chapter provides a brief overview of the reasons this work is being undertaken and summarises the objectives for this research.

2. **Background information**: The precipitation of glauconitic minerals and the depositional environments of glaucony formation are outlined along with the an overview of the current sources of K and the expected demands for K in the future.

3. **Geological setting and stratigraphy:** The broad geological settings are introduced for the Waitaki Basin, the Waipara Greensand and the Stoney Creek Limestone. This is based on previous authors work.

4. **Materials and Methods**: This chapter describes the methods used for sample collection, sample preparation and the geochemical analysis used to provide data for this thesis.

5. **Results:** The results are divided into 4 main categories: 1) sedimentary descriptions and observations of glaucony characteristics. 2) Elemental concentrations from the solid phase, including results for major, trace and Rare Earth Elements (REE). 3) Structural analysis of glaucony, including X-Ray diffraction and Raman spectroscopy. 4) Solubility of glaucony - two separate solubility analysis were conducted to test the release of elements from the solid phase into solution.

6. **Discussion**: The results presented in Chapter 5 are discussed with respect to the geochemical variations between outcrops, the influence of host material on geochemical signature and the geochemical evolution of glauconitic minerals. The palaeoredox conditions are interpreted from REE's and an interpretation of the incorporation of Cr into glauconitic minerals is described. The release of elements from glaucony under different conditions is evaluated before a discussion on the benefits and drawbacks of using glaucony as a source of K is presented.

7. **Conclusions**: Some concluding statements are made to summarise the findings of this research.

2 Background Information

2.1 Authigenic precipitation of glaucony

The general formula for glaucony is $K_{(x+y)}(Si_{4-x}, Al_x)_{\sim 4}(Fe^{3+}, Al, Mg, Fe^{2+})_{\sim 2}O_{10}(OH)_2$ (where x is 0.2-0.6 and y is 0.4-0.6) (Huggett, 2005). Precipitation occurs as crystallites infilling the pore spaces within sedimentary host grains or in porous structures on hard ground surfaces (Odin and Matter, 1981; Huggett, 2005). Parent grains can be composed of a range of materials including faecal pellets, bioclasts, silicate minerals and clay minerals (Burst, 1958; McRae, 1972; Odin and Matter, 1981). Pore spaces within granular particles provide a semi-confined micro-environment which creates a passageway for the exchange of ions between ambient sea water, the interstitial fluids of the underlying sediments and the local chemical environment within the parent material itself (Odin and Matter, 1981). As glauconitisation proceeds inside the grain, so does dissolution of the parent material, eventually breaking the parent grain through cracking, fissuring or displacement of pre-existing planes of weakness (Huggett, 2005).

The terms maturation and evolution are often used to describe the mineralogical nature of glaucony. Potassium is regarded as the key indicator for the maturity or evolutionary state of glaucony, where K enrichment represents more mature minerals than K depleted grains. Chemical maturation involves the progressive enrichment in K and Fe with depletion in Al. Structurally, immature glaucony occurs as Fe-rich smectite clays which are pale green in colour. As grains mature and incorporate K as the interlayer cation they evolve into minerals with illite to micaceous structures and appear as dark green to black colours. The maturity of glaucony is classified as nascent (<4% K_2O), slightly evolved (4-6% K_2O), evolved (6-8% K_2O) and highly evolved (>8% K_2O) (Odin and Matter, 1981; Amorosi et al., 2007). Variations in mineral chemistry and structure has resulted in the terms 'glaucony' and 'glauconitic minerals' being used to describe the mineral as a facies, with the term 'glauconite' being reserved for grains with >6 weight % K_2O and micaceous structures (McRae, 1972; Odin and Matter, 1981; Stille and Clauer, 1994; Amorosi et al., 2007).

The key factors controlling the maturation of glaucony include sedimentation rate and host material characteristics. Glaucony precipitates near the seafloor-seawater interface where near neutral to slightly sub-oxic redox conditions are prevalent, allowing Fe and K to remain mobile and diffuse through grains (Baldermann et al., 2012). Low sedimentation rates allow grains to remain in this sub-oxic zone of glauconitisation for longer periods of

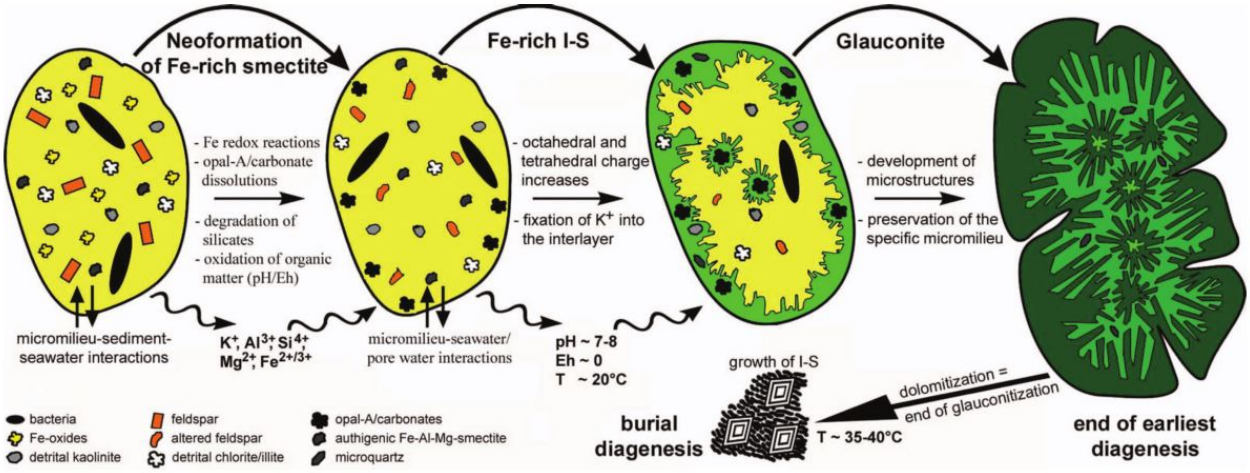

Figure 1 – Model for the precipitation and maturation of glauconitic minerals. Progressive uptake of K as the interlayer cation satisfies the negative surface charge resulting in a transition from smectite to illite and eventually micaceous clay mineral structures (Baldermann et al., 2012). I-S stands for illite-smectite clays

time and subsequently increase in maturity. Parent materials which are prone to dissolution or degradation are better suited to allowing glauconitisation to proceed because they create new pore space for crystallites to precipitate in. Faecal pellets and bioclasts are more prone to dissolution than silicate precursor minerals, therefore it is not surprising that these are the two most common host materials for glaucony (Odin and Matter, 1981). It follows that the evolution of glauconitic grains is dominantly controlled by the physical properties of the host grain (porosity and tendency to dissolve) and the environment of deposition (see below), more so than the chemistry of the parent material. Although parent minerals may contribute ions to the local chemical environment, the common occurrence of glaucony infilling material such as foraminiferal tests or quartz grains (which are devoid of or contain only trace amounts of K, Fe and Al) suggests that the chemistry of ambient seawater and the interstitial fluids of the sedimentary grains on the seafloor creates a local chemical environment with sufficient amounts of the critical ions necessary to precipitate glaucony (Odin and Matter, 1981).

2.2 Depositional environments of glaucony formation

Marine shelf and shelf break environments in water depths between 50-500 m are common environments for glaucony precipitation, as this is where sedimentation rates are low and decaying organic matter on the seafloor creates near neutral to sub-oxic conditions (Odin and Fullagar, 1988; Amorosi, 1997). Close to the shore the higher energy (oxygenated)

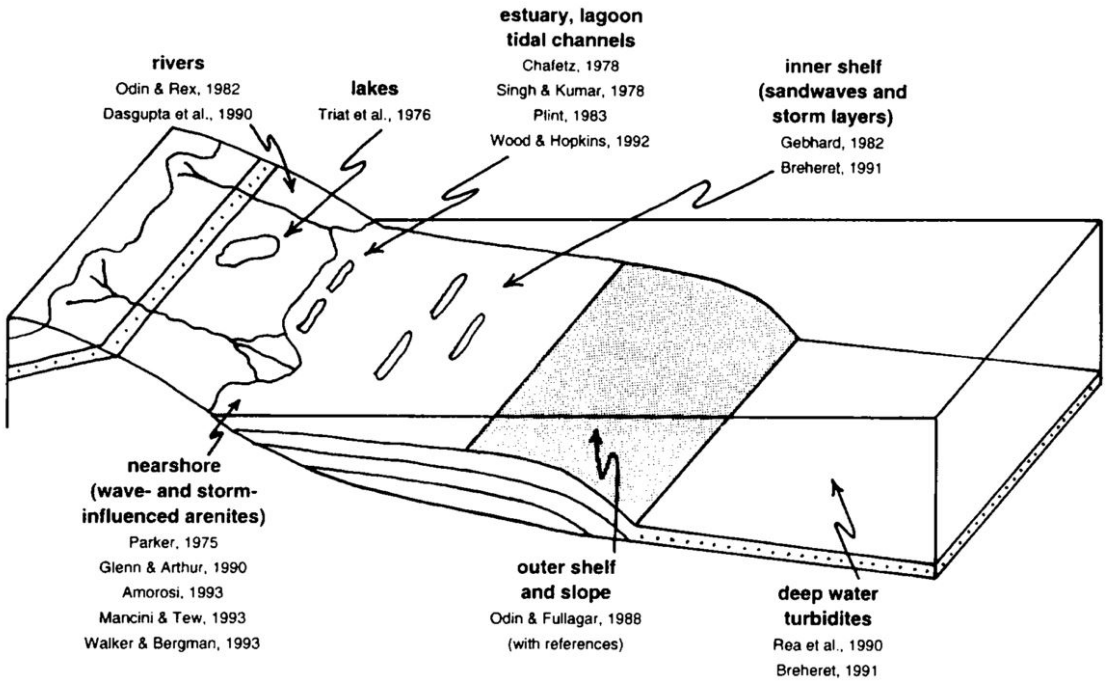

Figure 2 – Various environments of allochthonus (transported or reworked) glaucony reported from the literature. Authochthonous (precipitating in situ) glaucony precipitates on the shelf break in marine settings (grey stipple) (Amorosi, 1997)

environment and influx of detrital grains inhibits precipitation, as does the accumulation of winnowed sediment below the shelf break in deeper settings. It is between this zone where both deposition and erosion are minimal that glaucony has sufficient time to grow and mature (Odin and Matter, 1981).

Marine transgressions are commonly associated with glaucony deposits, where continentally derived detrital grains and inner shelf carbonates become sufficiently drowned to an area of low sediment accumulation. The drowned continent has less sub-aerial exposure leading to decreased sediment flux to the seafloor. The inner-shelf to shelf-break area is also a likely place to accumulate faecal pellets and carbonates, two of the most favourable parent substrates for glaucony (Odin and Matter, 1981; Banerjee et al., 2012b).

Although the environment described above is the commonly accepted zone of glauconitisation, deposits are not restricted to this environment. Banerjee et al. (2012a) document authigenic glaucony forming in a back barrier lagoon environment and these grains show similar geochemical characteristics to deposits from deep water environments. Glaucony has also been reported to have formed in neritic environments close to an estuary (Kapoutsos, 2005) and in shallow water environments (Kapoutsos, 2005; Chafetz, 2007). This suggests that the water depth and energy do not strictly influence whether or not

glaucony will precipitate, and the more important controls are sedimentation rate and the parent materials' physical characteristics.

2.3 The demands for K and previous use of glaucony as fertiliser

In 2018 the global fertiliser demand is expected to exceed 200 Mt for the first time ever. Between 2012 and 2018 demand for K is expected to increase by 2.8% per year to 34 Mt, this is faster than demand increases for P (1.9% p.a to 46 Mt) and N (1.5% p.a to 120 Mt) fertilisers (Heffer and Prud, 2014). Potash (K_2O derived from minerals) is currently derived from soluble mineral salts bearing high elemental proportions of K (25-30% K_2O representing high grade ore) (Fixen and Johnston, 2011). Economic deposits of K occur as ancient inland seas (evaporites), salt lake deposits or natural brines and commonly contain the minerals sylvite (KCl), sylvinite (KCl + NaCl), hartsulz (ore deposits with sulfate salts) and langbeinite ($K_2SO_4.2MgSO_4$). Canada, Russia, Belarus and Germany contain 92% of the global potash reserve collectively, with Canada alone having 53% of the global reserve. Based on current production, world potash has a reserve life of 235 years (Fixen and Johnston, 2011).

Greensand has been used a fertiliser in the past and is currently being investigated or used on a small scale in some areas. India has identified 3,000 Mt of indigenous glauconitic sandstone which could offer a cheap, locally derived source of slow releasing potash fertiliser (TIFAC, 2009). Brazil is currently trying to decrease its reliance on imported potash and is using *verdete,* a metamorphosed greensand with 8-10% K_2O which provides a slow release of K and other nutrients, whilst removing the issue of chlorinisation associated with KCl (Franzosi et al., 2014). In the Perth Basin, Western Australia, Potash West is developing a large (2,119 km^2), shallow deposit of greensand and phosphate rock, with the intention of producing potash and superphosphate as commercial fertiliser products (Doepel, 2013).

Trace elements, including heavy metals, have been identified in glauconitic minerals and can contaminate soil. Elevated concentrations of As (7-31 ppm), Be (5-18 ppm), Cd (<0.2-1.2 ppm) and Cr (130-1000 ppm) were identified in greensands that were used as fertilisers on New Jersey pastoral land (Dooley, 1998). During the 1880's, 1 Mt of greensand was applied to New Jersey farmland per year, sometimes at rates up to 100 t per acre (Tedrow, 2002). Arsenic concentrations up to 5.95 $\mu g/L$ in New Jersey stream-waters exceeded the state standard and were chemically fingerprinted to have derived from glauconitic sediments present in the groundwater environment (Barringer et al., 2011).

3 Geological Setting and Stratigraphy

This chapter outlines the general geological setting for the Waitaki Basin, the Waipara Greensand and the Stoney Creek Limestone (Oparara Quarry). Brief overviews of the geological history and depositional environments are based on previous authors work. Sedimentary descriptions and stratigraphic logs compiled from the current research are presented in Chapter 4.

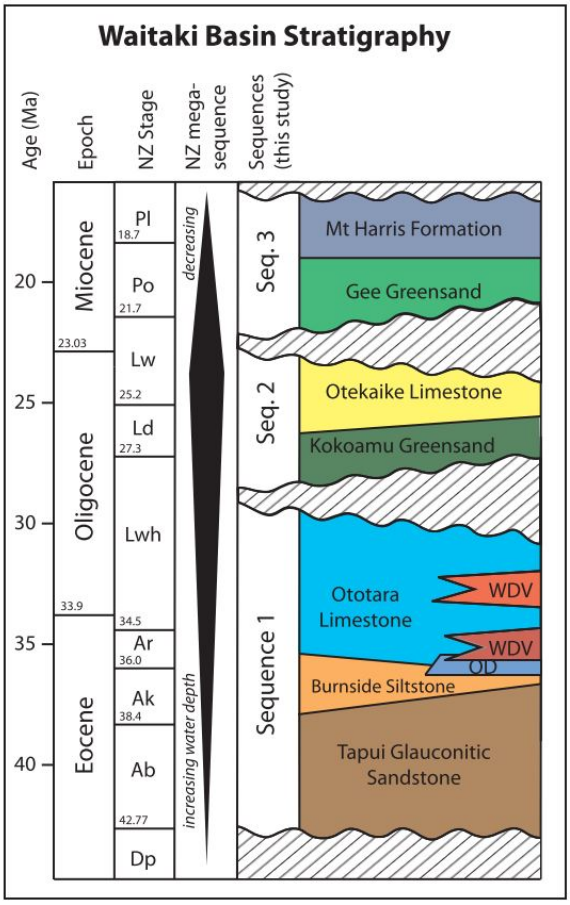

Figure 3 – Stratigraphy of the Waitaki Basin (Thompson et al., 2014a) (modified from Gage (1957); Forsyth (2001); Cooper (2004); Hollis et al. (2010)). WV-WD are the Waiareka-Deborah Volcanics; OD is the Oamaru Diatomite. Ab, Bortonian; Ak, Kaiatan; Ar, Runangan; Dp, Porangan; Ld, Duntroonian; Lw, Waitakian; Lwh, Whaingaroan; Po, Otaian; Pl, Altonian

3.1 Overview of stratigraphy for the Waitaki Basin

Late Cretaceous to Late Oligocene marine rocks around the Oamaru region that are of interest to this research consist of limestones, marls and calcareous greensands. The system can be described as broadly transgressive from the Late Cretaceous until the Latest Oligocene, and regressive from the Miocene. During the Late Cretaceous, the New Zealand continent rifted from Gondwana and slowly subsided, resulting in a relative sea level rise. Deposition of fluvial conglomerates of the Taratu Formation were replaced by shallow marine rocks of the Kauru Formation, the Tapui glauconitic sandstone and the Raki siltstone (Gage, 1957; Forsyth, 2001). Further sea level rise in the Eocene resulted in deposition of the Alma Group; a dominantly carbonate hosted system with sporadic episodes of volcanism. These rocks consist of the Ototara Limestone and Deborah/Waiareka Volcanic suite.

3.2 Alma Group Rocks

The Alma Group consists of the Ototara Limestone and the Waiareka/Deborah Volcanic suite. These rocks overly terrestrial and marginal marine rocks of the Taratu Formation and the Kauru Formation.

3.2.1 Ototara Limestone

In the east of the Waitaki basin the Ototara Limestone is a clean, bryozoan rich grainstone. At Parkside quarry a minimum thickness of 70 m is observed. Where it is underlain by volcanic material the deposits thin drastically due to the influence of topographical highs. In the east of the basin, the ramps of volcanic cones impeded terrestrial sediments from the west, producing a rimmed cool-water shelf platform which dominated by branching bryozoans (Thompson et al., 2014a). Further to the west the Ototara thins and terrestrial muds are introduced from a sediment source consisting of low relief islands of Rakaia Terrane (Mortimer, 2004). The units here are wackestones referred to as the Earthquakes Marl and the Amuri Limestone, which were both deposited on the mid to outer shelf.

The Ototara Limestone represents deposition during the highstand systems tract (HST), and was deposited between the Runangan (Late Eocene) and Whaingaroan (Early Oligocene) (Thompson et al., 2014a). Inner to mid shelf environments and shallow reefs created

through topographic highs are interpreted as likely palaeoenvironments in the east, grading into mid to outer shelf settings in the west (Gage, 1957; Forsyth, 2001; Thompson et al., 2014a).

In the east the Ototara Limestone is capped by a karst surface (Figure 10), representing the regional Marshall Paraconformity of Carter and Landis (1972). This surface represents a hiatus of 2-4 My, with significant sub-aerial exposure forming dissolution cavities (Forsyth, 2001). Further to the west the karst surface is absent, being replaced instead with a sub-marine unconformity showing trace fossil infilling by over lying units. This suggests sub-aerial exposure was limited to the topographical high created by the underlying volcanic material in the east. The Marshall Paraconformity coincides with the separation of Tasmania and South America from Gondwana, resulting in the onset of the Antarctic Circumpolar Current, producing a eustatic sea level fall due to the growth of Antarctic polar ice caps (Cooper and Cooper, 1995).

3.2.2 Waiareka/Deborah Volcanic Suite

The intraplate Waiareka/Deborah volcanic suite is comprised mainly of basaltic lapilli tuff deposits, the Kakanui Mineral Breccia, and pillow basalts. Eruptions were Surtseyan style, with submarine pyroclastic density flows building up the flanks of volcanic cones at Kakanui North and South. Basalt intrusions are seen as large sills at Tokarahi and the Moeraki quarry. Volcanic activity occurred during the Late Eocene until the Early Oligocene, with intrusions of basaltic pillows into carbonate sediments and blanketing of palaeocones showing this volcanism occurred on a continental shelf setting (Cas et al., 1989).

3.3 Kekenodon Group Rocks

The Kekenodon Group unconformably overlies the Alma Group. It consists of the Kokoamu Calcareous Greensand and the Otekaike Limestone which were deposited in the Duntroonian and Waitakian Stages (Late Oligocene to Earliest Miocene) during a marine transgression (Gage, 1957; Forsyth, 2001). Contacts between the Ototara Limestone and these overlying units are sharp. In the east the Kokoamu and Otekaike fill cavities of the karst surface of the Ototara Limestone, creating very thin to non-existent beds. This is reworked material which has been distributed over the topographic high by sub-marine currents. In

the west, contacts occur as trace fossil infilling of Kokoamu Greensand into Ototara Limestone (Forsyth, 2001).

3.3.1 Kokoamu Calcareous Greensand

The Kokoamu Greensand is a glaucony rich packstone. In the eastern part of the Oamaru basin, the unit is a thin surface drape or karst infilling, as was observed at Gee's Point and Campbell's Beach. Here it is indistinguishable from and likely mixed in with reworked Otekaike Limestone. Further to the west, beds thicken to 3-4 m, although the true thickness is arbitrary as the contact with the overlying Otekaike Limestone is highly gradational. Progressive submergence of the continental block to the west diminished sediment supply which suppressed glaucony precipitation (see section 2.5). The Kokoamu Greensand is Late Whaingaroan (Late Oligocene) stage (Forsyth, 2001) and is interpreted to have formed during a transgressive systems tract (TST) (Thompson, 2013). Sedimentation rates overall are slow and discontinuous (Gage, 1957; Thompson, 2013). The contact with the overlying Otekaike Limestone is gradational and is defined by decreasing glaucony content.

3.3.2 Otekaike Limestone

The Otekaike Limestone overlies the Kokoamu Greensand. The distinction between units is drawn on the change in glaucony content, grading from 30-40% in the Kokoamu Calcareous Greensand to 15-20% at the base of the Otekaike Glauconitic Limestone. The thickest deposits are in the west where prominent limestone cliffs up to 30 m high appear as a pale creamy-grey unit, often with nodular concretionary bands forming well indurated horizons which are resistant to weathering. In the east the Otekaike thins, occuring as thin surface drapes or stratigraphically absent beds over the karst surface of the Ototara Grainstone. A detrital silt component containing visible quartz and mica is present throughout the unit suggesting a source of subaerially exposed continent was being constantly eroded during the entire period of deposition of the Otekaike Limestone. A slight increase in terrestrial input was observed up section by (Gage, 1957).

Deposition of the Otekaike was during the falling-stage systems tract (FSST) which created shallow water depths and strong submarine currents (Thompson, 2013). It is dated as Upper Late Duntroonian (Late Oligocene) to Waitakian (Early Miocene) (Thompson,

2013). Depositional environments were still, relatively clear water on the mid shelf with a distal terrestrial sediment supply to the west (Gage, 1957). The upper contact of the Otekaike is erosional in the east. Inconspicuous signs of a karst surface or at least submarine winnowing indicate a depositional hiatus, with sharp contacts of the overlying younger strata. In the west of the basin, the contact with the overlying Gee Greensand is gradational according to Gage (1957).

3.4 Otakou Group Rocks

The Otakou Group unconformably overlies the Kekenodon Group rocks and is comprised of the Gee Greensand and the Mount Harris Formation.

3.4.1 Gee Greensand

In the east of the basin, the Gee Greensand unconformably overlies the Otekaike glauconitic packstone or is seen in direct contact with the Ototara grainstone where the intervening sediments are missing. This unit is only found in the east of the basin as inland deposits have been eroded due to poor induration. The Gee Greensand is of Latest Waitakian to Otaian (Early Miocene) age and was deposited during a TST (Thompson, 2013). An inner shelf environment with slow sedimentation rates was interpreted by (Gage, 1957). The presence of phosphorite and intense bioturbation suggests the seafloor sediments and bottom waters were rich in organic material (Thompson, 2013). Phosphorite formation was due to upwelling cold, nutrient enriched water on the volcanic ramp. Enhanced primary production and subsequent degradation of sedimentary organic material would have increased the dissolved phosphate concentration in pore waters, allowing francolite to precipitate (Pufahl, 2010).

3.4.2 Mount Harris Formation

The Mount Harris Formation marks a change in the sedimentation regime from the broadly transgressive sequence deposited during Late Cretaceous to Early Miocene time, to a regressive sequence indicating the initiation of major uplift to the west. The contact with the underlying Gee Greensand is gradational. At its' type locality 'Old Rifle Butts' it is a massive, green-grey, well sorted calcareous mudstone with occasional concretionary bands.

Minor amounts (< 3%) of glaucony are present near the base, appearing as forest green, fine sand sized grains.

3.5 The Occurrence of Glaucony in Oamaru Rocks

Glauconitic minerals are classically associated with precipitation during marine transgressions, highstand systems tracts and the development of maximum flooding surfaces (McRae, 1972; Odin and Matter, 1981; Amorosi, 1997), which drown continents and reduce clastic sedimentation to the seafloor. The Oamaru region displays the opposite relationship between glauconitisation and sequence stratigraphy (Thompson et al., 2014b). In periods of maximum continental flooding following marine transgressions the carbonate systems are devoid of glaucony, as seen in the Ototara Limestone. In contrast, glaucony rich deposits immediately follow sea level lowstands, as seen in the Kokoamu Calcareous Greensand and the Gee Greensand. Figure 4 displays the precipitation of glaucony in a sequence stratigraphic framework in the Waitaki Basin.

The lack of glaucony during sea level highstands suggests that concentrations of the critical ions required for glauconitisation to occur (Fe, Al and K) were too low for direct precipitation. During periods of highstand there was insufficient delivery of these ions to the shelf environment, therefore inhibiting the growth of glaucony and instead allowing a carbonate factory to develop on the volcanic highs. The fact that minor glaucony is observed in the Earthquakes Marl and not in the clean Ototara bryozoan rich grainstone suggests that the input of terrestrial mud in the west of the basin is enough to favour glaucony precipitation, whereas the lack of terrestrial input to the east is insufficient to precipitate glaucony.

The gradational contact between the Kokoamu Greensand and the Otekaike glauconitic limestone shows that glaucony precipitation was fueled during sea level lowstand by increased detrital flux from a proximal continental source. As transgression progressively drowned the continental block this sediment supply is suppressed, leading to decreasing glaucony content up section through the Kokoamu Greensand and Otekaike limestone (Thompson et al., 2014b).

In carbonate hosted settings such as those mentioned above, it appears that having a source of terrestrial sediment input is crucial for the precipitation of glauconitic minerals (Thompson, 2013). It is important to also note that sedimentation in carbonate systems is

different to that of siliciclastic systems. During the transgressive systems tract and development of maximum flooding surfaces, a siliciclastic dominated system sees a reduction in sedimentation rate. Under the same circumstances a carbonate hosted system will continue to deposit sediment as bioclasts accumulate on the seafloor. Therefore it appears that in carbonate hosted systems the precipitation of glauconitic minerals is largely influenced by the presence or absence of critical ions in the seafloor sediment pile, whereas precipitation in siliciclastic hosted deposits are influenced primarily by sedimentation rate. Both systems probably have a unique 'sweet spot', where the delivery of terrestrial sediments is enough, but not too much, to allow the glauconitisation process to occur uninterrupted and with the necessary ions.

3.6 Mid Waipara Section

3.6.1 Overview of stratigraphy and previous work

The mid-Waipara section lies on the south-eastern limb of the Doctors Anticline and consists of Late Cretaceous to Cenozoic rocks unconformably overlying deformed Mesozoic Torlesse Supergroup rocks (Wilson, 1963). The cover sequence begins with the Haumurian (Late Cretacous) Broken River Formation, consisting of terrestrial conglomerates and sandstones (Morgans, 2005). Gradationally overlying the Broken River Formation is the 185 m thick Conway Formation of Late Haumurian age (Latest Cretaceous) (Roncaglia et al., 1999). This calcareous siltstone marks the beginning of a marine transgression and the transition from terrestrial to marine sedimentation. The Loburn Mudstone conformably overlies the Conway Formation and is Teurian (Paleocene) in age. Conformably overlying the Loburn Mudstone is the Waipara Greensand of Teurian to Waipawan (Paleocene to Early Eocene) age. The Waipara Greensand is subsequently overlain by the Ashley Mudstone which is Early Waipawan to Kaiatan (Early to Late Eocene) (Browne and Field, 1985). The final unit in the sequence is the Kaiatan to Runangan (Late Eocene to Oligocene) Amuri Limestone, this is the age equivalent unit to the Ototara Limestone found in the Oamaru basin. The Loburn Mudstone and the Waipara Greensand are the units of interest to this research.

Research on the mid-Waipara section has focused on the presence of the Cretaceous-Tertiary (K/T) boundary layer in the Conway Formation (Vajda and Raine, 2003; Hollis

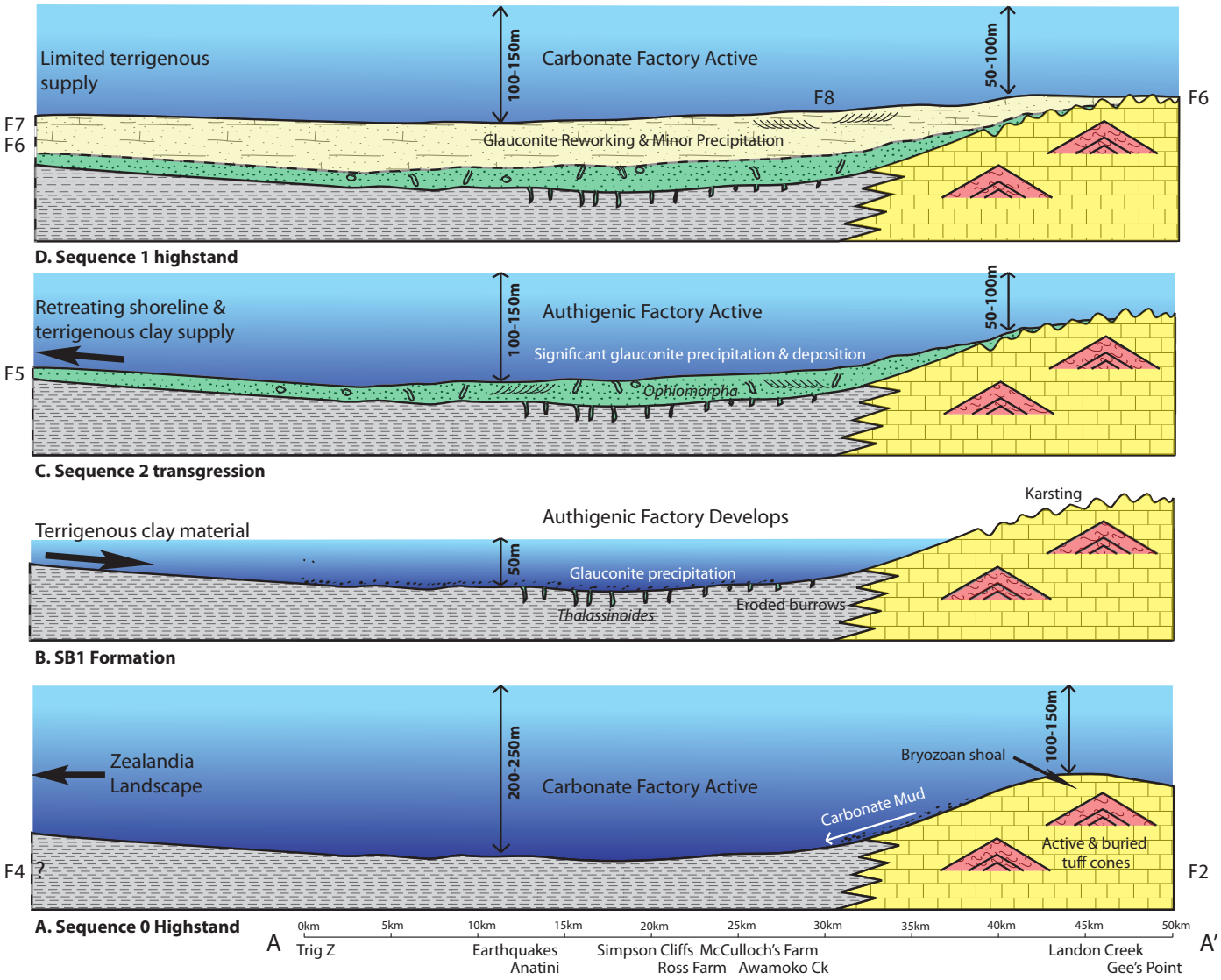

Figure 4 – Controls on the precipitation of authigenic minerals in the Waitaki Basin (Thompson et al., 2014b)

and Strong, 2003), the palaeontology of the marine sediments (Haast, 1871; Hutton, 1894; Fordyce et al., 1986; Morgans, 2005) and more recently the mid-Waipara has been the subject of palaeoclimatic studies (Creech et al., 2010; Hollis et al., 2013, 2014). The palaeo-temperature proxy TEX_{86} suggested that sea surface temperatures (SST) during deposition of the Loburn Mudstone and Waipara Greensand hovered around 20°C before a short term cooling event in the Latest Paleocene resulted in deposition of the organic rich Tartan Formation, and intense warming during the Paleocene-Eocene climatic optimum raised SST to ∼30°C and bottom waters to 20°C (Hollis et al., 2013).

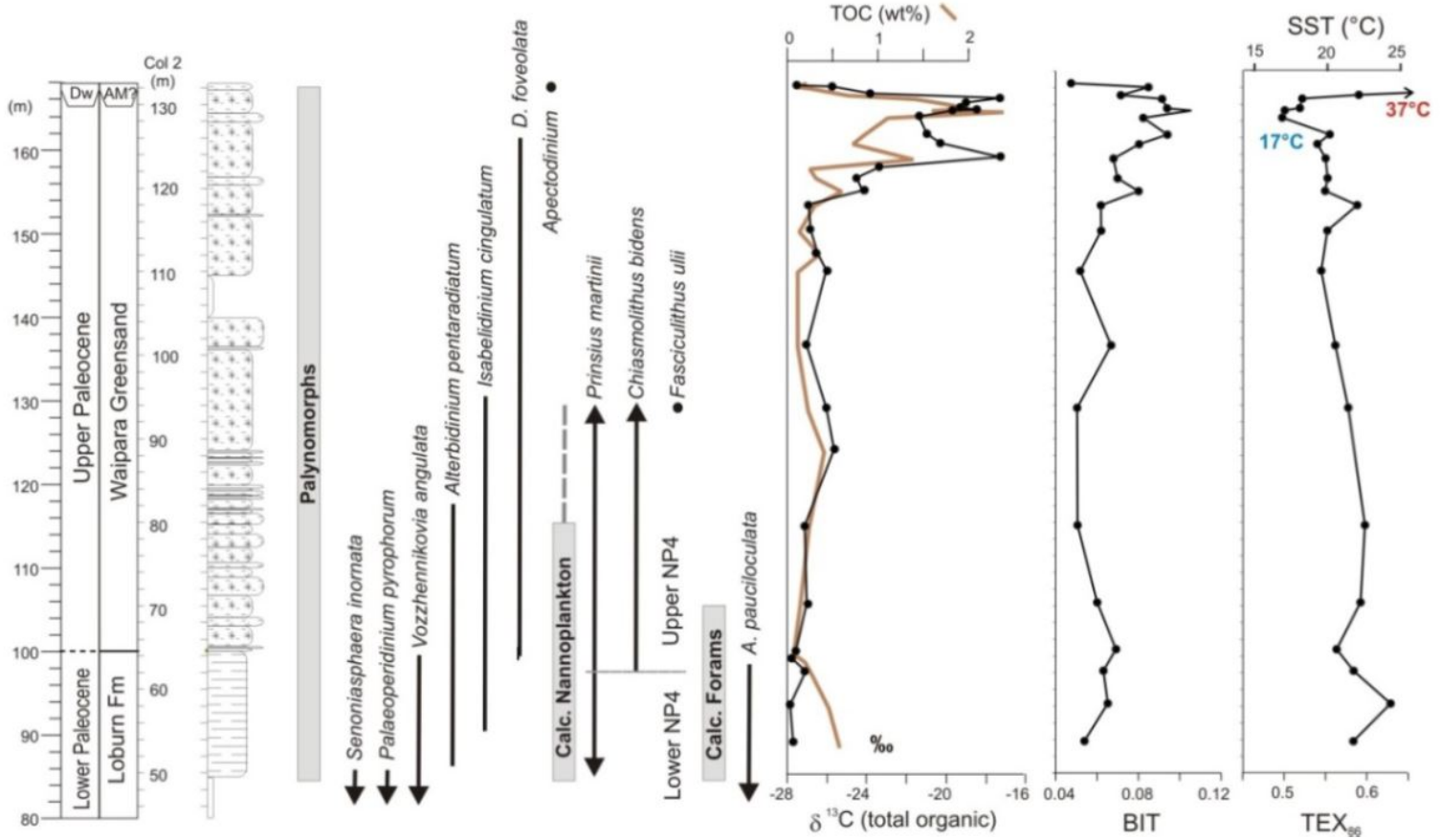

Figure 5 – Stratigraphy and environmental conditions based on palynmorph, calcareous nanoplankton and calcareous foraminifera assemblages, as well as Total Organic Carbon (TOC), Branched and Isoprenoid Tetraether index (BIT) and TEX_{86} for the Upper Loburn Mudstone and Waipara Greensand (Hollis et al., 2013)

3.6.2 Loburn Mudstone

The Loburn Mudstone is finely laminated, grey, very well sorted, moderately indurated with pale yellow jarosite staining and nodular concretions (Morgans, 2005). Trace amounts of glaucony are present and concentrated in burrows. A thickness of 10 m was measured, although this is a minimum value as the contact with the underlying Conway Formation was not observed. Kapoutsos (2005) measured a total thickness of 12 m. The fine grained, very well sorted nature of the sediment and abundant feeding trace fossils suggests the Loburn Mudstone was deposited in an outershelf marine environment with low sedimentation rates. The presence of Fe-Sulfide minerals suggests the seafloor was sub-oxic.

3.6.3 Waipara Greensand

The Waipara Greensand conformably overlies the Lobun Mudstone (Morgans, 2005). The gradational contact is arbitrarily defined as in increase in glaucony content from <5% to 20-30%. Thomson (1920) divided the formation into lower alternating hard and soft greensand and and upper unit of softer dark greensand with argillaceous matter and shaly partings. The formation was divided into the lower Mount Ellen Member and the upper Stormont Member by Browne and Field (1985). The Waipara Greensand is well sorted with a dark grey silt matrix and 30-60% fine grained glaucony grains. The presence of dark green mature glaucony suggests deposition in a marine environment with low sedimentation rates.

3.7 Oparara Quarry Limestone, Karamea

3.7.1 Overview of stratigraphy

Calcareous sediments of the Karamea region relevant to this research are those from the Nile Group. This group encompasses Oligocene calcareous rocks of Buller and north Westland and is comprised of two formations, the Little Wanaganui Formation and the Karamea Limestone Formation (Nathan, 1973). The Little Wanganui Formation is comprised of three members; the Kohaihai Limestone, the Glasseye Mudstone and the Kongahu Member, and is Whaingaroan to Waitakian aged. In the Karamea region the Little Wanganui Formation is only represented by the Kohaihai Limestone Member, whereas further south the Glasseye Mudstone and Kongahu members are present as either conformably

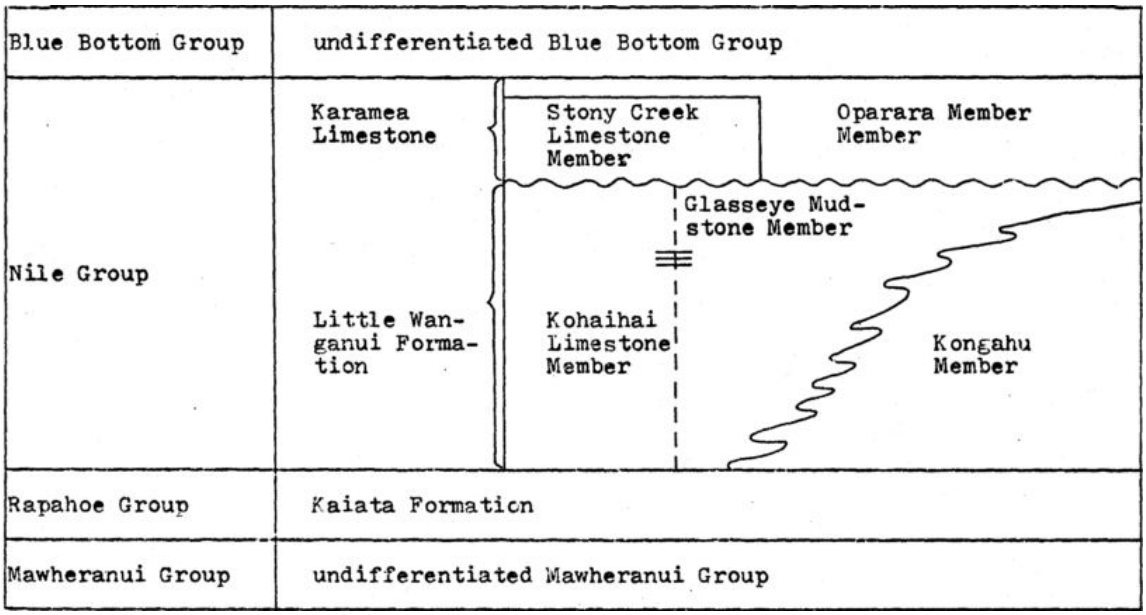

Figure 6 – Overview of the northern West Coast stratigraphy (German, 1976)

overlying the terrestrial Mawheranui Group or unconformably overlying Paparoa Granite. The Waitakian aged Karamea Limestone Formation comprises two units; a lower Stoney Creek Limestone and an upper Oparara Member, and unconformably overlies either calcareous rocks of the Little Wanganui Formation or the Karamea Granite. The Nile group is conformably overlain by the Blue Bottom Group sediments (German, 1976).

3.7.2 Stoney Creek Limestone (a member of the Karamea Limestone)

The Stoney Creek Limestone is Late Duntroonian to Early Waitakian (Late Oligocene) in age (Neef, 1981) and is the only unit sampled in this research. It is present as a well exposed outcrop of tilted, finely bedded limestone at the Oparara Quarry where it is ∼40 m thick. In the Oparara valley, sharp unconformable contacts are seen between the Karamea Granite and the Stoney Creek Limestone (German, 1976). Intervening sediments from the terrestrial Mawheranui Group (Brunner Coal Measures) and the Kohaihai Limestone were eroded during a period of localised uplift in the Duntroonian (German, 1976; Neef, 1981), exposing the surface of the Karamea Granite. Renewed subsidence in the Waitakian resulted in deposition of the Stoney Creek Limestone on a shallow wave cut platform, dominated by communities of bryozoans. Small islands of Karamea Granite provided minor lithic components which decreased upsection as the water depth progressively increased. German (1976) suggested water depths were likely 20-80 m as this is the zone of vigorous bryozoan growth.

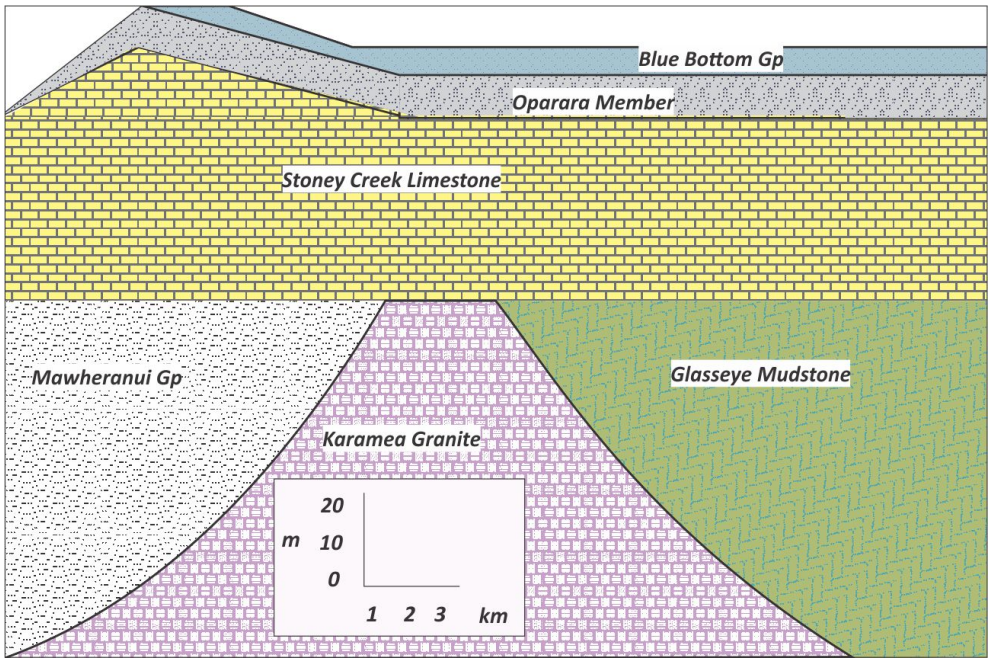

Figure 7 – Cross section showing the Stoney Creek Limestone unconformably overlying the Karamea Granite, modified from German (1976)

3.7.3 Karamea Granite

The Karamea Batholith extends from Kahurangi Point southwards to the Alpine Fault, a distance of 200 km with an average thickness of 20 km. It is a coarse grained, porphyritic biotite granite containing large, pink alkali feldspar megacrysts. The groundmass is composed of quartz, oligoclase, microcline, biotite and muscovite with accessory minerals including zircon, iron oxide and apatite (Muir et al., 1996). The Karamea Batholith is comprised of high-K calc-alkaline rocks ranging in composition from metaluminous to strongly peraluminous. The granites were considered as S-type by Kutsukake (1988) and both I and S-type by Muir et al. (1996).

4 Materials and Methods

4.1 Field work and sample collection

Field work was undertaken in March 2014 at Oamaru, the mid-Waipara River and the Oparara Quarry, Karamea. Geological descriptions and field logs were drafted of all units that were relevant to aid in interpreting the geological setting (see Section 2). Samples were collected from all units containing visible glaucony. In weakly indurated rocks, fresh samples were collected by removing the outside 10-20 cm of weathered rock. Approximately 1 kg of rock was taken for each sample, placed in a zip lock bag and labelled. The subscripts WP, OP, EQ, RF, CB and GB represent Waipara, Oparara, Earthquakes, Ross Farm, Campbells' Beach and Gees' Beach, respectively. GPS measurements were recorded where samples were collected. All samples are stored in the Department of Geological Sciences rock and mineral collection at the University of Canterbury.

4.2 Sample preparation

Weakly indurated samples were disaggregated in warm water. This was done by hand in a plastic container to minimise mechanical fragmentation to the grains. Loose sediments were then wet sieved into 1000-500 μm, 500-212 μm and 212-63 μm grain size fractions before being dried at 45° C for 24 hours.

Glauconitic minerals were then separated from the bulk sample using a Frantz isodynamic magnetic separator. The purest separation was achieved by doing two runs for each sample; beginning with the voltage set at 1 A, 14° sideways tilt and 20° longitudinal tilt, followed by a run using the same orientation of the unit and 0.5 A. This produced a sample of green grains which was free of sediment that was not of interest for chemical analysis.

Concentrated glaucony samples were then rinsed in dilute HCl (10%) to remove any traces of carbonate components aggregated to the surface of the glaucony grains, followed by rinsing 5 times with distilled water. A short ultrasonic bath (3 s) was the final stage of purification before the sediment was again oven dried at 45° C for 24 hours.

Grains were handpicked using a fine paint brush under the binocular microscope. One-hundred hand picked grains were mounted on epoxy resin stubs and used for Raman spectroscopy, Laser Ablation Induction Coupled Plasma Mass Spectroscopy (LA-ICP-MS)

and the Scanning Electron Microscope using Energy Dispersive X-ray Spectroscopy (SEM + EDS). From the non-indurated rocks 11 samples were chosen to pick grains from. Three were from the Waipara River section and 8 were from various outcrops around the Oamaru region. This allowed the comparison of grains from different depositional environments both up-section in an outcrop and across a sedimentary basin. Where possible, 3 grains were picked from each grain size for each sample, resulting in 9 grains representing a sample. Grains were picked that best represented the majority of the glaucony from a sample; this was based on colour, parent material and rounding. All of these grains were examined and photographed under the binocular microscope before the stubs were polished (grain images are presented in Appendix B).

Stubs were mounted with grains of the same size fractions to make the polishing surface close to an even elevation. The grain mounts were polished using gradually finer polishing agents, beginning with 120 fixed grit silicon carbide paper, followed by 3 μm, 1 μm and eventually 0.5 μm diamond paste on 450 Lampan cloth. Unfortunately due to the softness of glaucony some of the 212-63 μm grains were lost and a total of 77 grains remained on the stubs.

Thin sections of the weakly indurated samples were cut after being impregnated with epoxy resin (Epotek 301). These were used for petrographic examination to show grain relationships and examine the internal morphology of glaucony. No further geochemical analysis were performed with these sections.

Indurated samples were only present at the Oparara Quarry. These grains could not be disaggregated by hand and mechanical crushing of the rock would have pulverised the glaucony making further analysis impossible. Instead the rock was cut into thin sections which were polished using the same method as described for the epoxy mounts above. These sections were used for Raman spectroscopy, LA-ICP-MS and SEM + EDS.

4.3 Optical Petrography

Components of the bulk sediment were analysed using a Meiji Techno EMZ-13 binocular microscope. Proportions of authigenic minerals, carbonate components and detrital material were estimated, along with the degree of rounding, the colour of glaucony and the nature of the parent material of glaucony. Thin sections were examined under a Leiko petrographic microscope. Images were taken at 4x and 10x magnification in both plane and cross polarised light.

4.4 Scanning Electron Microscopy

Twenty grains were mounted on a 12.5x10 mm grooved slug-type SEM mount using 12 mm carbon tapes as the mounting adhesive before being gold coated. Grains were not polished as it was found that polishing removed the surface features from grains. A Jeol 7000 Field Emission SEM was used to analyse grains. Images were saved in a tiff format with information about operating mode, voltage, magnification, scale bar and working distance included on each image.

4.5 LA-ICP-MS trace element measurement

Sixty grains from the polished mounts were chosen to be analysed for trace and REE. These grains were selected to include all sampled outcrops and to cover a range of host material and maturity levels of glaucony. A total of 50 grains were selected to be measured with LA-ICP-MS, 40 from the polished stubs and 10 from the polished thin section.

Trace and rare earth elements were measured by LA-ICP-MS using facilities In the Otago Community Trust Center for Trace Element Analysis at the University of Otago. Laser ablation was conducted with a Resonetics RESOlution M-50-LR laser ablation system incorporating a Coherent CompexPro 102 193 nm ArF excimer laser and Laurin Technic two-volume sample cell. The laser was operated at a constant energy of 100 mJ and 12.5% transmission for an on-sample fluence of 4 J/cm^2. Ablated material was carried by He gas (650-750 ml/min) from a two-volume sample cell, mixed with Ar (650-750 ml/min) and N_2 (2-6 ml/min), and input into an Agilent 7500cs ICP-MS. Data for 52 mass peaks were collected in time resolved mode with one point per peak. Integration times were 10 ms for ^{3}Li, ^{4}Be, ^{23}Na, ^{24}Mg, ^{27}Al, ^{29}Si, ^{31}P, ^{39}K, ^{43}Ca, ^{45}Sc, ^{49}Ti, ^{51}V, ^{53}Cr, ^{55}Mn, ^{57}Fe, ^{59}Co, ^{60}Ni, ^{65}Cu, ^{66}Zn, ^{71}Ga, ^{72}Ge, ^{75}As, ^{85}Rb, ^{88}Sr, ^{89}Y, ^{90}Zr, ^{93}Nb ^{133}Cs, ^{137}Ba, ^{139}La, ^{140}Ce, ^{141}Pr, ^{146}Nd, ^{147}Sm, ^{158}Eu, ^{157}Gd, ^{159}Tb, ^{163}Dy, ^{165}Ho, ^{166}Er, ^{169}Tm, ^{172}Yb, ^{175}Lu, ^{177}Hf, ^{181}Ta, ^{202}Hg, ^{206}Pb, ^{207}Pb, ^{208}Pb, ^{232}Th and ^{238}U.

Background (laser off) data were acquired for 20 s followed by 40 s with the laser using spot diameters of 75 μm, a 5 Hz repetition rate, a 200 μm long track at 5 μm/s, and approximately 20 μm deep giving about 100 mass scans. Each set of 9-12 samples was bracketed by analysis of standard glasses NIST 610 and 612 from Pearce et al. (1997).

Raw mass peak count rates were background subtracted, corrected for mass bias drift and converted to concentrations using an offline spreadsheet. After triggering, it takes

several seconds for a steady signal to be reached, so these initial data were excluded from the calculations. Trace-element concentrations were obtained by normalising count rates for each element to those for Si in the sample and standard using known SiO_2 and trace element concentrations in NIST 610 Pearce et al. (1997) and the SiO_2 in the sample estimated by summing the major element oxides to 100 wt%.

4.6 Scanning Electron Microscope with Energy Dispersive X-ray Spectroscopy (SEM + EDS)

Major element concentrations were measured using a JEOL JSM 6100 SEM with an Oxford Aztec EDS analysis system at the University of Canterbury. Polished epoxy grain mounts and a polished thin section were carbon coated prior to anlaysis. Measurements were made at 800x magnification with a 4 s acquisition time. Two squares were drawn on each grain to select the area to be scanned, these were about 100 μm^2 and were drawn in the most homogenous looking part of the grain. Images were taken of each grain prior to chemical analysis.

Chemical data for 87 grains (77 from stubs and 10 from the thin section) were collected as elemental weight %. Microsoft Excel spreadsheets were used to recast data as oxide weight % and to calculate stoichiometric mineral formulas. Total Fe was calculated as Fe_2O_3 and mineral formulas were calculated as being anhydrous as no loss on ignition data was obtained.

4.7 Raman Spectroscopy

Raman spectroscopy was used to assess chemical variation between single grains of glaucony. Analysis was conducted at the Department of Chemistry, University of Otago. Raman spectra were measured for all 77 grains on the polished epoxy mounts with a Senterra dispersive Raman microscope (Bruker Optics, Ettlingen, Germany). Grains were measured using a 785 nm diode laser frequency at 10 mW laser power. It was found that using lower laser frequency and higher laser power would burn the clay minerals and lead to excess fluoresence overprinting the spectra of glaucony. The objective was focused using 50x magnification with an aperture of 50 μm.

Each grain was analysed by setting a rectangular grid with 9 points to be scanned by the laser. The integration time was 5 s and we used 10 co-additions per site (each of the

9 spots making the rectangle was collected 10 times and averaged). Data was collected between the spectral range of 90-3200 cm^{-1} at a resolution of 9-18 cm^{-1}. Software used to analyse the data and create spectra was Opus Version 6.5 from Bruker Optik Gmbh 1997-2007. 'The Unscrambler' multivariate analysis software was used to assess variation between spectra.

4.8 XRD

The crystalline structure of glaucony was analysed by XRD at the Department of Geological Sciences, University of Canterbury. Twelve samples were magnetically separated to isolate glaucony before grains were crushed in an agate mortar and pestle. Oriented mounts were created by mixing the finely crushed powder with ethanol to form a slurry which was then transferred to a glass slide and allowed to dry at room temperature.

Analysis was carried out using a Philips PW1820/1710 X-ray diffractometer with Cu tube and PW1752/00 monochromator. Samples were scanned from 3° to 70° 2θ with a step size of 0.02° 2θ and scan speed of 0.02° per θ per second. X-rays were generated using a PW1729 X-ray generator (50kV/40mA).

To test whether glaucony would swell or not the samples were placed into a desiccator with ethylene glycol solution overnight in an oven at 60° C. The slide was scanned from 3° to 30° 2θ once it had cooled to room temperature. To test the effect heat has on glaucony the glycolated slides were placed into a muffle furnace for one hour at 550° C. The slide was scanned from 3° to 30 2θ once the slide had cooled to room temperature.

4.9 Solubility testing

Two separate experiments were conducted to assess the release of elements from glaucony into solution over time.

1. Glaucony solubility was measured in H_2O over a 16 day period. ~0.37 g of glaucony from the 212-500 μm grain size fraction of WP07 and WP10 were left in 40 mL of ultrapure water. Tubes were lying horizontally on a table shaker (IKA model KS260) operating at 50 revolutions per minute, giving a gentle stirring action. Extractions of solution were made at 25, 73, 190 and 382 hours. Ten mL of solution was extracted

from 3 tubes resulting in a triplicate analysis for each time period. The extractions were filtered using 2 μm filters to remove trace solid particulates. The samples were kept in a room at 22° C throughout the experiment. Two samples of the ultrapure water were taken for analyses, one at 25 hours and one at 382 hours. This was done to ensure no contamination was introduced from the water itself, and all elemental proportions are due to dissolution of the glaucony.

Following each extraction pH measurements were taken using a Mettler Toledo Seven GoDuo Pro SG78 pH/conductivity probe. The pH of the neutral ultrapure water dropped from 7.0 to 3.6 within the first day of testing. This was initially of concern and restarting the experiment using a buffered solution was considered, however, after deciding to continue on to see what would happen it was found that the pH fluctuated only slightly (ranging from 3.47 - 3.69, averaging 3.58) over the full 16 days.

Elemental proportions were measured using Induction Coupled Plasma Mass Spectroscopy (ICP-MS) in the Chemistry Department at the University of Canterbury. Solutions were protonated to pH 2 to stop ions sticking to the sides of plastic tubes. Measurements of Na, Mg, Al, P, K, Ca, V, Cr, Mn, Co, Fe, Ni, Cu, Zn, As, Sr, Zr, Ru, Cd, Sn, Sb, Cs, Ce, Ti, ^{206}Pb, ^{207}Pb, ^{208}Pb, Th and U were made using an Agilent 7500cx ICP-MS with 2-260 Atomic Mass Units quadrupole mass analyser.

2. The second experiment tested the influence of birnessite (a high valent Mn oxide known to be a strong oxidising agent in soil environments) on elemental release from glaucony. This experiment was run over 103 hours at 25°C using 0.25 g of magnetically separated glaucony from WP04 and EQ01. Samples were left in 10 mL of solution on a table shaker operating at 80 rotations per minute. The solutions were a pH 4.6 acetate buffered solution and a pH 8 NaOH buffered solution. Birnessite (0.015 g) was added to one of two samples at both acidic and basic pH, resulting in the analysis of glaucony solubility with and without birnessite at both high and low pH. Elemental concentrations were measured using ICP-MS at Stanford University. The elements selected for analysis were Mg, Al, K, Ca, Cr, Mn and Fe.

5 Results

5.1 Sedimentary descriptions and glaucony characteristics

This section will present results of field observations and sampling. A discussion of glaucony morphology is included first as a guide to the terminology used in the following sections.

5.1.1 Morphological and colour variations

Glauconitic minerals occur in a wide range of morphologies. This is due to the variety of the host material's shape and size, the wide range of controls that can influence the maturity of a glauconitic mineral and the aggregate nature of precipitation (Odin and Matter, 1981; Amorosi et al., 2007). It is a rare exception that a grain of glaucony retains the surface morphology of the host material and this tends to prevail in only immature glaucony and where mechanical fragmentation has been minimal. With this in mind, it is possible to tentatively assign a morphological category to grains only when the original host material is considered a significant factor. Grain morphologies that were encountered during this research, in order of decreasing occurrence include:

- Amorphous grains which are broken or cracked and have irregular morphologies (Figure 8I). Some of these are undoubtedly derived from pellets, bioclasts or vermicular grains, however to assign a distinct morphological class to them is difficult at best. These grains take on the full colour range of glaucony from pale grey-green to dark black-green.

- Capsule or ellipsoid morphologies, sometimes with segmented surfaces resulting in botryoidal shapes (Figures 8G and H). These are usually medium to dark green in colour and have a rounded surface. Grains of this nature were determined to originate from faecal pellets (Triplehorn, 1966; Odin and Matter, 1981; Banerjee et al., 2012a) and will be referred to as pellets from here.

- Grains which preserve the morphological expressions from bioclast tests (Figures 8C, D, E and F). The internal spaces of the calcite tests become filled with glaucony and eventually preserve the structures of the host grain once the test itself has dissolved. These can take on a variety of morphologies and commonly occur as a pale green

colour compared to the darker pellets. Benthic foraminifera are especially favourable host materials, with bryozoans and echinoderm spines appearing only rarely.

- 'Bookshelf' or 'accordian' shaped grains and are derived from growth and expansion inside the cleavage planes of micaceous minerals and are referred to as vermicular grains (Triplehorn, 1966; McRae, 1972; Odin and Matter, 1981). These occur as straight or slightly curved rectangular shapes with surface cracks running perpendicular to the long axis of the grain (Figures 8A and B). The colour of vermicular grains ranges from very pale grey-green through to dark black-green.

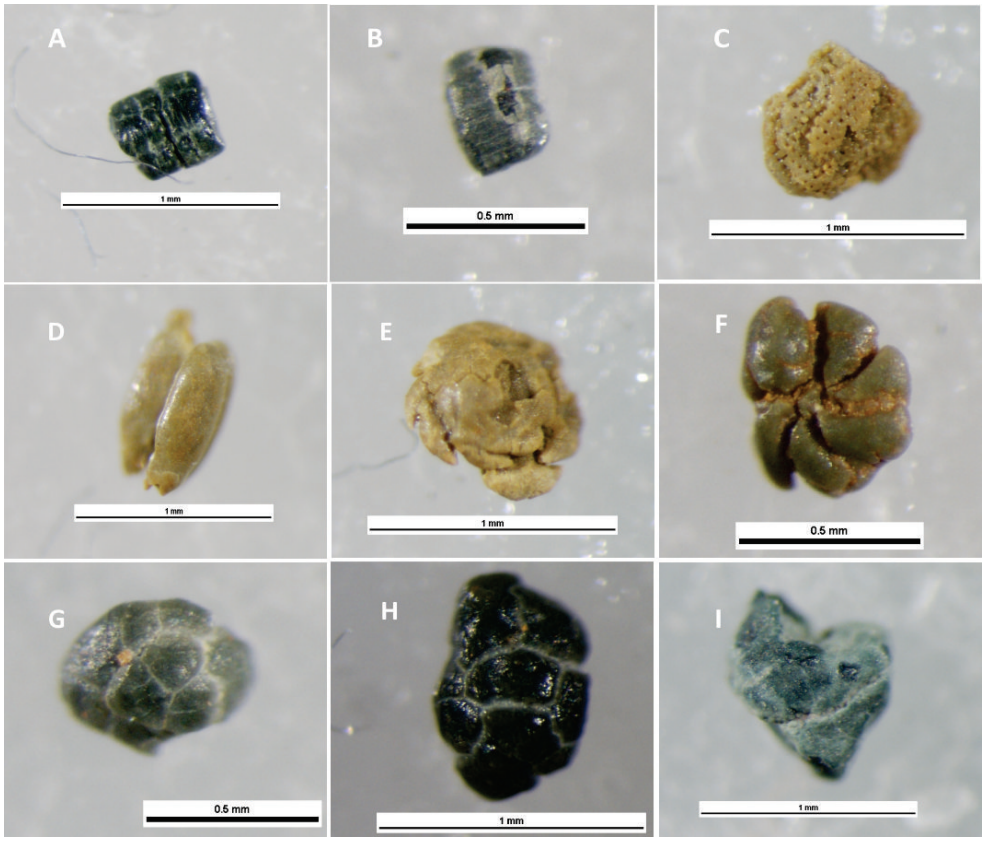

Figure 8 – Grains of glaucony on double sided tape prior to being mounted and polished on epoxy resin. **A** and **B** - medium-dark green vermicular glaucony from Campbell's Beach (Gee Greensand) and Earthquakes (Kokoamu Greensand) respectively. **C** - Well preserved pale green glaucony derived from echinoderm host grain - Gee's Beach (Gee Greensand). **D**, **E** and **F** - Pale green growth inside benthic foraminifera - Gee's Beach. **G** and **H** - Glaucony pellets from Earthquakes (Kokoamu Greensand) and the Waipara (Waipara Greensand), respectively . **I** - Amorphous grain, possibly derived from lithic material - Waipara

Figure 9 – Locations of outcrops sampled and measured in the Waitaki basin

Figure 10 – Images of features observed in Oamaru outcrops. A) Otekaike Limestone infilling karst surface of Ototara Limestone at Gee's Beach, B) Otekaike Limestone infilling trace fossil burrows on the surface of the Earthquakes Marl, C) Melatodes near base of the Gee Greensand, D) Cross beds in Gee Greensand at Gee's Beach.

5.2 Sedimentary descriptions

5.2.1 Earthquakes

The 'Earthquakes' outcrop was accessed via the Earthquake Road off the Livingstone-Duntroon Road. Eight samples were collected at Earthquakes and 3 were chosen for chemical analysis, these were EQ02 and EQ06 which represent the base and top of the Kokoamu Greensand, respectively, and EQ08 represents the base of the Otekaike Limestone. The Kokoamu Greensand was deposited during the onset of a transgressive sequence directly above the Marshall Paraconformity and the Otekaike Limestone was deposited during a late stage of transgression and highstand systems tract. The stratigraphic column for Earthquakes is shown in Figure 11.

The Ototara Limestone is present as the **Earthquakes Marl** and measures a minimum thickness of 0.8 m. The Earthquakes Marl is a creamy white, impure wackestone with 2-5% glaucony, trace amounts of mica and ∼10-15% terrestrial silt, most of which is sub-angular quartz. The upper contact is heavily bioturbated with *Thallasinoides* trace fossils. Trace fossil burrows at the contact between the Earthquakes Marl and Kokoamu Greensand suggest the unit did not become sub-aerially exposed during the Marshall Paraconformity

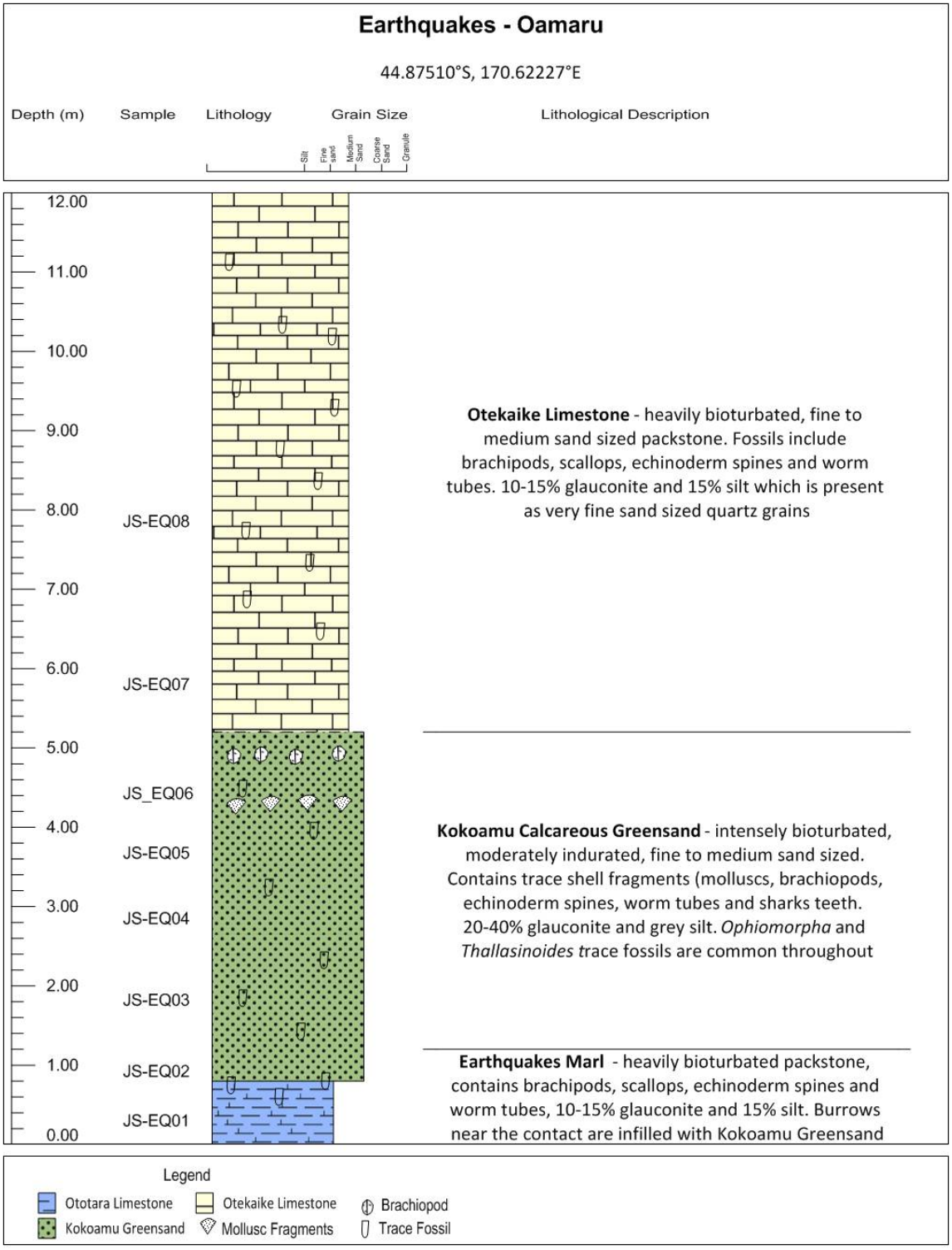

Figure 11 – Stratigraphic log for Earthquakes

and stiff seafloor sediments were present (Figure 10B). The Earthquakes Marl was not sampled for chemical analysis due to the low glaucony content.

The base of the **Kokoamu Greensand** measures 4.2 m and is massive. It contains 30-40% glaucony, decreasing to 25-30% near the top. Glaucony from both samples is concentrated in the 500-212 μm grain size. The grains are dominantly of the dark green pelletal variety and are rounded with well defined segments (Figure 8G). Yellow-olive coloured glaucony is also present and is more angular than the darker grains. In the 212-63 μm grain size the proportion of pale grains increases at the expense of the dark green pellets, however these are a minor component of the overall sediment. Faecal pellets are the dominant host material, with trace amounts of both vermicular grains and bioclast replacement.

The bioclastic component of the Kokoamu Greensand is similar between the base and the top of the unit. At the base, benthic foraminifera dominate the assemblage whereas near the top the proportion of planktic:benthic foraminifera increases to ∼50%. Echinoderm spines (30%), Mollusc fragments (24%) and worm tubes (1%) account for the remaining bioclastic components. *Ophiomorpha* trace fossils are present throughout the Kokoamu Greensand. The terrestrial silt content is highest near the base of the Kokoamu Greensand where it accounts for 5-10% of the bulk sediment, this decreases near the top of the unit to 2-5%.

The **Otekaike Limestone** measures a minimum thickness of 7 m at Earthquakes and is massive. The contact between the Kokoamu Greensand and the Otekaike Limestone is arbitrarily defined as a decrease in glaucony content from ∼30% in the Kokoamu to ∼5-10% in the Otekaike. Glaucony comprises only 10% of the bulk sediment in the Otekaike Limestone. This is dominated by very dark green to black pelletal glaucony with minor amounts of the pale yellow-green grains. Glaucony is concentrated in the 500-212 μm grain size and is present as pellets with trace amounts of vermicular shapes. Grains are sub-rounded to rounded and have surface segmentation creating botryoidal shapes.

The bioclastic component is comprised of brachiopods, mollusc fragments, echinoderm spines, worm tubes and both benthic and planktic foraminifera. Terrestrial material increases slightly up section (from ∼2-5%) and is dominantly fine sand sized, sub-angular quartz grains and trace amounts of mica.

5.2.2 Ross Farm - Oamaru

Ross Farm was accessed via Taylors Road off the Duntroonian-Georgetown Road (Highway 83) with access from the landowners. Four samples were collected from Ross Farm and 2 of these were chosen for chemical analysis. RF01 represents the base of the Kokoamu Greensand directly above the contact with the Earthquakes Marl, and RF03 is taken from near the top of the unit. Figure 12 shows the stratigraphic column for Ross Farm.

A thin exposure of the **Ototara Limestone** is present as the basal unit and measures 20 cm thick. The contact with the overlying Kokoamu Greensand is sharp and weak banding was observed, suggesting sea levels underwent minor fluctuations between the low-stand and the onset of the next major transgressive sequence. The Earthquakes Marl is a bryozoan rich packstone with ∼20% glaucony. Glauconitic grains are medium to dark green and dominantly of the pelletal variety, with only trace amounts of vermicular grains (no bioclast infillings were observed). Bioclasts are dominantly bryozoans, with benthic and planktic foraminifera, mollusc fragments and echinoderm spines being present as minor components. Terrestrial components make up 5-10% of the bulk sediment and are fine sand sized, sub-angular quartz grains.

The **Kokoamu Greensand** is 2 m thick, massive, well sorted and moderate-poorly indurated. Glaucony is concentrated in the 500-212 μm grain size and is generally present as 50-60% of the bulk sediment by volume. Grains are medium to dark green and contain occasional pale green overgrowths. Pellets are the dominant host grain material, with <2% vermicular grains and no grains which could confidently be labelled as bioclast infilling. The sample RF03 is taken from the most glaucony rich rock found in the Oamaru region. Here it comprises 80% of the bulk sediment. Grains are dark green-black with only very minor amounts of yellow-pale green grains. Overgrowths are absent and glaucony appears homogenous. Morphologies are dominantly rounded, segmented grains interpreted as pelletal glaucony, although in the 212-63 μm grain size fraction there are minor amounts of pale green grains which preserve features of benthic foraminifera tests. Vermicular grains are present in trace amounts.

The bioclastic component of the Kokoamu Greensand comprises of planktic foraminifera, mollusc fragments, worm tubes and echinoderm spines. *Ophiomorpha* trace fossils are present throughout. Terrestrial material is present in low amounts (∼2%) and is mainly present as sub-angular quartz and mica.

The **Otekaike Limestone** is at least 3.5 m thick at Ross Farm, although only the base of

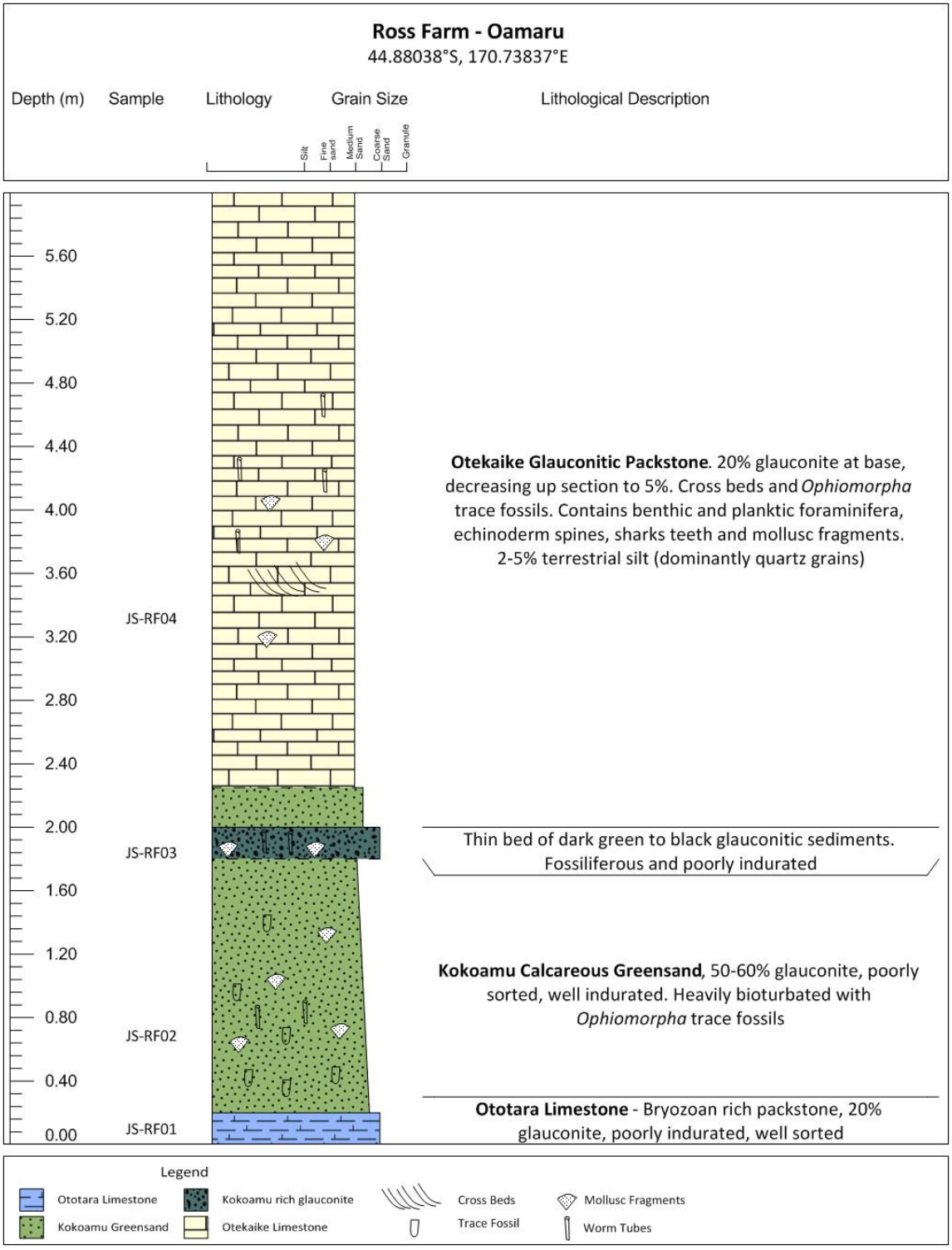

Figure 12 – Stratigraphic log for Ross Farm

the unit was able to be measured due to steep exposure. It shows well defined cross beds and contains concretionary bands which form ledges resistant to weathering. The rock is very well indurated and no samples were collected for geochemical analysis for this reason. The contact is with the underlying Kokoamu Greensand was difficult to define and was based on the change in glaucony content from 20% near the top of the Kokoamu to 5-10% in the Otekaike.

Bioclasts include benthic and planktic foraminifera, echinoderm spines, sharks teeth and mollusc fragments. *Ophiomorpha* trace fossils are common and the terrestrial silt content is 2-5%, comprising mainly of sub-angular quartz grains.

5.2.3 Gee's Beach - Oamaru

Gee's Beach was accessed via Beach Road ∼2 km north of the township of Kakanui. Seven samples were collected from Gee's Beach and 2 were chosen for chemical analysis. GB07 was taken from an outcrop near the southern end of the beach (towards Kakanui) and GB04 was taken ∼300 m further north, where Beach Road first accesses the beach. The Gee Greensand rests unconformably on top of the Otekaike Limestone and represents deposition following the beginning of a transgressive sequence. Figure 13 displays the stratigraphic log for both measured outcrops at Gee's Beach.

The **Ototara Limestone** is the basal unit present at Gee's Beach and measures 1.5-2.0 m (depending on the base level of the beach sands). It is a very well indurated, creamy white, bryozoan grainstone. Dissolution cavities on the surface of the Ototara Limestone marks sub-aerial exposure and chemical weathering during the Marshall Paraconformity (Figure 10A). Trace amounts (<2%) of glaucony, quartz and mica are present. No samples were collected for chemical analysis due to the low glaucony content and the indurated nature of the rock.

The **Kokoamu Greensand** and **Otekaike Limestone** are present only as a thin surface veneer draping the dissolution cavities of the underlying Ototara Limestone. Glaucony comprised 30-50% of the Kokoamu and is present as medium green fine sand sized grains. Phosphorite is present as brown grains in the calcareous greensand and as a surface coating above the Ototara Limestone. Medium sand sized basalt lithics are present as ∼2-5% of the rock.

The **Gee Greensand** is 1.6 m thick in the outcrop to the north and ∼3 m thick in the southern exposure. It is moderate to poorly sorted, medium to coarse sand sized grains and

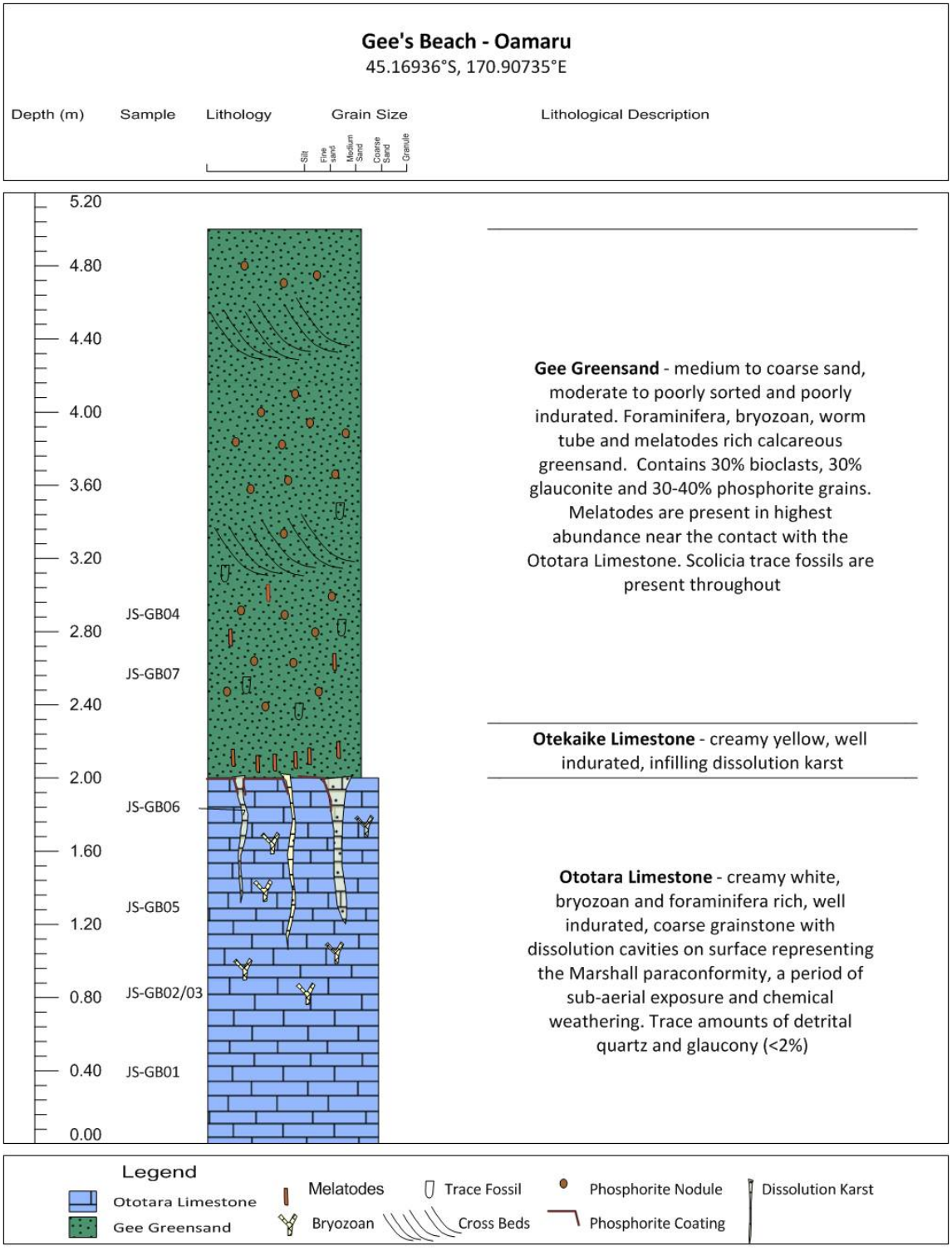

Figure 13 – Stratigraphic log for Gee's Beach. This log shows the section measured at the southern end of Gee's Beach and this is where GB07 was collected from. GB04 was taken from an outcrop 300 m to the north although the unit is stratigraphically the same (hence GB04 being above GB07 in the sample column of the log)

is poorly indurated. In the northern outcrop the unit is massive and in the south there are large scale cross beds (20-30 cm between beds) (Figure 10D). Glaucony comprises 30-50% of the bulk sediment and is present as pale yellow-green to dark green. Host materials include bioclasts, pellets and vermicular grains, and some of the best examples of bioclastic replacement was observed from these samples (see Figure 8D, E and F). Benthic foraminifera and echinoderm tests are common hosts for glaucony at Gee's Beach. Most grains have a faint brown-orange surface coating resulting from co-precipitation of phosphorite.

The dominant bioclastic components of the Gee Greensand are bryozoans (55%) and benthic foraminifera (30%), with melatodes, worm tubes, echinoderm spines, scleractinian corals and mollusc fragments making up the remaining bioclast components. Basalt lithics (<2%) are present at both outcrops and detrital terrestrial components are present only as trace amounts of sub-rounded quartz. Scolicia trace fossils are present throughout the unit.

5.2.4 Campbell's Beach - Oamaru

Campbell's Beach was measured and sampled on the southern side of the Kakanui Peninsula and was access was via Harbour Terrace. Only one sample was collected for chemical analysis, this was CB01 and was taken from the Gee Greensand. Figure **??** displays the stratigraphic log for Campbell's Beach.

The **Ototara Limestone** is ∼2.5 m thick at Campbell's Beach. It is a well indurated, creamy white, bryozoan grainstone. Glaucony content is <2% and the unit contains ∼5% basalt lithics. No terrestrial material was observed. Dissolution cavities are 5-15 cm deep and are infilled with a thin surface veneer of reworked **Kokoamu Greensand/Otekaike Limestone.** The infilling material is a a creamy grey, well indurated, poorly sorted rudstone.

The **Gee Greensand** is ∼2 m thick at Campbell's Beach. It is massive, a dark green-grey colour, medium to coarse sand sized, moderate to poorly sorted and poorly indurated. Glaucony comprises 40-60% of the bulk sediment and is concentrated in the 500-212 μm grain size. Host materials are bioclasts, pellets and vermicular grains and these are present as olive green to dark forest green colours. As in the Gee Greensand sampled at Gee's Beach, benthic foraminifera and echinoderms are common bioclast host materials.

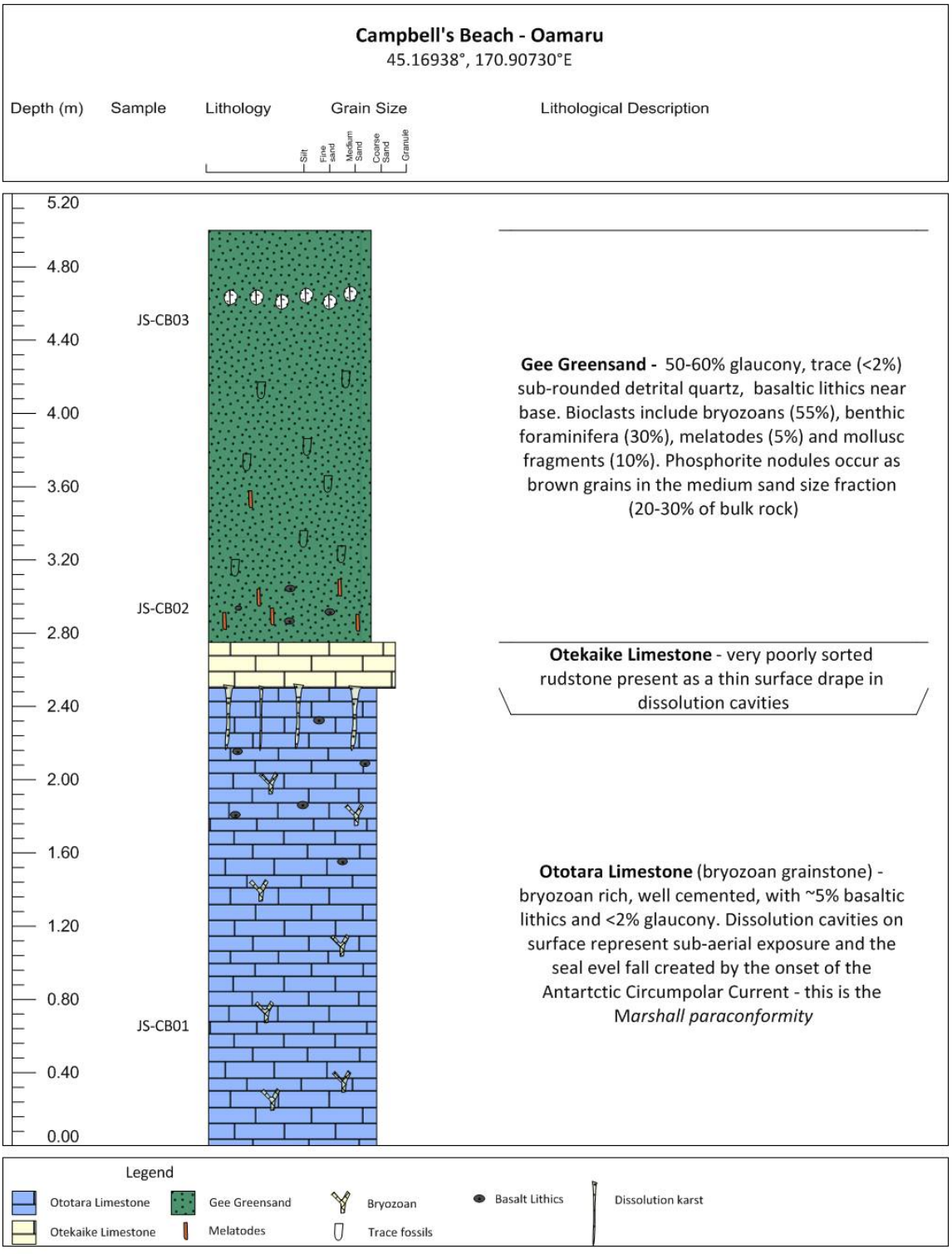

Figure 14 – Stratigraphic log for Campbell's Beach

The bioclastic component of the Gee Greensand contains benthic foraminifera, bryozoans, melatodes, echinoderm spines and a thin fossiliferous horizon containing mollusc fragments. Basaltic lithics are present at the base (2-5%) and decrease up section. Terrestrial material is present as <2% sub-rounded quartz grains.

5.2.5 Waipara Greensand - North Canterbury

The mid-Waipara River section was accessed via Laidmore Road off Ram Paddock Road. Three samples were collected from the Loburn Mudstone and 7 from the Waipara Greensand. Of these, WP04, WP07 and WP10 were chosen for geochemical analysis and WP07 was chosen for solubility analysis. Only the Loburn Mudstone and the Waipara Greensand were measured for this research. The stratigraphic column for the mid-Waipara section is displayed in Figure 16.

The **Loburn Mudstone** measured a minimum thickness of 10 m. It is a finely laminated, grey, very well sorted, moderately indurated mudstone with fritted weathering and yellow sulphur staining on the surface (Figure 17C). Glaucony is present in low concentrations (3%) as fine sand sized, medium green specks. *Planolites* trace fossil burrows are present and the glaucony is concentrated in these (Figure 17A). Marcasite (Fe-sulphide) nodules are common and measure 1-5 cm long (Figure 17D).

The **Waipara Greensand** measures a total thickness of 66 m. This should be regarded as a minimum as the contact with the overlying Ashley Mudstone was obscured. The greensand is monotonous and massive, with concretionary bands present throughout the unit appearing as nodular horizons of well indurated rock ranging in thickness from ∼20-150 cm (Figure 17D). These bands are compositionally identical to the rest of the unit. The matrix of the Waipara Greensand is a dark grey silt and sub-angular quartz and mica grains are present at ∼20-30% and <2% respectively throughout. No microfossils were observed in the samples from the Waipara Greensand. Occasional marcasite nodules are present near the base of the unit and become increasingly sparse up section. *Ophiomorpha* trace fossils are present and are filled with glaucony concentrated sediment. Near the top of the unit quartz grains become visible (30%) and the rock appears as a highly weathered, black greensand.

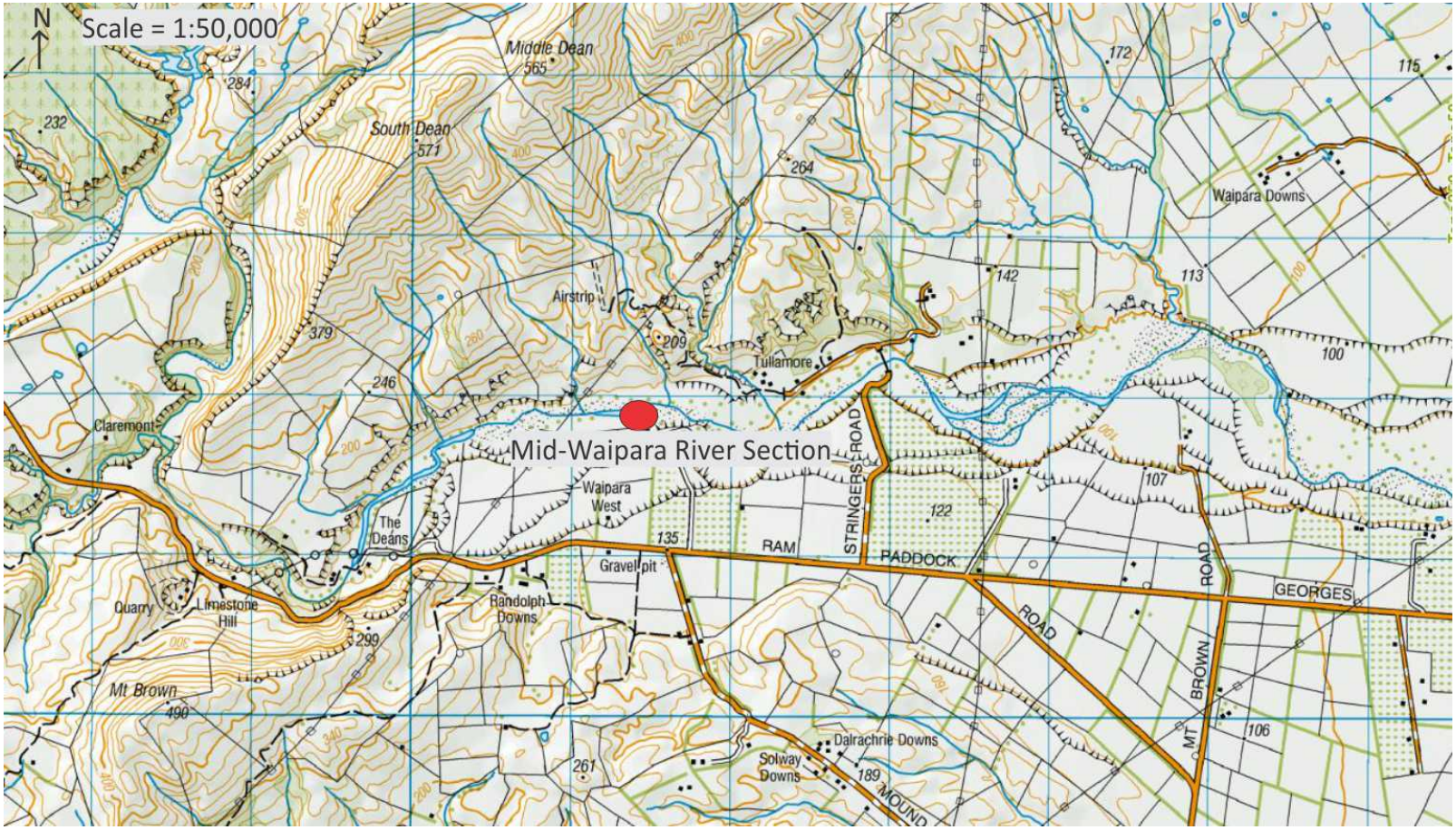

Figure 15 – Topographical map showing location of the section measured at the Mid-Waipara River

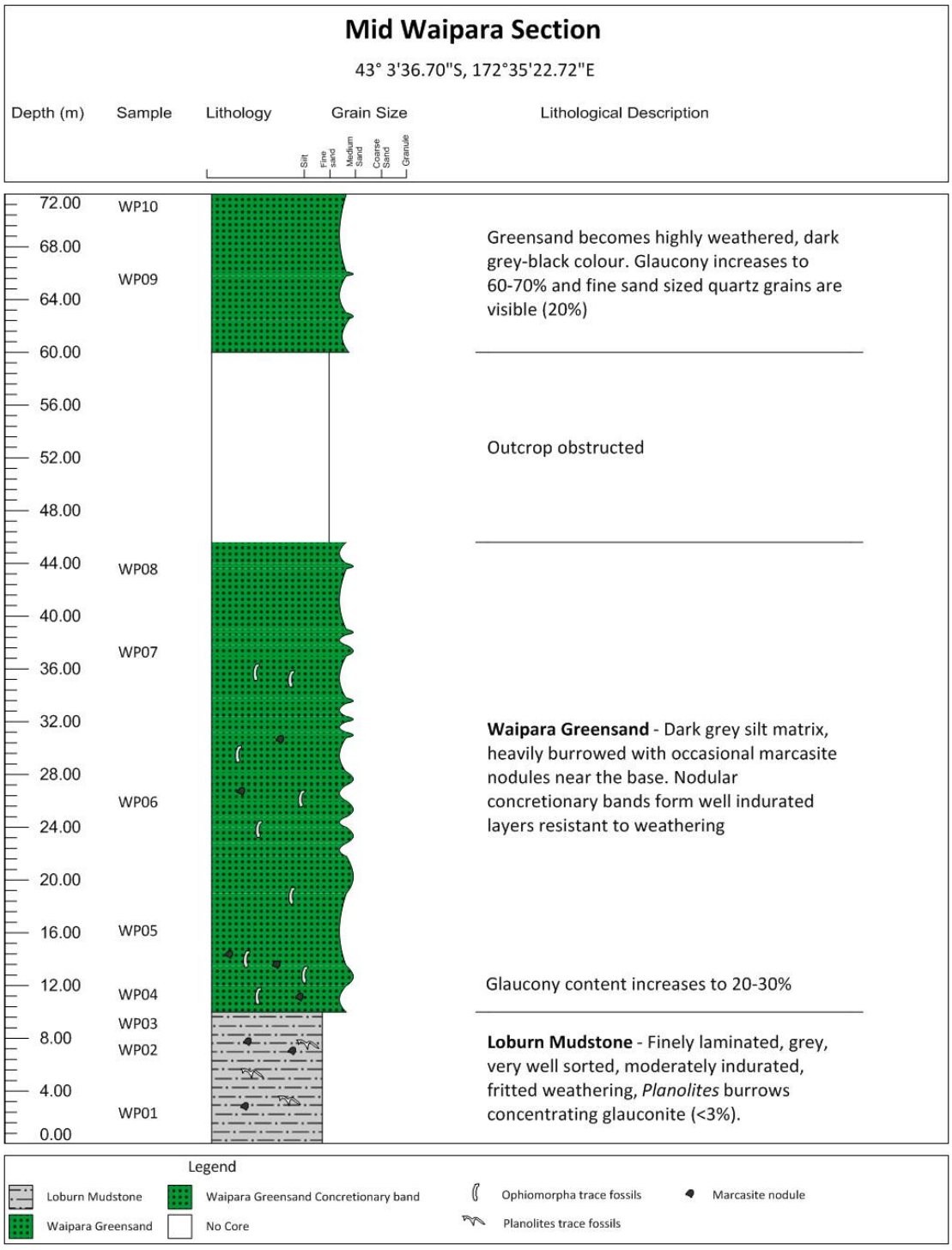

Figure 16 – Mid-Waipara stratigraphic log

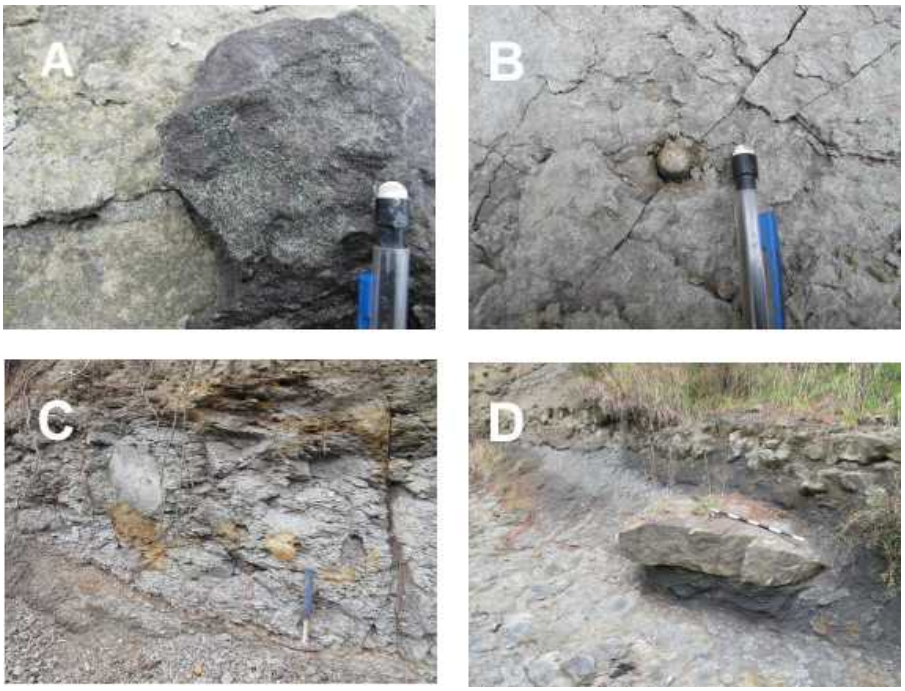

Figure 17 – Images from the Mid-Waipara section. A - concentrated glaucony in *Planolites* trace fossil. B - marcasite nodule in the Loburn mudstone. C - sulphur staining in the Loburn mudstone. D - concretionary banding in the Waipara Greensand

Glaucony generally comprises 40-50% of the bulk sediment from the Waipara Greensand, although this increases to 60-65% near the top of the unit. The green grains are dominantly sub-rounded dark green pellets and sub-angular amorphous shapes which show signs of mechanical fragmentation beyond the point of host material recognition. These are concentrated in the 500-212 μm grain size. Minor amounts of pale grey-green glaucony are present and pale green overgrowths on darker grains are common. Under the binocular microscope the dark grains have a finely aggregated crystalline appearance. Host materials which can be recognised are dominantly pellets and trace amounts of vermicular glaucony. It is likely that the amorphous grains are pellets which have been fragmented, although some may derive from quartz and feldspar host grains.

5.2.6 Stoney Creek Limestone - Oparara Quarry, Karamea

The Stoney Creek Limestone member of the Nile group was measured and sampled at the Oparara Quarry, Karamea, with permission from the quarry owner, Peter Curry. Access was via Oparara road, $\sim$3 km north of Karamea township. A total of 6 samples were collected, although only one of these (OP05) contained glaucony. Only the Stoney Creek

Limestone (a member of the Karamea Limestone Formation of the Nile Group) was present at the quarry. The stratigraphic column for the Oparara Quarry is presented in Figure 19.

At the Oparara Quarry the Stoney Creek Limestone is a creamy yellow echinoderm - bryozoan biomicrite with sparry cement infilling bryozoans. Quarrying has exposed 30-40 m of the **Stoney Creek Limestone**, however dense vegetation obscures contacts with the underlying Karamea granite and the overlying Oparara member. The limestone is ∼30 m thick and consists of well defined, slightly undulating beds measuring 4-8 cm thick (Figure 20A) which have been tilted from post depositional tectonic activity. Due to the well indurated nature of the Stoney Creek Limestone no whole separated grains of glaucony were observed. Glaucony was only present in one thin section where it comprised ∼5% of the total rock (Figure 21B) and is present as pale green homogenous grains. Host morphologies are difficult to distinguish in thin section, although bioclast infilling (planktic Foraminifera) was observed in a few grains, whereas vermicular grains and pelletal glaucony were both absent. Trace amounts of Fe oxides are present in thin section, both on glauconitic minerals and on the carbonate bulk material.

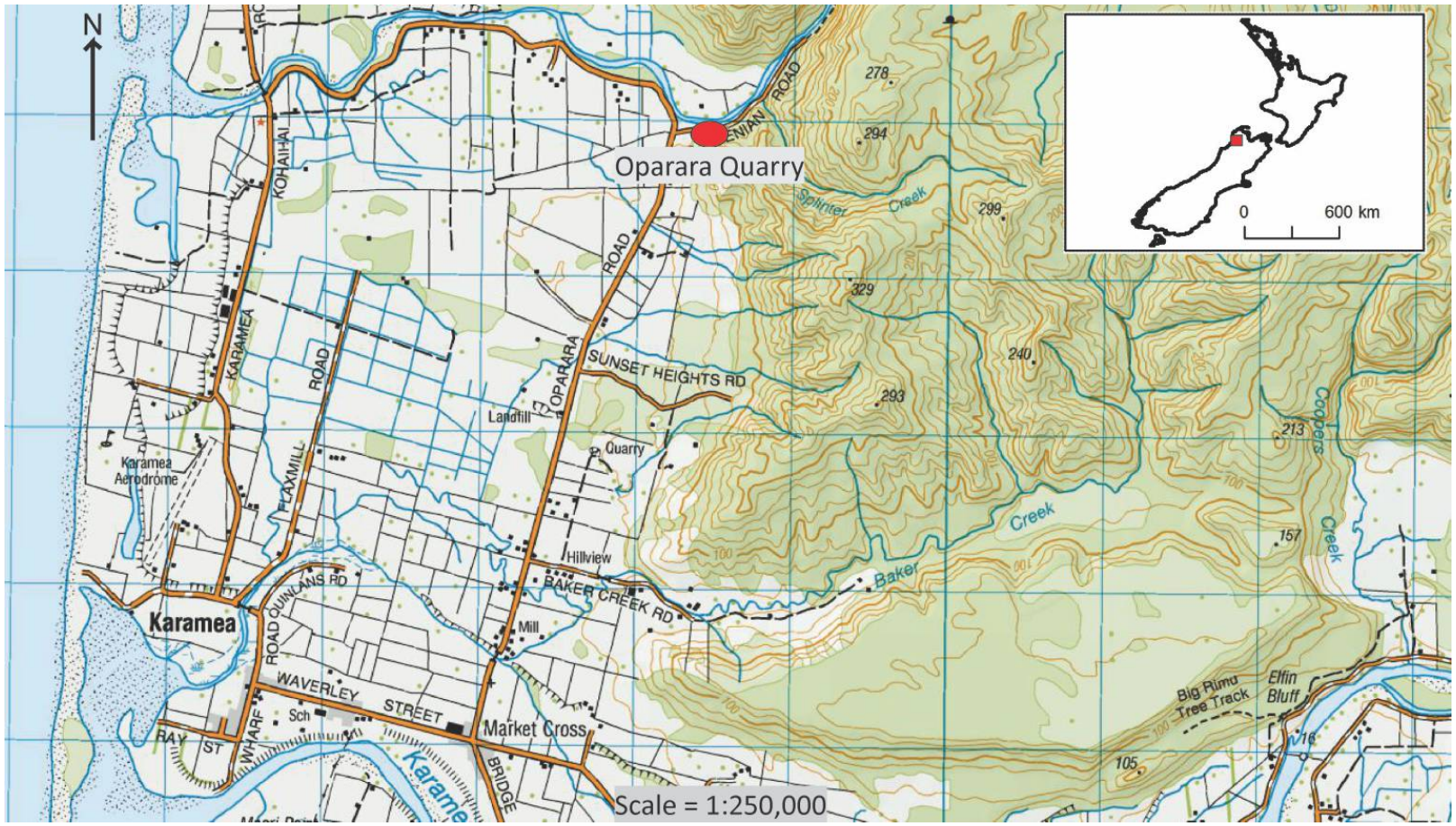

Figure 18 – Topographical map showing location of the Oparara Quarry, Karamea

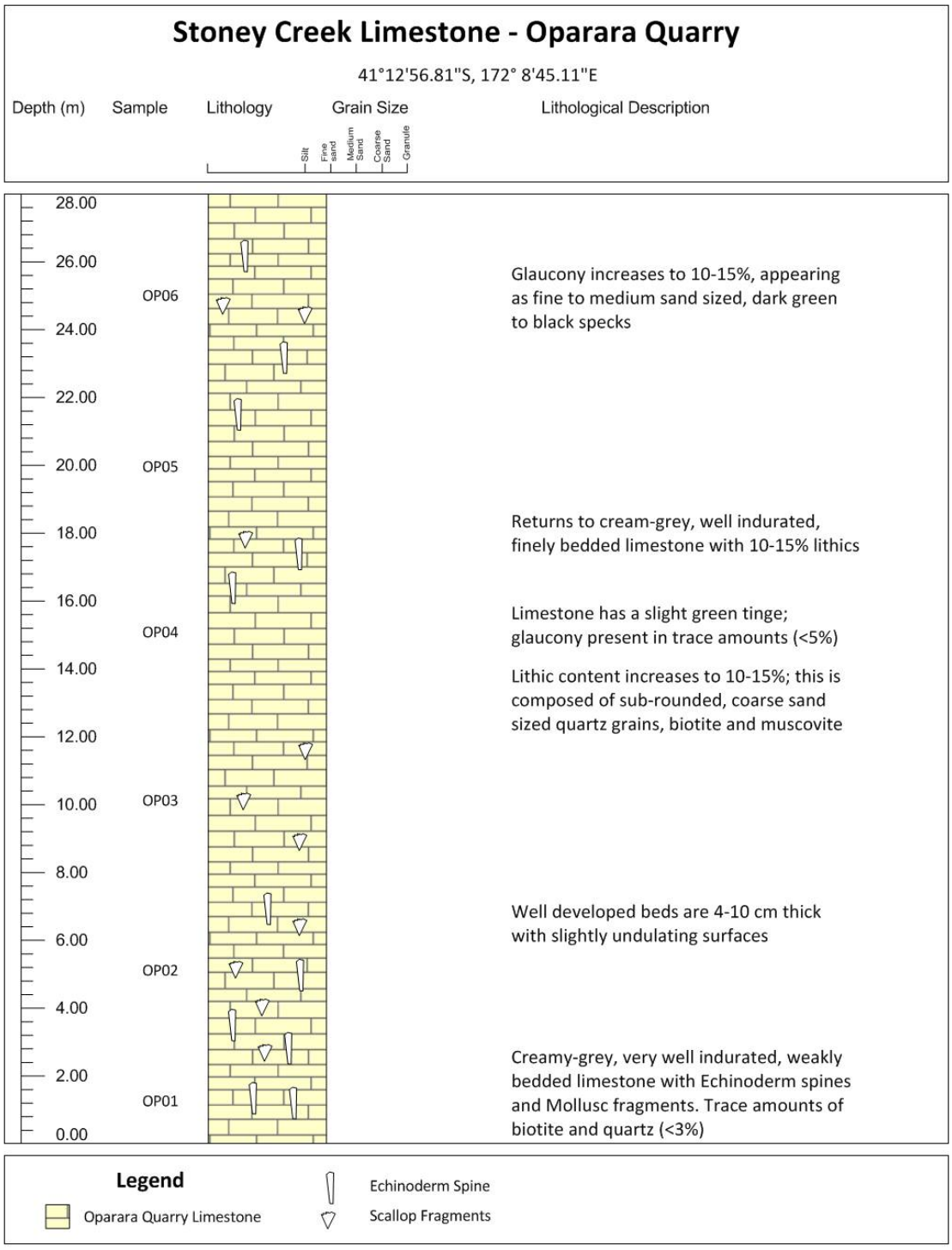

Figure 19 – Oparara Quarry Limestone stratigraphic log

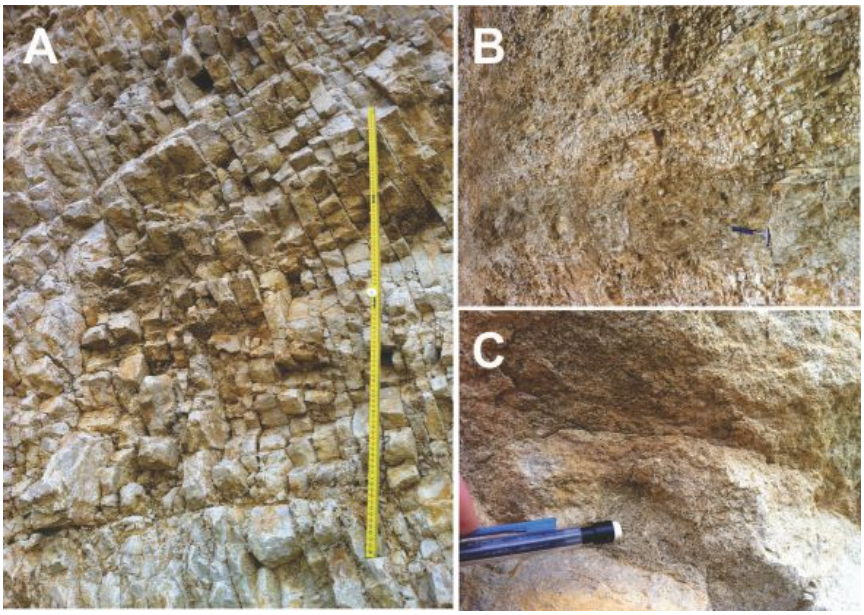

Figure 20 – Field images from the Oparara Quarry. A - finely bedded limestone. B - slightly glauconitic band (faint green/grey tinge) within non-glauconitic limestone. C - example of the most glaucony rich rock from the quarry (20% glaucony)

The bioclastic component of the Stoney Creek Limestone is dominated by bryozoans and echinoderm spines, with mollusc fragments and foraminifera making up minor components of the bulk rock. Lithic content is 2-5% and is composed of sub-angular to sub-rounded quartz and mica grains, however the detrital quartz content increases to ∼20% in one discrete bed, this also happens to be where the glauconitic minerals appear (OP05).

Table 2 – Summary of outcrops and units sampled for further geochemical analysis with glaucony % of bulk sediment by volume and dominant host material interpretations

Outcrop	Samples	Units sampled	% Glaucony	Dominant host grain
Earthquakes	EQ02, EQ06	Kokoamu Greensand	25-40	Pellet + trace vermicular
	EQ08	Otekaike Limestone	10	Pellet + trace vermicular
Ross Farm	RF01, RF03	Kokoamu Greensand	20-80	Pellet + trace vermicular and bioclast
Gee's Beach	GB04, GB07	Gee Greensand	40-50	Bioclast + pellets + trace vermicular
Campbell's Beach	CB03	Gee Greensand	50-60	Bioclast + pellets + trace vermicular
Waipara	WP04, WP07, WP10	Waipara Greensand	40-65	Pellets + amorphous grains
Oparara Quarry	OP06	Stoney Creek Limestone	10	Bioclasts + amorphous grains

5.2.7 Petrographic Microscopy

Viewed in thin section under plane polarised light glaucony is pale green to dark greenish black and is weakly pleochroic. In cross polarised light the grains are cryptocrystalline and show aggregate polarisation. Crystal aggregates are randomly orientated. Detailed optical work on glaucony is limited due to the size of the crystallites being less than the thickness of the thin section (0.02 mm), however it is a straightforward mineral to identify based on its' colour.

5.2.8 SEM analysis

The nanostructures of glaucony are revealed with the Scanning Electron Microscope. Figure 22D shows the ill defined, globular nature of immature glaucony. The thin, randomly orientated plates are typically 0.5-3 μm long and $<$0.1 μm wide. As maturation proceeds the crystallites coalesce into larger plates with smooth surfaces that have a more structured appearance. Figure 22E shows smooth plates up to 7 μm long and 2-3 μm thick which are overgrown with poorly structured thin globular blades of less mature glaucony. Highly evolved glaucony with well developed lamallae structures are shown in Figure 22F.

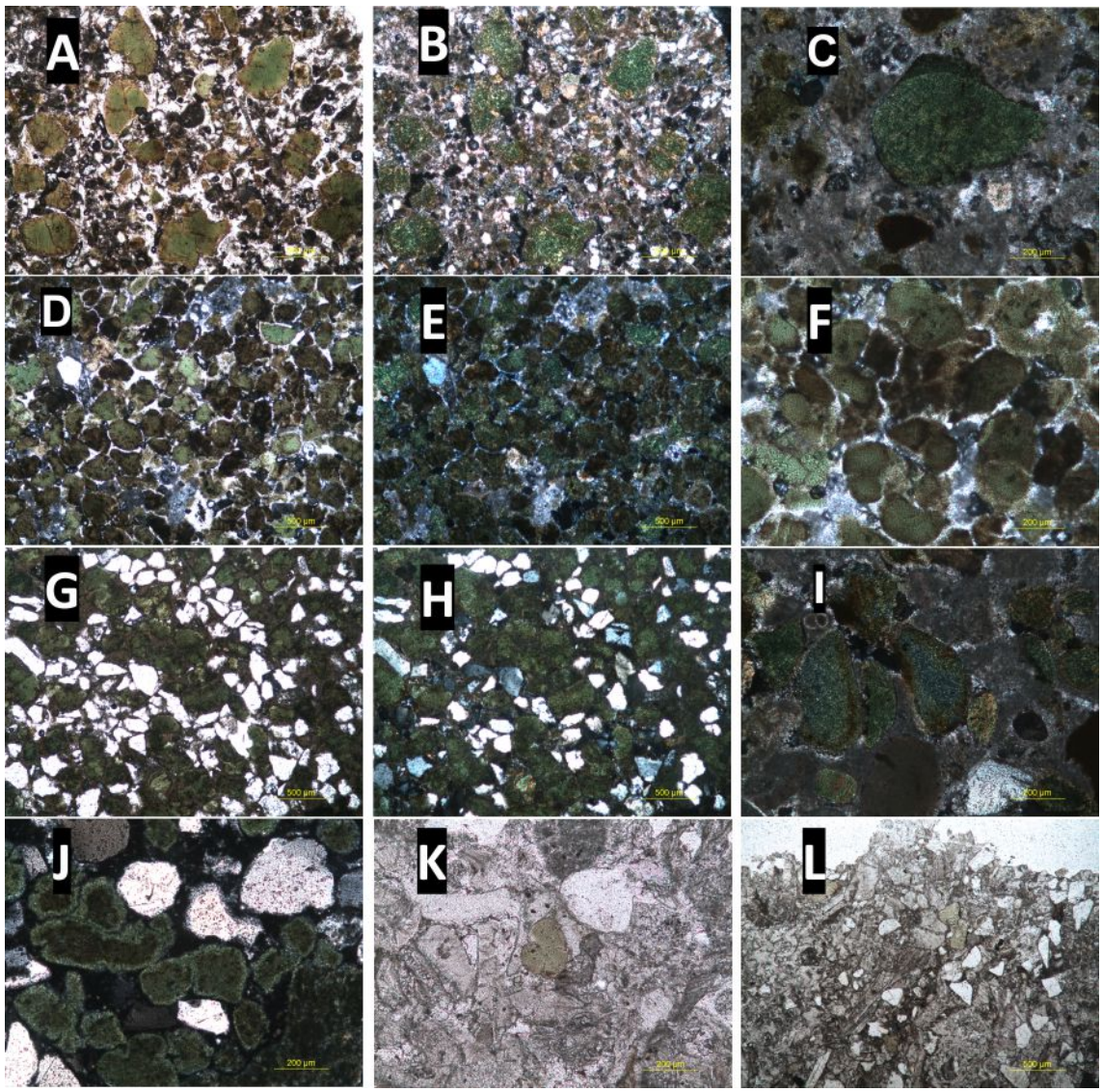

Figure 21 – Photomicrographs of glauconitic rocks in transmitted light under the petrographic microscope. **A** - Pale green faecal pellet replacement viewed in plane polarised light (ppl) - EQ05 (Kokoamu greensand sampled at Earthquakes). **B** - Same image in cross polarised light (cpl). **C** - Mature glaucony pellet showing aggregate polarisation in cpl - CB02 (Gee Greensand sampled at Campbell's Beach). **D** - Sub-rounded, medium-dark green glaucony pellets from Ross Farm (ppl) - RF02 (Kokoamu Greensand sampled). **E** - Same image in cpl. **F** - Pelletal glaucony from Ross Farm (RF02 - Kokoamu Greensand). **G** and **H** - Pelletal and amorphous glaucony and sub-rounded quartz grains from Waipara Greensand (ppl and cpl respectively) - WP08. **I** - Blue-green glaucony with brown phosphorite surface coatings - Gee's Beach - GB02. **J** - Amorphous glaucony with pale green rims around dark green center - Waipara Greensand - WP08. **K** and **L** - Pale green glaucony in Stoney Creek Limestone - Oparara Quarry, Karamea - OP05

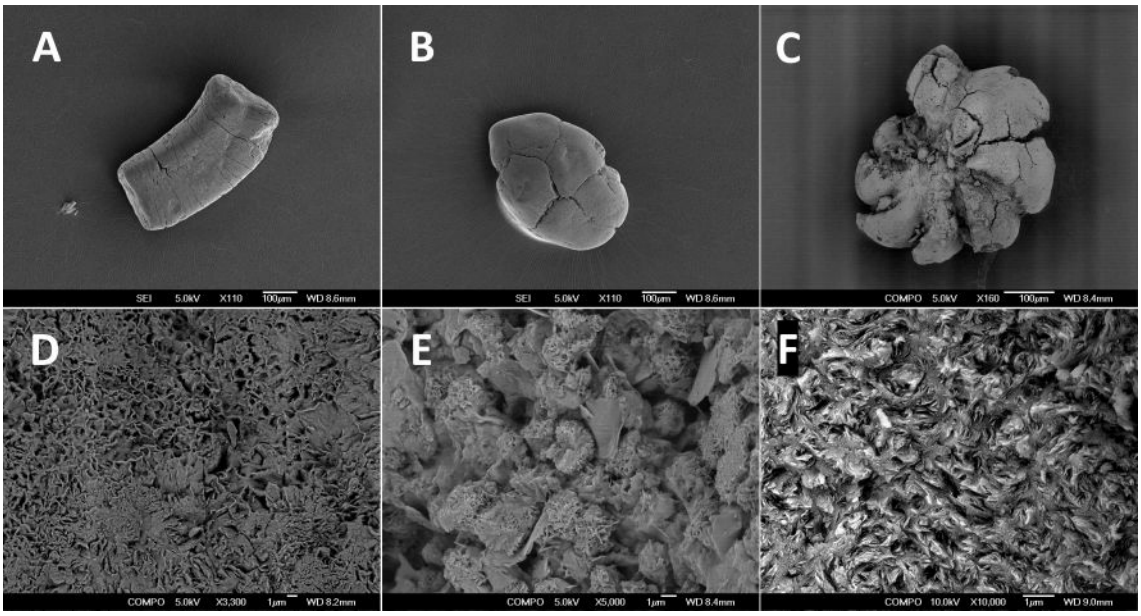

Figure 22 – SEM images of glaucony grain surfaces and nanostructures of glaucony crystallites. **A** - Vermicular grain with near parallel surface cracks - Ross Farm. **B** - rounded pellet with surface cracks - Campbell's Beach. **C** - Benthic foraminifera - Gee's Beach. **D** - Ill defined globules and caterpillar like structures showing aggregate nature of glaucony growth - Waipara Greensand. **E** - Well developed plates and rosette structures of mature glaucony with co-precipitation of less mature crystals - dark green pellet from Campbell's Beach. **F** - Lamellar structures in highly evolved glaucony

5.3 Chemical Analysis

5.3.1 Major Elements

Stoichiometric mineral formulas are presented in Tables 11 and 12 (Appendix B). The average formula for all 88 grains of glaucony analysed is $K_{0.74}$ $(Fe_{1.27}Al_{0.30}Mg_{0.39})_{1.96}$ $(Si_{3.77}Al_{0.23})_4$ $(O_{10})(OH)_2$. Calcium, Na, P and Ti are present in low concentrations with 0.55, 0.09, 0.08 and 0.10 weight % respectively; these are not considered structural components and are not included in the stoichiometric formulas. Iron is the main octahedral cation and Si dominates the tetrahedral layer. Potassium is present in all grains as the interlayer cation.

5.3.2 Elemental concentrations

Table 3 shows concentration averages, minima, maxima and standard deviations for SiO_2, MgO and Fe_2O_3 for all grains analysed using SEM+EDS. Overall, K content ranges from 6.75 to 9.84 weight %, with an average of 8.58 weight % and standard deviation of 0.81 (N=88). The average K concentration is highest in grains from Campbell's Beach (9.40 weight %), and decreases in the following order: Ross Farm, Earthquakes, Waipara, Gee's Beach and Oparara; these measure 8.95, 8.72, 8.66, 7.95 and 7.66 weight % respectively. Standard deviations for K range from 0.87 at Gee's Beach (N=12) to 0.32 at Campbell's Beach (N=11).

The minimum concentration of Fe measured was 18.45 weight % at Ross Farm. Gee's Beach contains the highest value of Fe with 34.15 weight %. The average Fe concentration for all measured grains is 24.97 weight %. Gee's Beach contains the highest average Fe concentration with 29.57 weight %; followed by the Waipara Greensand (25.38 weight %), Campbell's Beach (24.41 weight %), Ross Farm (23.99 weight %), Earthquakes (23.77 weight %) and the minimum average Fe concentration was at Oparara (22.15 weight %). Standard deviations range from 3.36 (N=12) at Gee's Beach to 0.98 (N=11) at Campbell's Beach and the standard deviaiton of all grains is 3.06 (N=88).

Aluminium concentration ranges from 3.45 to 15.55 weight %. The average Al concentration from all grains is 6.71 weight %. Oparara contains the highest average Al concentration with 12.34 weight %; followed by Earthquakes (6.73 weight %), Ross Farm (6.29 weight %), Campbell's Beach (5.84 weight %), Gee's Beach (5.72 weight %) and Waipara

Table 3 – Average, standard deviation, maximum and minimum concentrations for all grains measured by EDS. N represents the number of grains analysed

	MgO	**Al_2O_3**	**SiO_2**	**K_2O**	**Fe_2O_3**
	weight %				
Oparara Quarry					
Average	3.74	12.34	54.11	7.66	22.15
Standard Deviation (N=9)	0.29	1.78	1.30	0.57	2.22
Minimum	3.03	10.07	52.29	6.77	19.47
Maximum	4.09	15.55	55.94	8.51	25.55
Earthquakes					
Average	4.06	6.73	56.72	8.72	23.77
Standard Deviation (N=19)	0.41	1.26	0.97	0.66	1.21
Minimum	3.27	4.19	54.66	7.48	21.64
Maximum	4.90	8.97	58.50	9.65	26.08
Ross Farm					
Average	4.20	6.29	56.57	8.95	23.99
Standard Deviation (N=14)	0.46	1.48	1.45	0.82	2.35
Minimum	3.51	4.41	55.14	6.97	18.45
Maximum	5.38	9.59	59.83	9.84	27.17
Campbell's Beach					
Average	4.35	5.84	56.00	9.40	24.41
Standard Deviation (N=11)	0.17	0.73	0.33	0.32	0.98
Minimum	4.10	4.88	55.47	8.91	22.62
Maximum	4.54	7.04	56.35	9.81	25.48
Gee's Beach					
Average	3.53	5.72	53.23	7.95	29.57
Standard Deviation (N=12)	0.52	0.96	2.14	0.87	3.36
Minimum	3.00	4.37	49.35	6.75	23.85
Maximum	4.41	7.18	57.02	9.73	34.15
Waipara Greensand					
Average	3.71	5.70	56.55	8.66	25.38
Standard Deviation (N=27)	0.34	1.99	1.70	0.59	2.58
Minimum	2.72	3.45	51.35	7.34	19.16
Maximum	4.33	13.76	59.58	9.64	31.73

with the minimum average value of 5.70 weight %. Standard deviations for Al range between 0.73 at Campbell's Beach (N=11) and 1.99 at Waipara (N=27). The standard deviation for Al from all grains is 2.47 weight %.

The minimum Mg concentration was found at Waipara (2.72 weight %) and the maximum was from Ross Farm (5.38 weight %). Average Mg content from all grains is 3.89 weight %. Gee's Beach contains the highest average value of Mg with 4.35 weight %; followed by 4.20 weight % at Ross farm, 4.06 weight % at Earthquakes, 3.74 weight % at Oparara, 3.71 weight % at Waipara and 3.53 weight % at Gee's Beach. Standard deviations range between 0.17 at Campbell's Beach (N=11) and 0.52 at Gee's Beach (N=12). The standard deviation for Mg from all grains measured is 0.46 weight %.

Silica is the most abundant element in glaucony. Overall, the average value from all grains is 55.84 weight % and the standard deviation is 1.94 (N=88). The minimum value for silica was 49.35 weight % from Gee's Beach and Earthquakes contains the highest value with 59.83 weight %. The highest average Si concentration is from Earthquakes with 56.72 weight %, followed by Ross Farm (56.57 weight %), the Waipara Greensand (56.55 weight %), Campbell's Beach (56.00 weight %), Oparara (54.11 weight %) and Gee's Beach (53.23 weight %). Standard deviations range from 0.33 at Campbell's Beach (N=11) to 2.14 at Gee's Beach (N=12).

5.3.3 Major element correlations

Figure 23 shows SiO_2, MgO and Fe_2O_3 concentrations as a function of K_2O. Table 17 (Appendix A) lists R^2 values between these elements. When relationships between elements are analysed for all measured grains the correlations are weak. When elemental relationships are analysed as separate sample localities the patterns become clearer and the R^2 values increase.

Iron correlates poorly with K when all grains are taken into account (R^2=0.0, N=88). Glaucony from the Oparara Quarry and Ross farm show strong positive correlations between Fe and K (R^2=0.91, N=9 and 0.70, N=14 respectively). Weak positive correlations are present in the Waipara Greensand, Earthquakes and Campbell's Beach (R^2= 0.24, 0.47, and 0.13 respectively). Gee's Beach is the only location which shows a negative correlation between and Fe and K (R^2=-0.65, N=12).

The total R^2 value for Al concentration versus K concentration is -0.25. Aluminium shows an inverse relationship with K in all separate outcrops. The Oparara Quarry and Ross

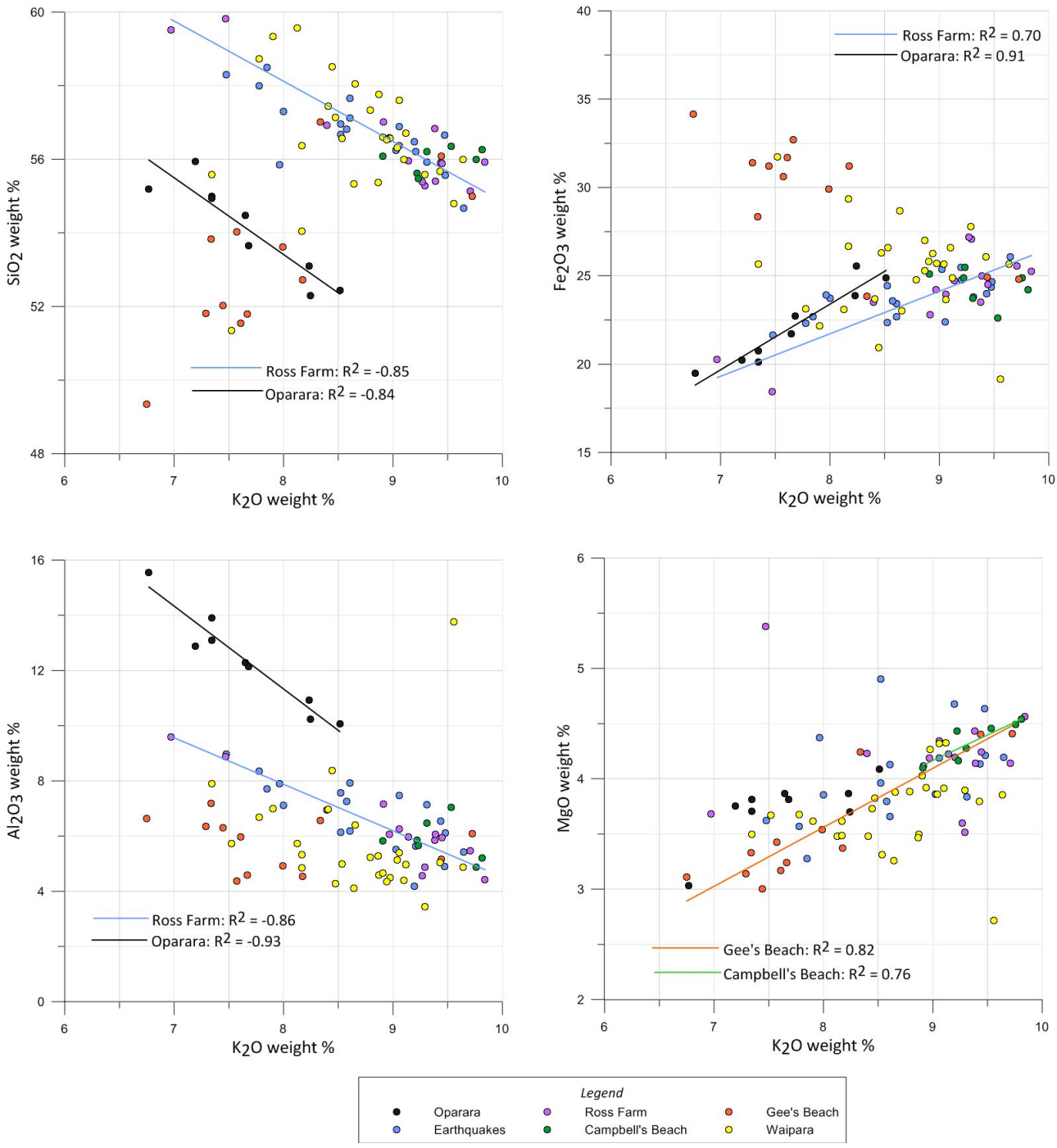

Figure 23 – Major elements x-y plots showing EDS results for SiO_2, MgO and Fe_2O_3 plotted against K_2O. Lines of best fit are plotted for R^2 values > 0.70. R^2 values for all outcrops are presented in Table 17 (Appendix A)

farm have the strongest R^2 values with -0.93 and -0.86 respectively. Weak to moderate correlations between Al and K are present at Earthquakes and Waipara (R^2= -0.57 and -0.37 respectively). Gee's Beach and Campbell's Beach both have weak negative correlations between Al and K (R^2= -0.11 and 0.05).

Magnesium positively correlates with K in all outcrops, with a total R^2 value of 0.47 for all measured grains. Gee's Beach and Campbell's Beach have the strongest R^2 values (0.82 and 0.76 respectively). Moderate R^2 values are present in glaucony from Ross Farm, Earthquakes and the Oparara Quarry with 0.64, 0.61 and 0.53 respectively. The weakest correlation between Mg and K is found in grains from the Waipara samples (R^2=0.25).

Silica correlates poorly with K when all grains are taken into account (R^2= 0.04). Moderate to strong negative correlations are found in the Waipara greensand, at the Oparara Quarry and Ross Farm (R^2= -0.53, -0.84 and -0.85 respectively). Silica correlates positively with K in samples from Gee's Beach and Campbell's Beach (R^2= 0.55 and 0.14).

5.3.4 Relationship between elements and host material

Figure 24 shows K_2O, MgO, Fe_2O_3 and Al_2O_3 concentrations in bioclastic, faecal pellet and vermicular (biotite) host minerals. Only grains which could be assigned a parent material based on binocular microscopy were included and average values for these grains are included (black diamonds).

Pellet hosted grains are enriched in Fe_2O_3 and K_2O. When pellets are the host material K averages 8.82 weight %, Fe averages 24.79 weight % and MgO averages 3.87 weight %. Aluminium is depleted in pellets with an average value of 6.14 weight %.

Bioclast hosted grains are enriched in Al_2O_3 with an average value of 9.43 weight % from 26 grains. Magnesium is present in concentrations comparable to pellets with 3.81 weight % and Fe is slightly depleted compared to pellets with 23.35 weight %. Bioclasts are depleted in K_2O with an average concentration of 7.90 weight %.

Vermicular grains are enriched in MgO with 4.27 weight % from 8 grains. Iron and K_2O are present in concentrations comparable to other host materials, with average concentrations of 23.32 and 8.80 weight % respectively. Aluminium is depleted in vermicular grains compared to bioclasts with 6.55 weight %.

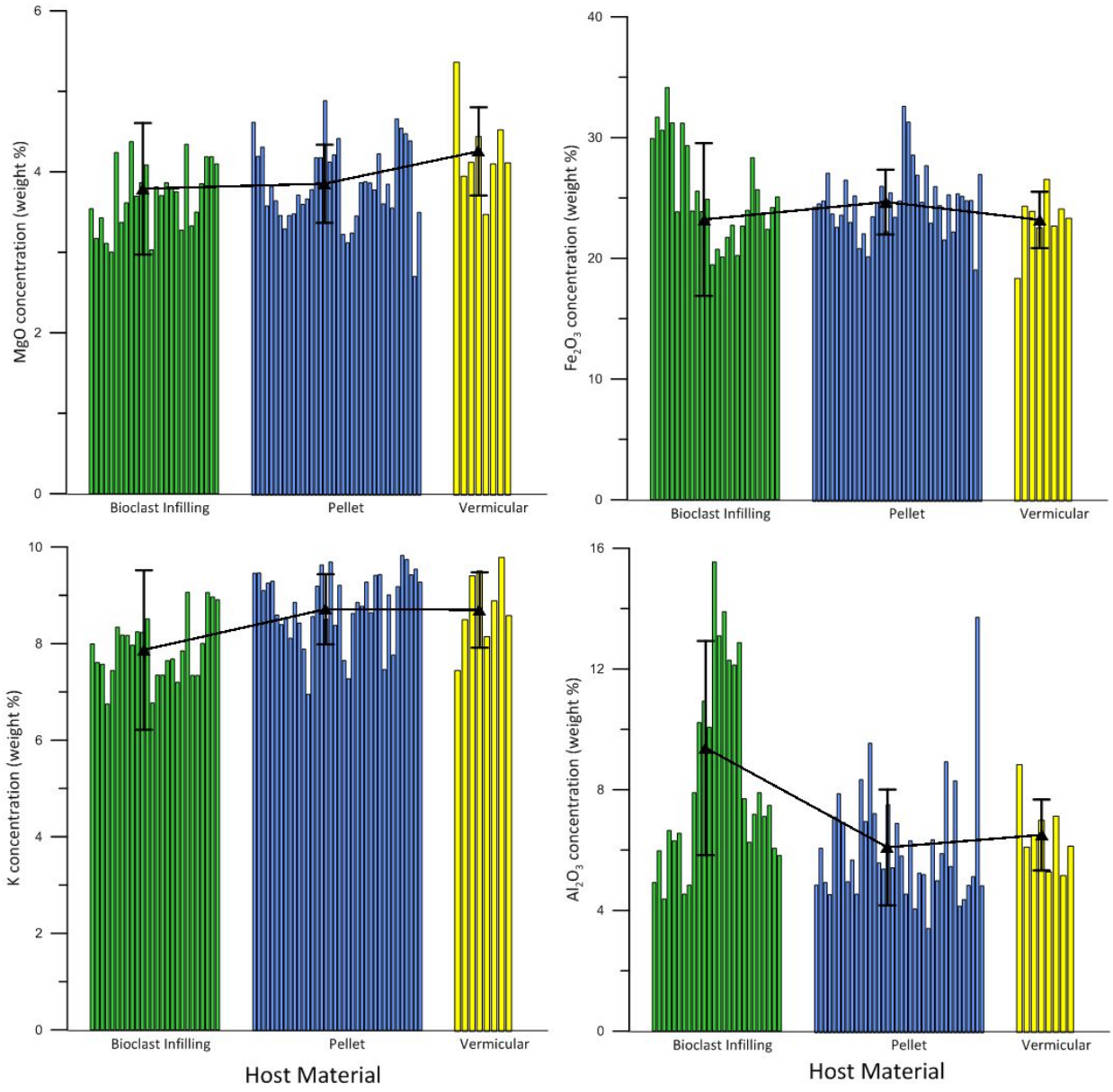

Figure 24 – Concentration of K, Fe, Al and Mg according to host material interpretation. Black triangles represent average values

Table 4 – Trace element averages and standard deviations for all grains measured by LA-ICP-MS. N = the number of grains analysed

Outcrop		Sc	Ti	V	Cr	Mn	Co	Ni	Cu	Zn	Ga	Rb	Sr	Y	Zr	Nb	Cs	Ba	Pb	Th	U	Total
		Concentration (ppm)																				
Oparara	Average	8.0	501.9	418.0	263.1	58.1	21.6	78.7	53.4	196.7	29.2	579.5	48.4	3.6	41.1	1.0	39.5	43.2	12.1	0.6	0.6	2398
	Standard Deviation (N=10)	2.4	103.1	60.6	35.8	27.0	2.8	10.6	18.3	19.1	4.2	46.7	25.5	6.9	3.9	0.2	10.0	10.1	5.4	0.5	0.4	
Earthquakes	Average	8.4	397.3	121.3	201.4	29.1	2.5	29.3	19.7	129.6	20.6	249.7	10.9	3.2	13.8	1.0	3.8	6.6	3.4	0.2	0.6	1252
	Standard Deviation (N=11)	2.0	176.8	63.2	56.4	19.1	1.1	5.7	14.1	48.4	3.6	20.1	2.5	2.4	5.4	0.2	1.7	5.6	1.5	0.1	0.2	
Ross Farm	Average	9.2	448.1	101.6	281.5	16.2	3.0	29.4	27.1	145.3	19.7	280.1	10.0	4.3	18.8	2.0	3.5	7.0	5.0	0.3	0.6	1412
	Standard Deviation (N=7)	5.3	237.5	27.6	68.8	14.8	1.2	3.5	11.4	30.8	3.8	32.6	7.0	4.6	3.5	0.4	1.6	7.0	2.9	0.3	0.1	
Campbell's Beach	Average	6.6	272.2	73.6	304.8	6.7	3.2	31.6	17.5	129.6	17.0	273.1	8.2	6.6	21.2	1.6	2.2	3.6	2.7	0.3	0.6	1183
	Standard Deviation (N=3)	0.2	95.7	3.4	69.3	0.7	0.3	1.9	5.5	20.4	0.3	7.2	1.1	3.0	1.4	0.1	1.0	0.4	1.8	0.3	0.1	
Gee's Beach	Average	6.2	570.0	153.0	174.2	44.6	10.5	61.2	30.6	200.2	12.3	253.3	11.2	5.4	24.2	2.2	6.2	15.3	11.5	0.4	0.4	1593
	Standard Deviation (N=8)	1.6	469.5	124.4	110.9	30.8	4.8	30.6	12.3	60.2	3.3	13.2	3.6	5.2	7.3	1.5	3.4	14.3	10.7	0.4	0.2	
Waipara	Average	18.3	914.8	251.4	334.2	55.7	4.1	18.6	21.4	188.5	25.0	335.4	7.0	1.2	26.4	4.6	5.8	24.1	5.0	1.2	0.8	2244
	Standard Deviation (N=20)	8.4	462.8	72.9	101.6	36.4	1.9	20.7	11.2	26.2	7.8	47.5	2.0	0.9	9.3	2.4	2.2	26.6	2.3	1.2	0.6	
Total for all grains	Average	11.5	615.5	211.7	268.0	42.2	7.2	37.8	27.8	172.0	22.0	335.8	15.2	3.2	24.8	2.6	10.2	19.4	6.6	0.7	0.7	1834
	Standard Deviation (N=59)	7.4	405.3	129.6	100.4	32.2	7.1	27.9	17.2	45.6	7.4	116.7	17.6	4.1	10.8	2.2	13.4	21.2	5.8	0.8	0.4	
GLO geostandard		8.0	-	65.0	140.0	-	14.0	36.0	3.5	38.0	13.0	238.0	19.2	13.2	36.0	3.7	3.3	6.0	-	0.2	0.3	640

5.3.5 Trace Elements

Table 4 shows trace element concentrations and the standard deviations for grains analysed using LA-ICP-MS. The sum of all trace elements for separate outcrops ranges from 1,183 ppm (Campbell's Beach) to 2,398 ppm (Oparara quarry). Samples from the Oamaru Basin contain total trace element sums of 1183, 1252, 1412 and 1593 ppm for Campbell's Beach, Earthquakes, Ross Farm and Gee's Beach, respectively. Glaucony from the Oparara Quarry and Waipara Greensand are enriched with trace elements compared to Oamaru, with 2,398 and 2,244 ppm total trace element sums respectively.

Titanium, V, Cr, Zn and Rb are present in significantly higher concentrations than all other trace elements in all samples, with average values across all outcrops of 616, 212, 268, 172 and 335 ppm respectively. Nickel is the next highest concentrated element with an average of 41 ppm across all outcrops. Titanium shows significant variation, with 272 ppm at Campbell's Beach and 915 ppm at Waipara. Average V concentration ranges from 74 ppm (Campbell's Beach) to 418 ppm (Oparara). Chromium is present in relatively consistent concentrations in all outcrops, ranging from 174 ppm at Gee's Beach to 334 at Waipara. Zinc concentration shows only minor variation, with Earthquakes and Campbell's Beach both measuring 130 ppm and Gee's Beach containing the maximum at 200 ppm. Rubidium is enriched at Oparara with 580 ppm. In outcrops from Oamaru Rb ranges from 250 to 280 ppm and the Waipara Greensand contains 335 ppm.

Measured values for trace elements normalised to the glaucony geostandard (GLO) (Govindaraju, 1994) and the absolute concentrations (ppm) for all trace elements are displayed in Figure 25. Vanadium, Cr, Cu and Zn are consistently enriched in all samples when normalised to GLO, with average values across all outcrops of 2.9, 1.9, 8.1 and 4.3 respectively. The Oparara quarry contains elevated concentrations relative to other outcrops with V, Cu, Cs, Ba and Pb measuring 6.4, 15.3, 12.0, 7.2 and 4.0 times higher than GLO respectively. Scandium, Ni, Co, Ga, Rb, Cs, Ba, Pb and U are generally close to 1.0 for all samples and Sr, Y, Zr and Nb are consistently depleted relative to GLO.

The relationships between K with V, Ti, Cr and Rb are shown in Figure 26 and Table 18 (Appendix A). Vanadium correlates positively with K in the Waipara Greensand (R^2= 0.37). All other samples show weak negative correlations with K. Titanium correlates negatively with K in all samples (R^2= -0.42 to -0.73) apart from the Waipara Greensand where no correlation is present (R^2= 0.00). Chromium shows weak correlations with K in all samples (R^2= 0.06 - 0.86) (note: R^2= 0.86 is for Campbell's Beach which only

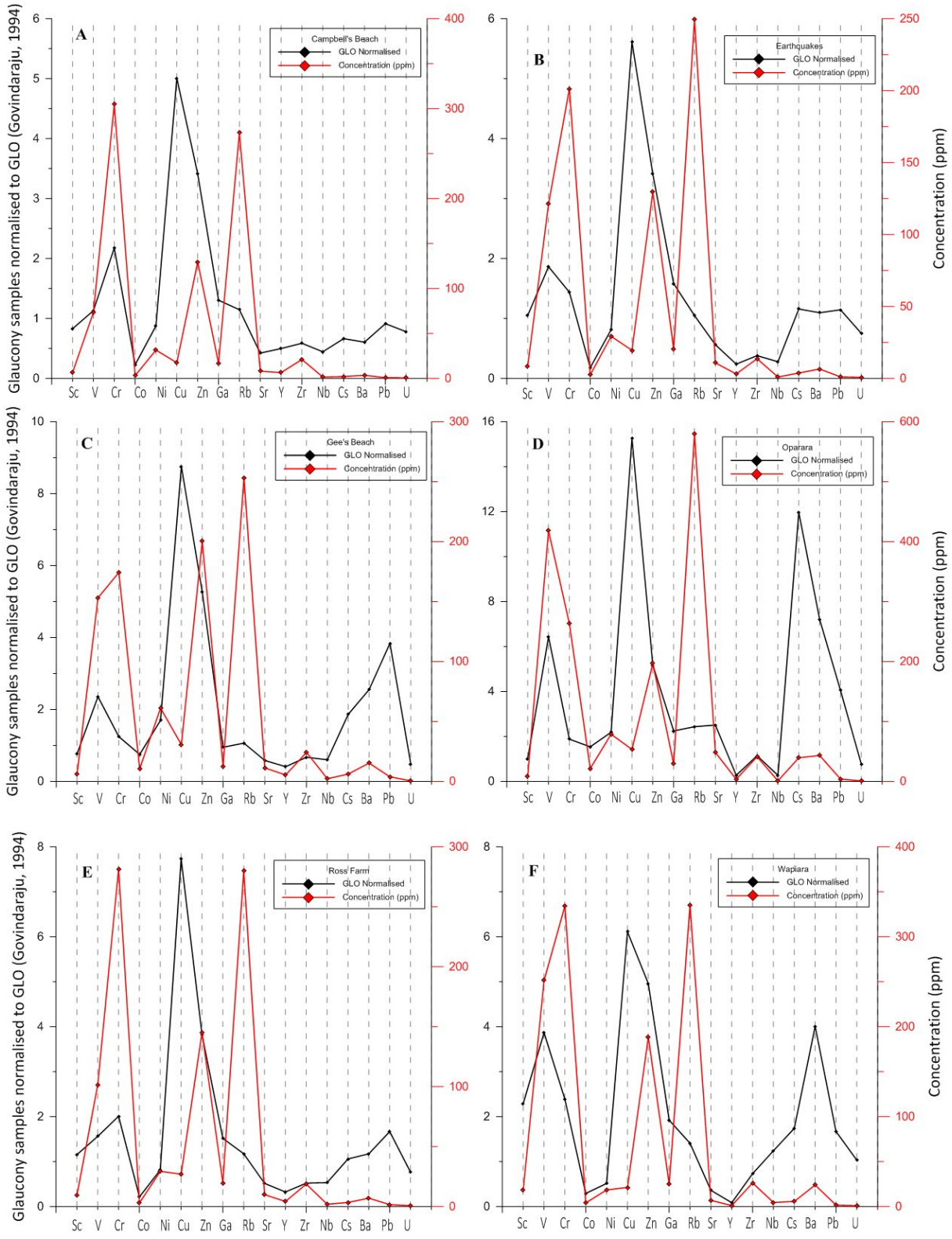

Figure 25 – Glaucony trace element concentrations (ppm) and measured concentrations from this research normalised to the glaucony geostandard (GLO) (Govindaraju, 1994) for all outcrops.

contains 3 measured grains and the overall scatter in the plot suggests no relationship exists between Cr and K). Rubidium correlates positively with K in all locations (R^2= 0.00 - 0.86).

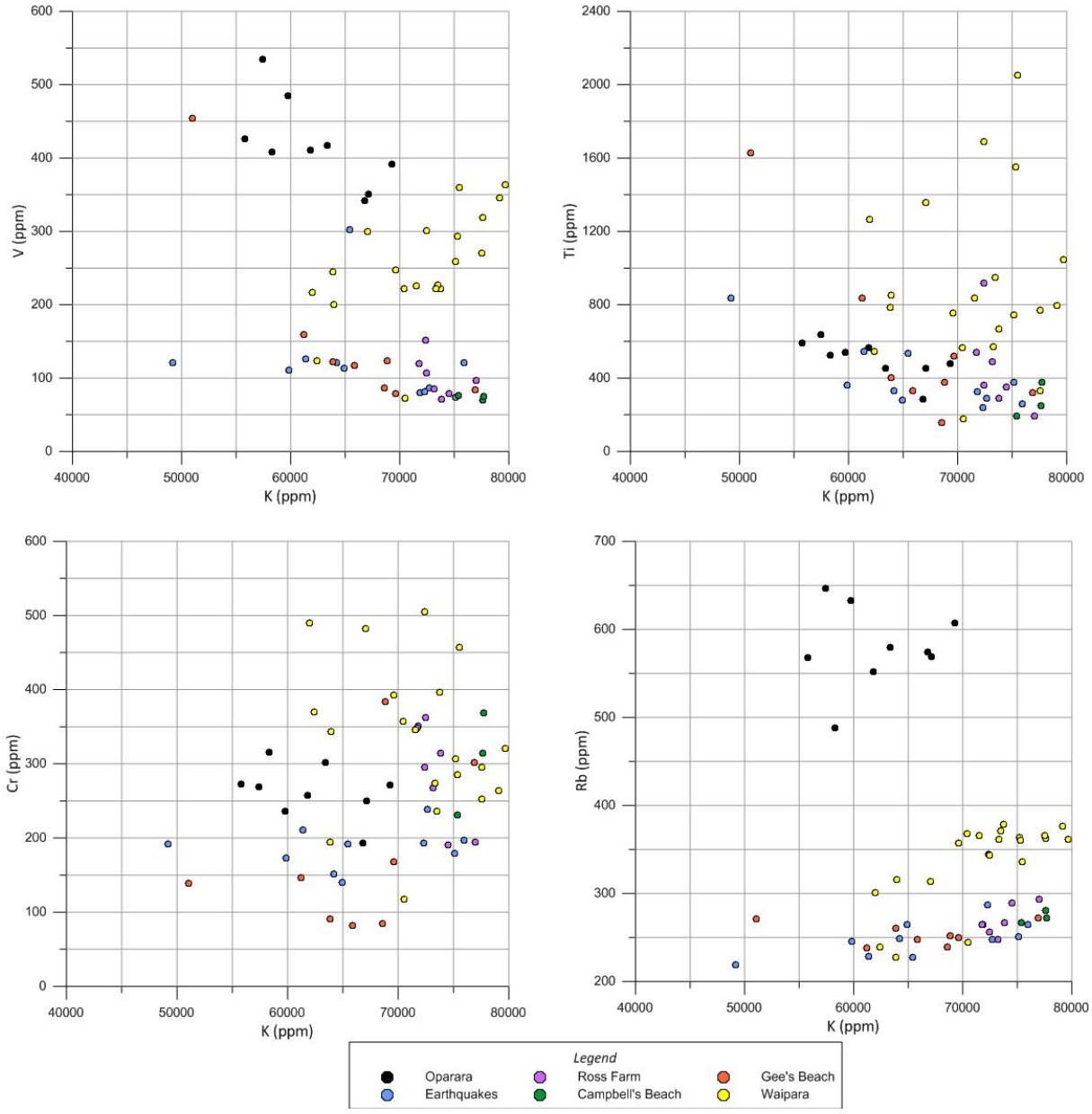

Figure 26 – Trace element x-y plots for V, Ti, Cr and Rb plotted against K for all locations.

Table 5 – Average REE concentrations for glaucony at all sampled outcrops as measured by LA-ICP-MS

Element	La	Ce	Pr	Nd	Sm	Eu	Gd	Tb	Dy	Ho	Er	Tm	Yb	Lu	Hf	Ta	∑REE
	Concentration (ppm)																
Oparara	2.872	5.418	0.965	4.570	1.074	0.233	0.926	0.124	0.647	0.116	0.273	0.031	0.180	0.024	2.758	0.078	20.289
Earthquakes	1.881	2.919	0.442	2.022	0.450	0.105	0.440	0.064	0.386	0.077	0.203	0.028	0.158	0.021	0.514	0.052	9.761
Ross Farm	2.947	3.395	0.629	2.918	0.598	0.136	0.599	0.080	0.472	0.122	0.258	0.033	0.247	0.032	0.791	0.094	13.351
Campbell's Beach	3.679	4.108	0.843	4.002	0.880	0.201	0.933	0.130	0.828	0.164	0.410	0.043	0.241	0.036	0.847	0.063	17.411
Gee's Beach	2.753	4.128	0.685	3.217	0.714	0.167	0.782	0.108	0.656	0.138	0.344	0.041	0.252	0.034	0.902	0.084	15.006
Waipara	4.263	15.543	1.116	4.214	0.765	0.135	0.456	0.057	0.280	0.048	0.114	0.017	0.115	0.016	0.866	0.085	28.092
Total	3.066	5.919	0.780	3.491	0.747	0.163	0.689	0.094	0.545	0.111	0.267	0.032	0.199	0.027	1.113	0.076	17.318

5.3.6 Rare Earth Elements

Average elemental concentration for the REE as determined by LA-ICP-MS are shown in Table 5. The Waipara Greensand is enriched in total REE with 29.1 ppm total, however this appears to be due to an anomalously high Ce value (15.5 ppm) relative to all other elements. Samples from the Oamaru region increase slightly towards the east of the basin. The Kokoamu Greensand sampled at Earthquakes and Ross Farm contain 9.8 and 13.4 ppm respectively, whereas the Gee Greensand sampled at Campbell's Beach and Gee's Beach total 17.4 and 15.0 ppm respectively. The glauconitic limestone sampled at the Oparara quarry contains 20.3 ppm total rare earth elements and is distinctly enriched in Hf (2.8 ppm) compared to Hf in all other deposits.

Glaucony REE concentrations from Table 5 are normalised to the geostandard for glaucony (GLO) (Govindaraju, 1994) and shown in Figure 27. All samples are consistently depleted by almost an order of magnitude with respect to the GLO standard. Depletion is greater in the light REE compared with the heavy REE, apart from the Waipara greensand which shows the opposite trend. Ytterbium is 0 in all samples and Hf is consistently the highest when normalised to GLO. Hafnium is the only element which shows an enrichment compared with GLO, although this is restricted to the Oparara samples only. Cerium is depleted relative to neighbouring elements in all samples excluding the Waipara Greensand in which it is enriched.

Figure 28 shows average REE for all outcrops normalised to the North American Average Shale Composition (NASC) (Gromet et al., 1984). All samples are depleted relative to the NASC. The average ratio for my results/NASC is 0.142. Earthquakes shows the strongest depletion, averaging 0.091, and Oparara is the least depleted with an average of 0.180. Table 28 (Appendix A) shows the maximum, minimum, average and range of rare earth elements for all outcrops sampled compared to the NASC.

Anomalies exist in Ce and Eu for all samples. Eu is depleted relative to neighbouring elements in every sample. Ce is depleted in all samples apart from the Waipara Greensand

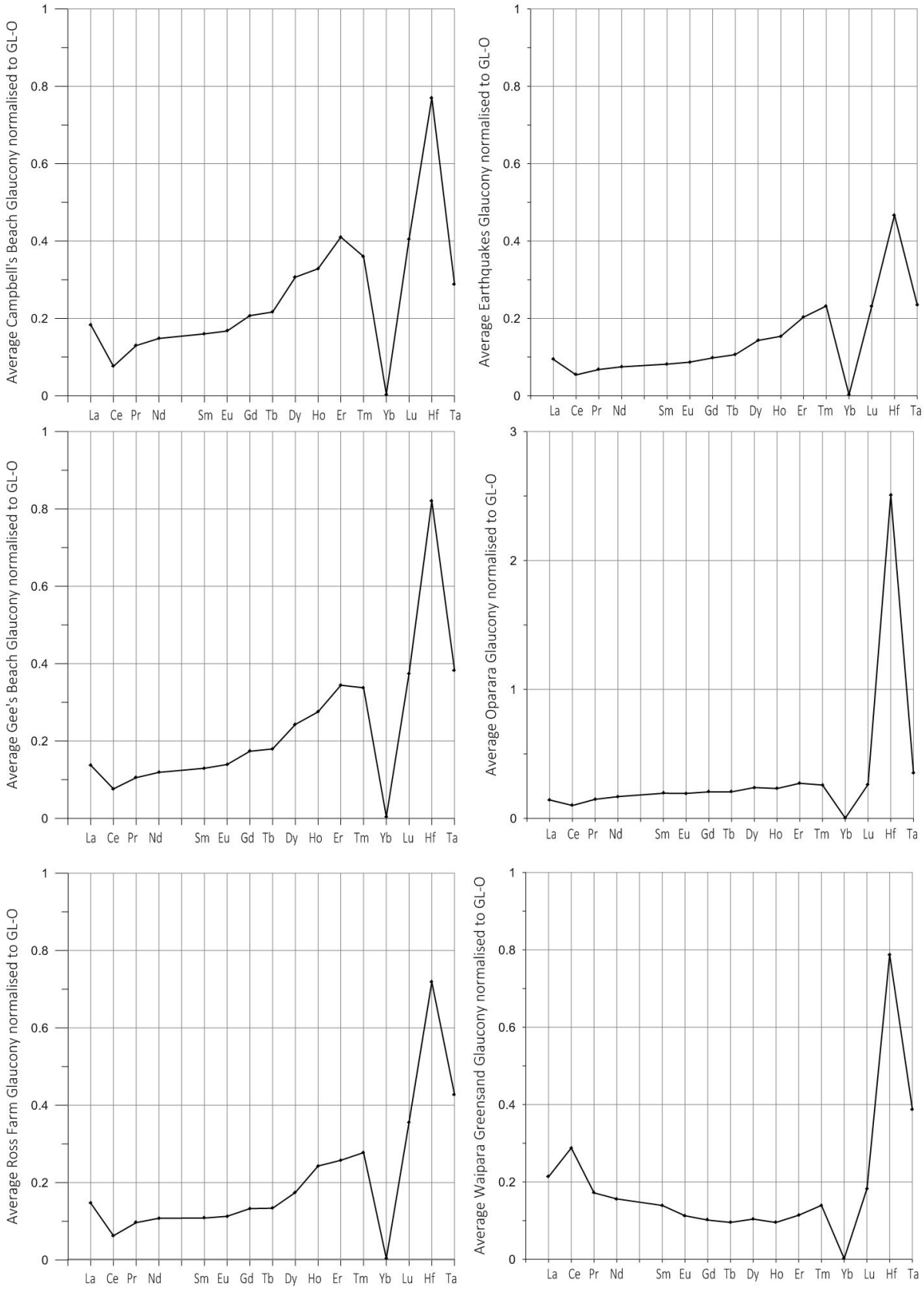

Figure 27 – REE for all sampled outcrops normalised to glaucony standard (GLO) (Govindaraju, 1994).

where it displays an enrichment relative to it's neighbouring elements. Figure 28 suggests that only the Waipara Greensand contains fractionation between the light and heavy rare earth elements. All other samples have a fairly flat profile, with the exception of Oparara which is slightly depleted in the heavy elements.

Ce and Eu can have multiple valence states. This differentiates Ce and Eu from other REE and provides insight into environmental conditions at the time of precipitation, as will be discussed further in section 5.2.3. Anomolies were calculated using the formula:

$Log(3Ce_n(2La_n + Nd_n))$ (Elderfield and Greaves, 1982)

where n is the measured value normalised against the NASC. The oxic - anoxic boundary at 0.1 is after (Wright et al., 1987).

Ce anomalies are within the range of -0.4 and 0.3. Figure 29 shows that the Waipara Greensand contains a distinctly more positive Ce anomoly than all other outcrops. The average anomoly value for Campbell's Beach is -0.31, Ross Farm is -0.26, Gee's Beach is -0.15, Earthquakes Marl is -0.15 and with 0.16 the Waipara Greensand is the only location to give a positive average Ce anomoly.

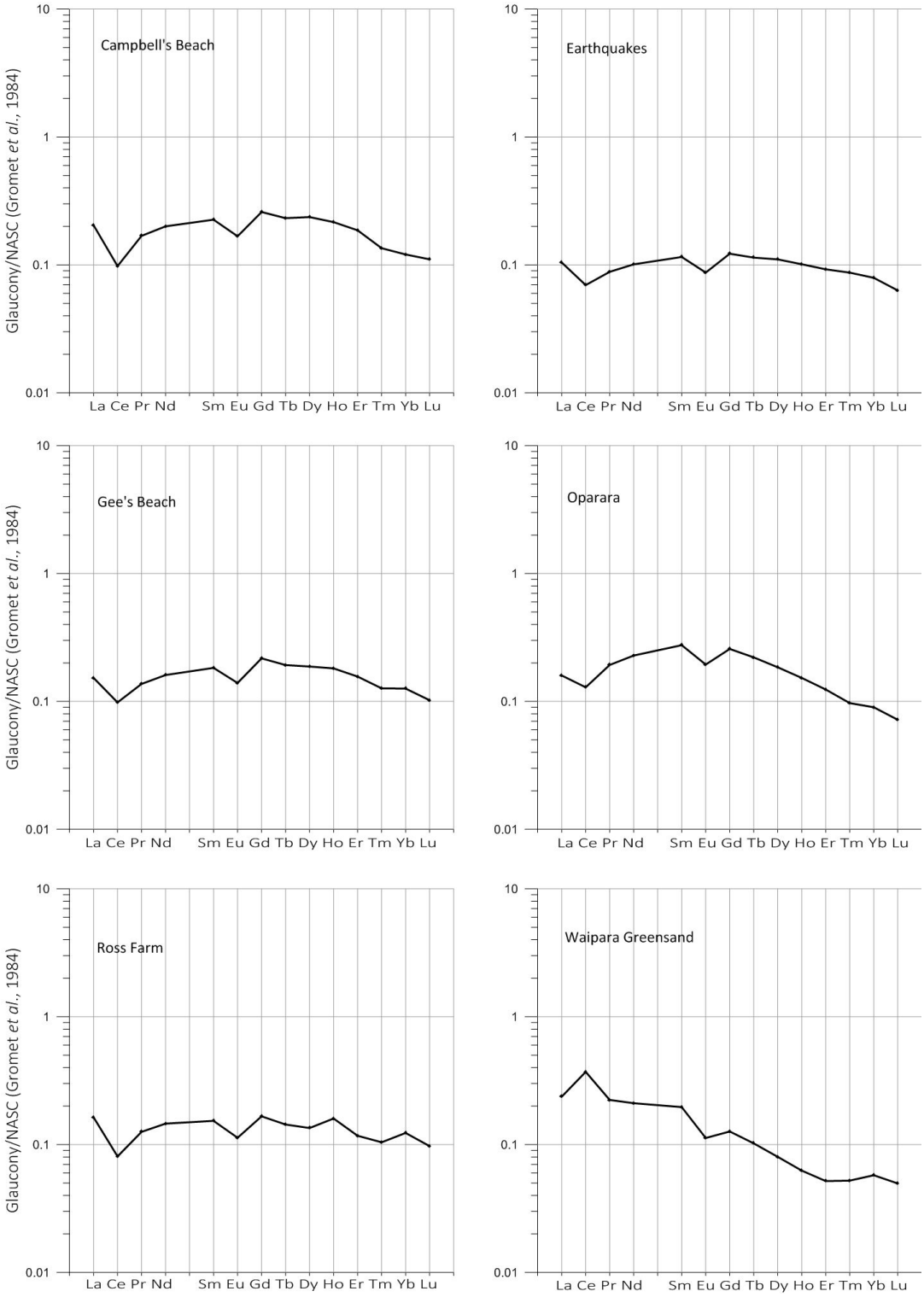

Figure 28 – Rare Earth Elements for all sampled outcrops normalised to the NASC (Gromet et al., 1984)

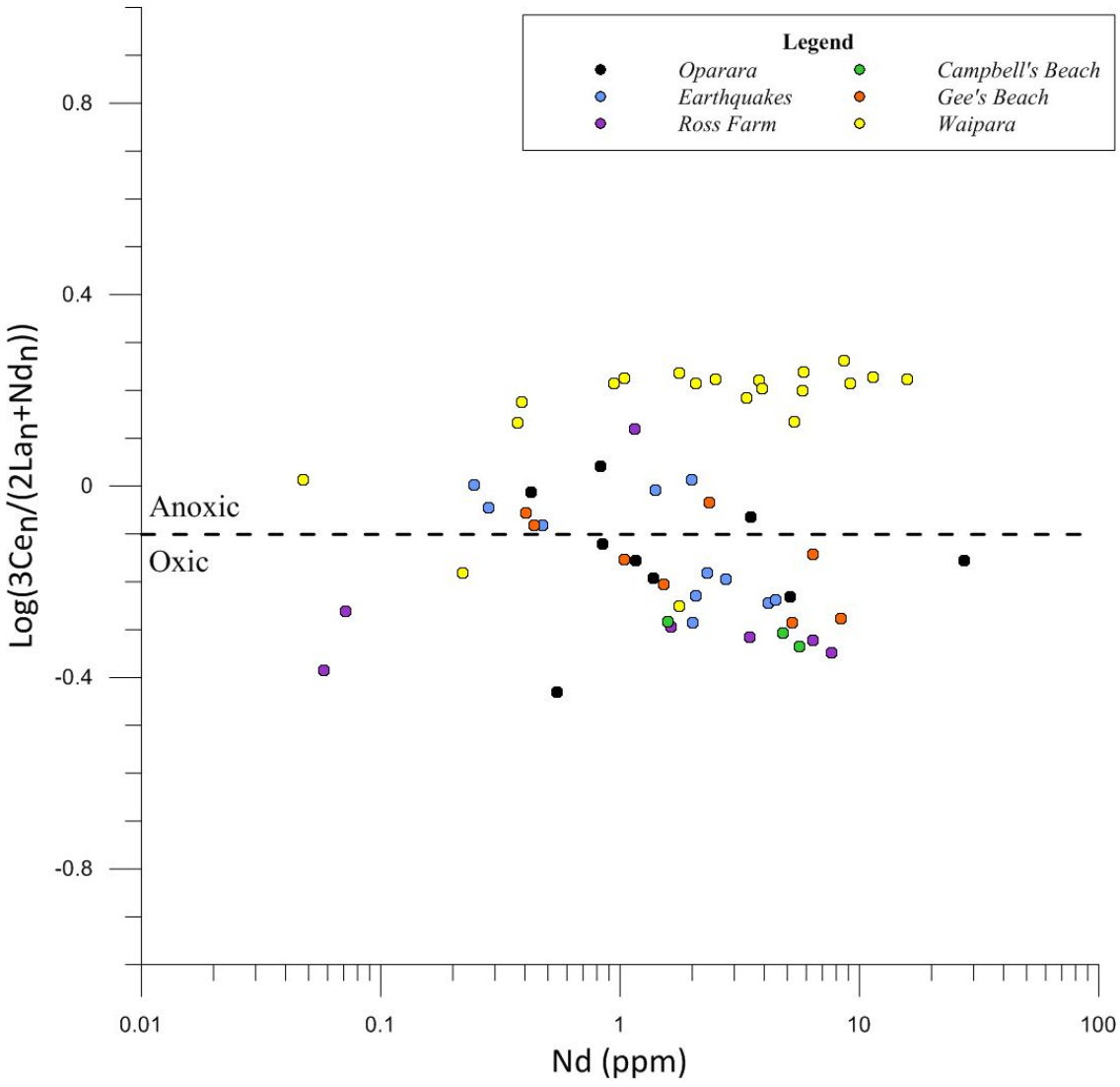

Figure 29 – Cerium anomalies for all sampled outcrops showing all grains analysed by LA-ICP-MS

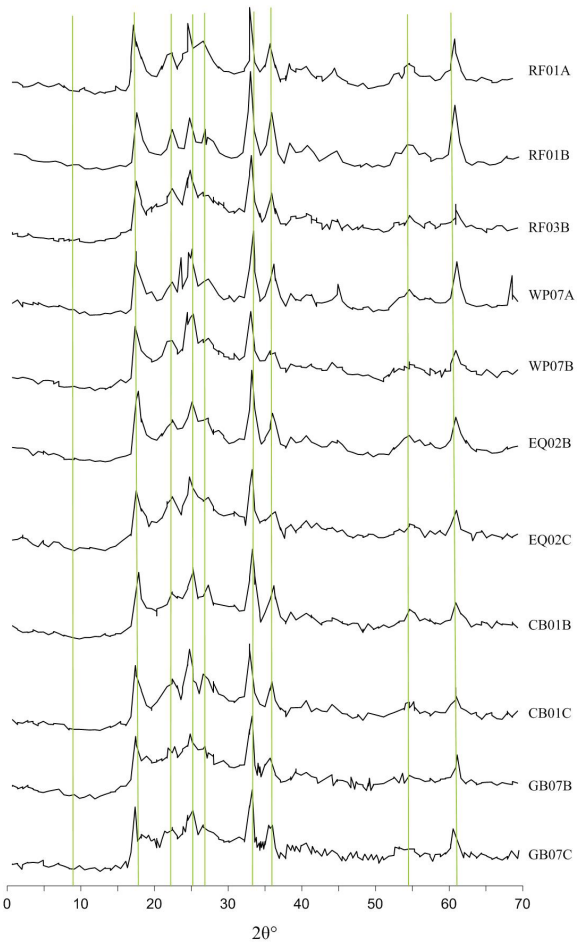

Figure 30 – X-Ray diffraction spectra of all air dried samples. Vertical green lines are the wavelengths of the peaks expected for glauconitic minerals

5.4 Structural analysis

5.4.1 X-Ray Diffraction

X-ray diffratograms for air dried samples are presented in Figure 30. Prominent peaks occur at 17°, 25°, 34°, 36° and 62° 2θ, with smaller peaks at 22° and 55° 2θ. These peaks line up with those expected of glauconitic minerals according to the Traces database (ICDD, 2015). The $d(001)$ value, representing the interlayer spacing, should occur around 10-14° 2θ (Odin and Matter, 1981; Amorosi et al., 2007), however this peak is missing from all measured samples. Peaks are consistent in their orientation and intensity relative to the background.

Diffractograms for air dried, glycolated and heat treated samples for EQ02, RF01 and

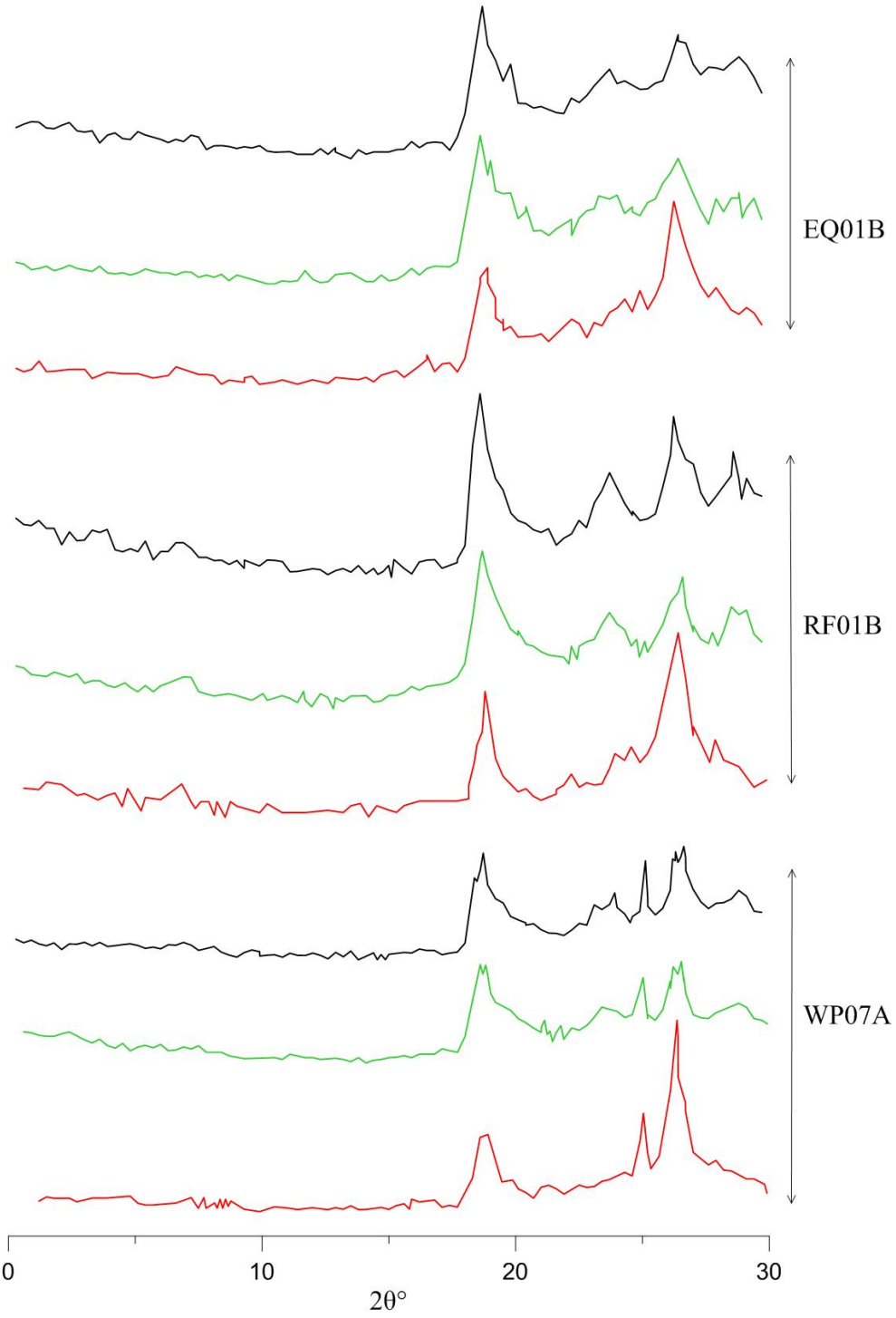

Figure 31 – XRD traces for EQ02B, WP07A and RF0B2 showing air dried (black lines), glycolated (green lines) and heated (red lines) samples

Table 6 – Prominent peaks from 33 grains of glaucony analysed by Raman spectroscopy

	Wavelength (cm^{-1})		
Average	1013.6	693.6	549.5
Minimum	927.0	684.0	539.0
Maximum	1093.0	699.0	559.0
Standard deviation	50.3 (N=31)	3.9 (N=24)	4.6 (N=33)

WP07 are displayed in Figure 31. Glycolated samples show no variation in peak location, width or intensity compared with the air dried spectra. Heated samples show a collapse of peaks at 23-24° 2θ and an intensification of the peak at ∼27° 2θ.

5.4.2 Raman Analysis

Raman analysis was used to assess chemical variation between galucony on a grain by grain basis. Figure 32 shows spectra measured from grains 34-66 (even numbers only). The spectra display many small peaks, most of which are due to fluorescence. Within the background there are several peaks which stand out in the spectra and occur consistently in all grains analysed. Peaks at ∼550 cm^{-1}, ∼690 cm^{-1} and ∼1010 cm^{-1} were consistently identified in the peak picking function in OPUS 6.5; these are displayed in Table 6. The peak at 550 cm^{-1} is the most prominent and shows only subtle variation in wavelength position between grains (standard deviation is 4.6 from 32 grains). The peak at 693 cm^{-1} is less intense than 550 cm^{-1} but still present in all grains and again shows only subtle variation in wavelength position (standard deviation of 3.9 from 23 grains). After 700 cm^{-1} there are numerous small peaks creating a messy spectra. A poorly defined hump is present between 900-1100 cm^{-1}, with an average peak position of 1013 and standard deviation of 50.3 from 30 grains. There are also peaks which were not identified by the peak picking software. These occur in all grains at ∼380-390 cm^{-1}, ∼250 cm^{-1} and ∼190 cm^{-1}.

The only grain to show significant variation from the others is JS02-62 (highlighted orange in Figure 32). Peaks at 550 cm^{-1} and ∼380 cm^{-1} are still present, however the background spectra is smoother and present at a higher intensity than all other grains.

Relationships between the three main Raman spectra peaks and major element concentrations are presented in Figure 33. There is no systematic variation between Fe_2O_3, Al_2O_3,

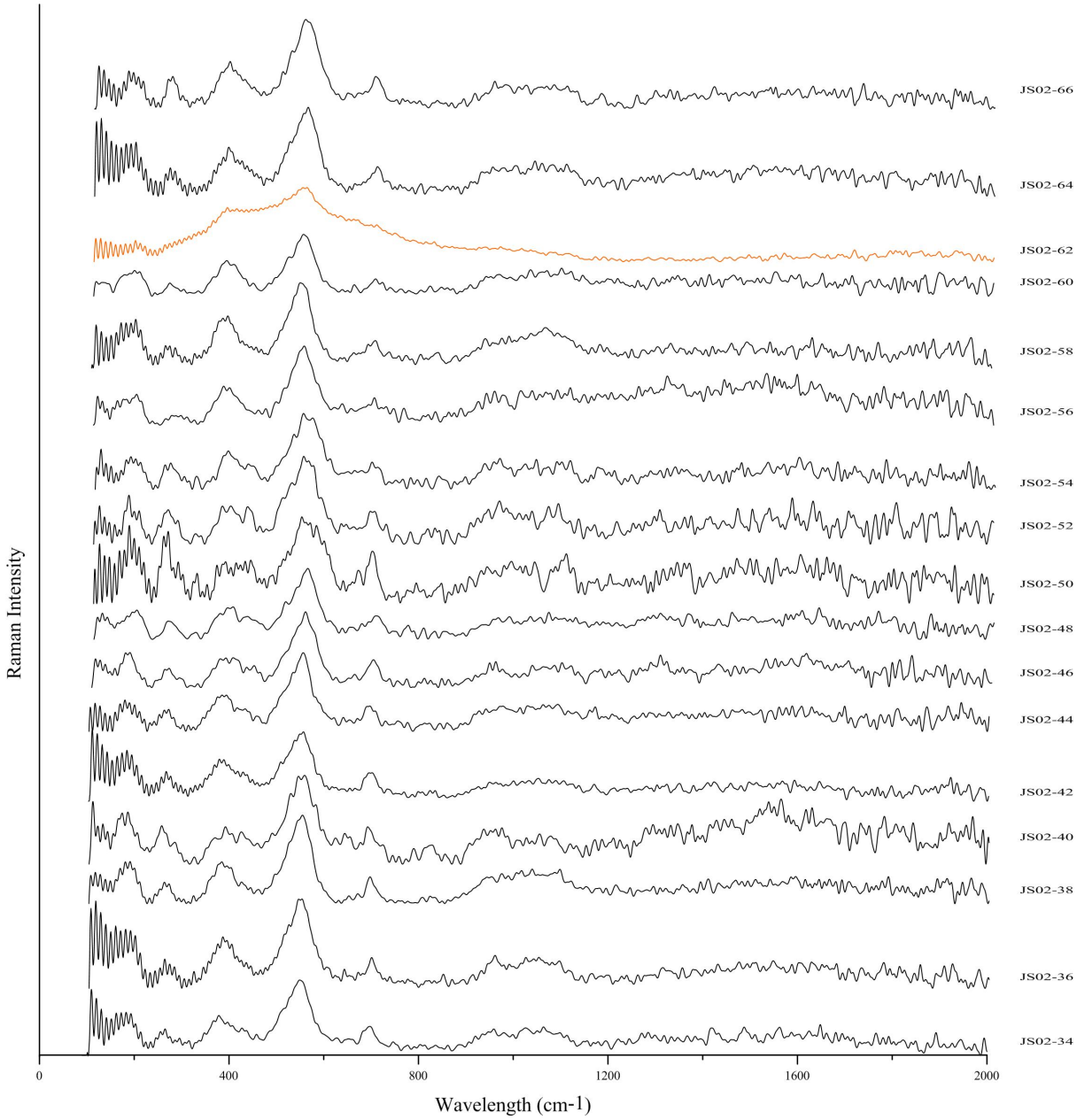

Figure 32 – Raman spectra for grains JS02-34-66 (only even numbers presented). Y-axis is arbitrary and allows comparison of peak heights between grains. The only grain (JS02-62) which shows significant variation from the rest is highlighted orange.

MgO or K_2O with any of the peaks. R^2 values are low in all peak-element plots (maximum $R^2 = 0.46$).

The principal component analysis (PCA) are displayed in Figures 34,35 and 36. Figure 34 is a PCA scores plot, grouping the spectra based on how similar they are to each other. Principal components 1 and 2 explain 33 % and 12 % of the variance respectively. The spectra generally cluster together and overlap, with only grain 39 occupying a distinctly separate portion of the plot. The PCA loadings plot shown in Figure 35 displays the wavelength of the spectra in which the major variations occur for the principal coordinates being considered. The stand out peaks in the loadings plot are at $\sim$370 cm^{-1} and 550 cm^{-1}. Figure 36 shows the explained variance for each principal component. The validation line is a theoretical calculation based on what the validation method (leverage correction in this case) thinks the line should look like. The calibration line shows that <50% of the first 2 principal components explain the variance within the spectra.

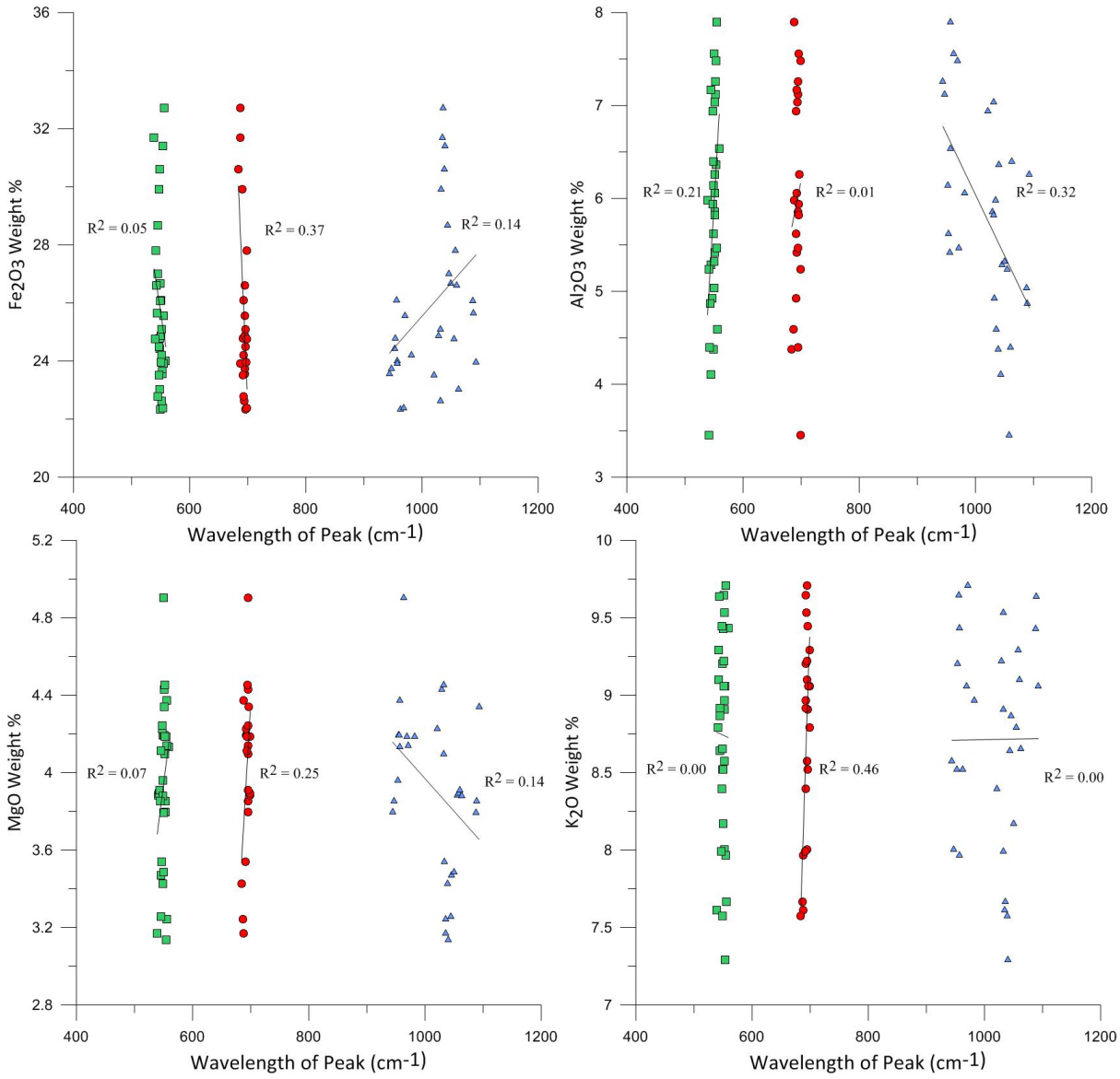

Figure 33 – Elemental concentrations for Fe, Al, Mg and K plotted against wavelength peak position acquired using Raman analysis for grains measured using both SEM+EDS and Raman microscopy. The peak at $\sim$ 1000 cm^{-1} shows greater scatter than the peaks at 550 and 700 cm^{-1}. The vertical profiles suggest that wavelength position does not vary as a function of elemental concentration

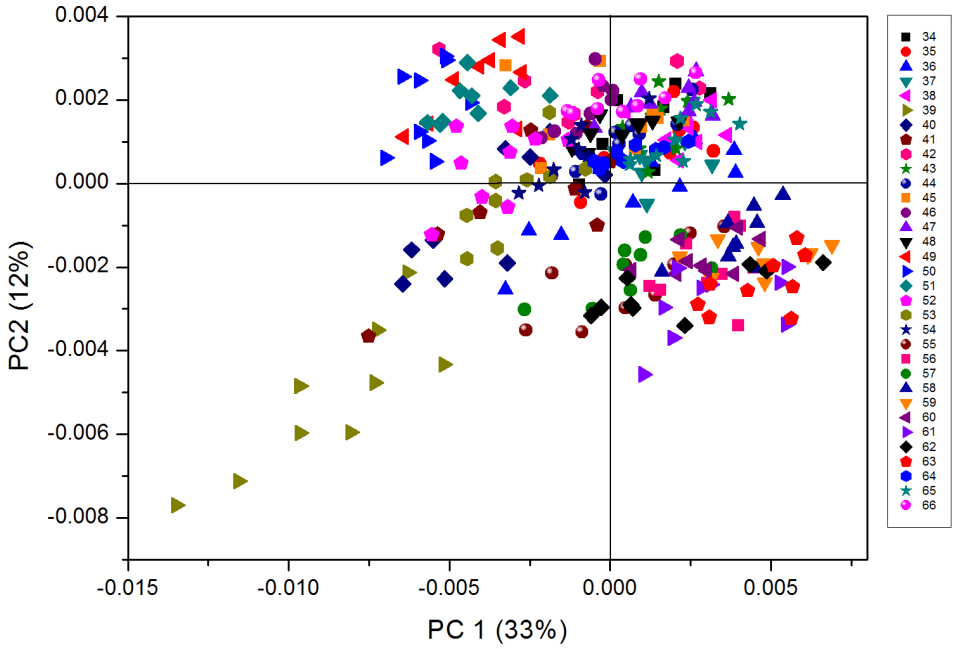

Figure 34 – PCA scores plot for all Raman spectra obtained from JS02

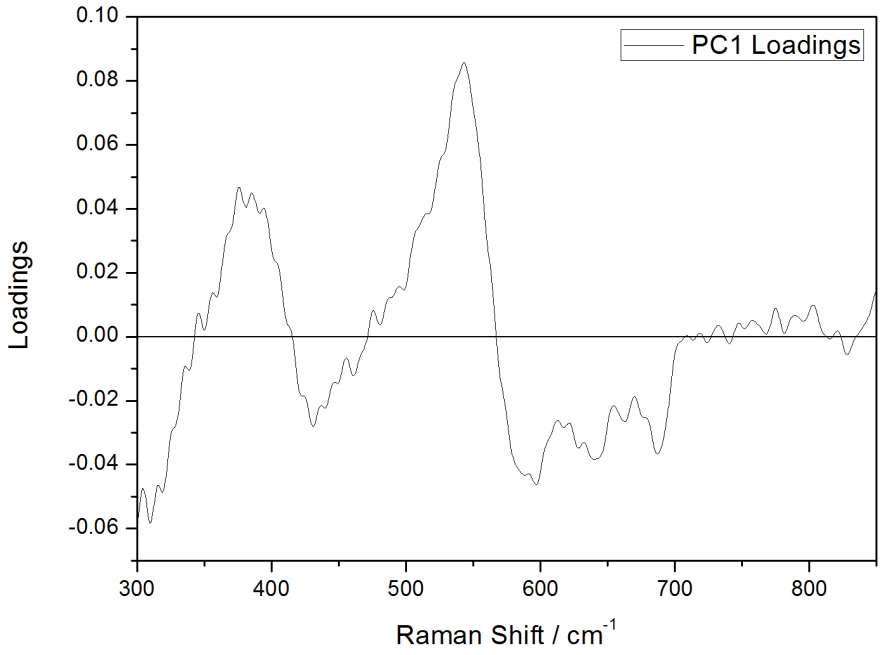

Figure 35 – PCA loadings plot for all Raman spectra from JS02

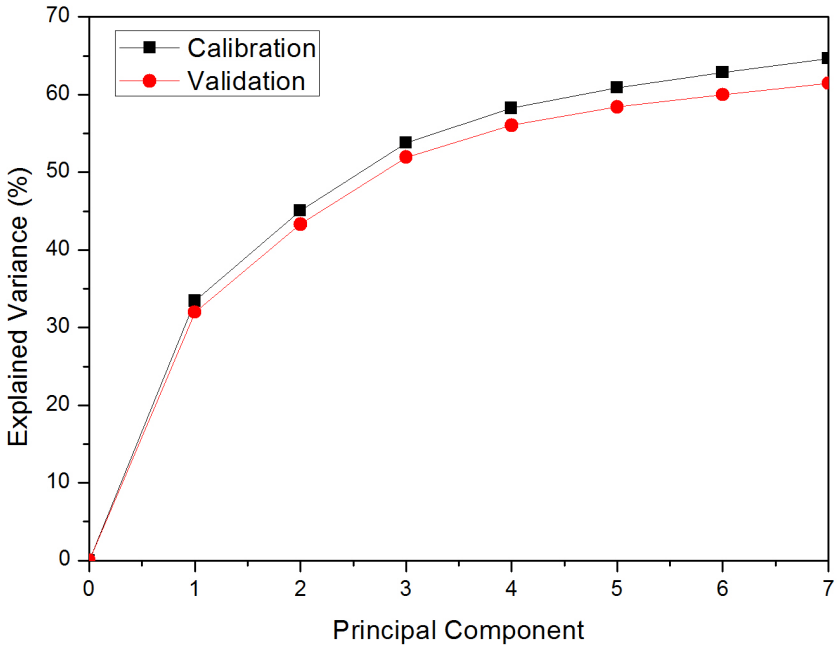

Figure 36 – PCA explained variance plot for all Raman spectra obtained from JS02. Validation is a theoretical line which the validation method (leverage correction) calculates what the line should look like. The low values for explained variance suggest that the principal components (prominent wavelength peaks) are not displaying variation between the different grains measured

5.5 Solubility of Glaucony

Experiment 1 - no birnessite at pH 3.7

Potassium concentration released from glaucony during lexiviation testing is shown in Figure 37. The first measured time interval at 25 hours contained 700 ppb K. After 73 hours the concentration of K increased to 800 ppb and after 190 hours K concentration reached 1400 ppb. Over the total 400 hours that grains were left to dissolve in acidified H_2O, 1640 ppb K was released into solution. The release of K was almost linear over the 400 hours. A straight line fit to the data produces the equation y = 2.69x + 696.16.

All other elements were released into solution in low concentrations. Sodium had the second highest concentration with a maximum value of 540 ppb. Calcium, P, Fe, Mg, and Al released maximum values of 74, 56, 26, 26 and 8 ppb respectively. Table 20 shows the concentrations for all elements measured by ICP-MS. All elements apart from P produced a positively sloping line of best fit.

Trace elements were released in very low concentrations. Copper had the highest concentration for all trace elements with 5 ppb, followed by Zn and As both of which measured 1 ppb. Chromium was undetectable in most analysis and measured a maximum concentration of 0.1 ppb from WP0A (the first measurement at 25 hours).

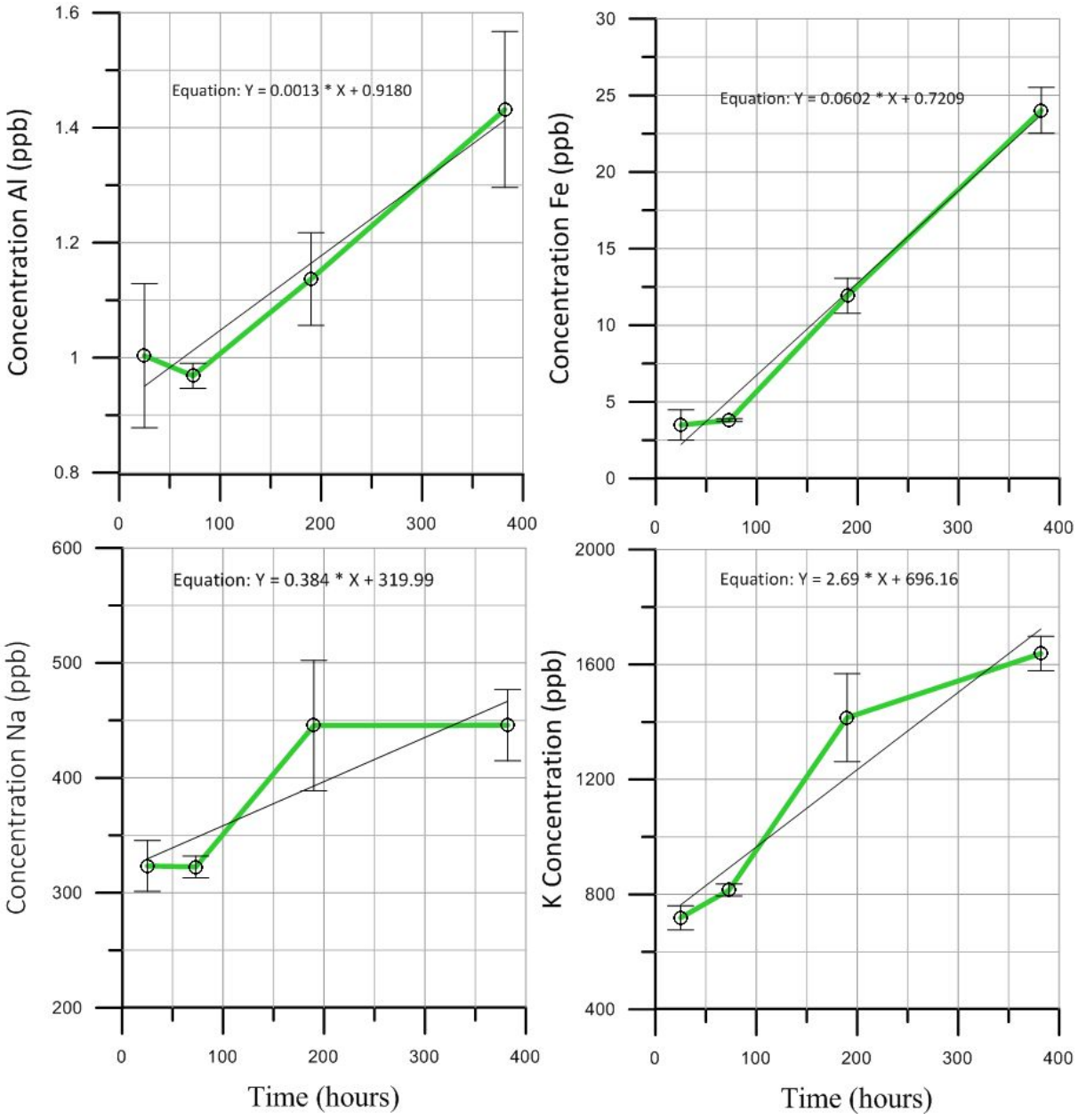

Figure 37 – Concentration of K, Al, Fe and Na dissolved from glaucony in acidified H_2O (pH 3.6) over 400 hours. Black lines are the line of best fit, green is the absolute values

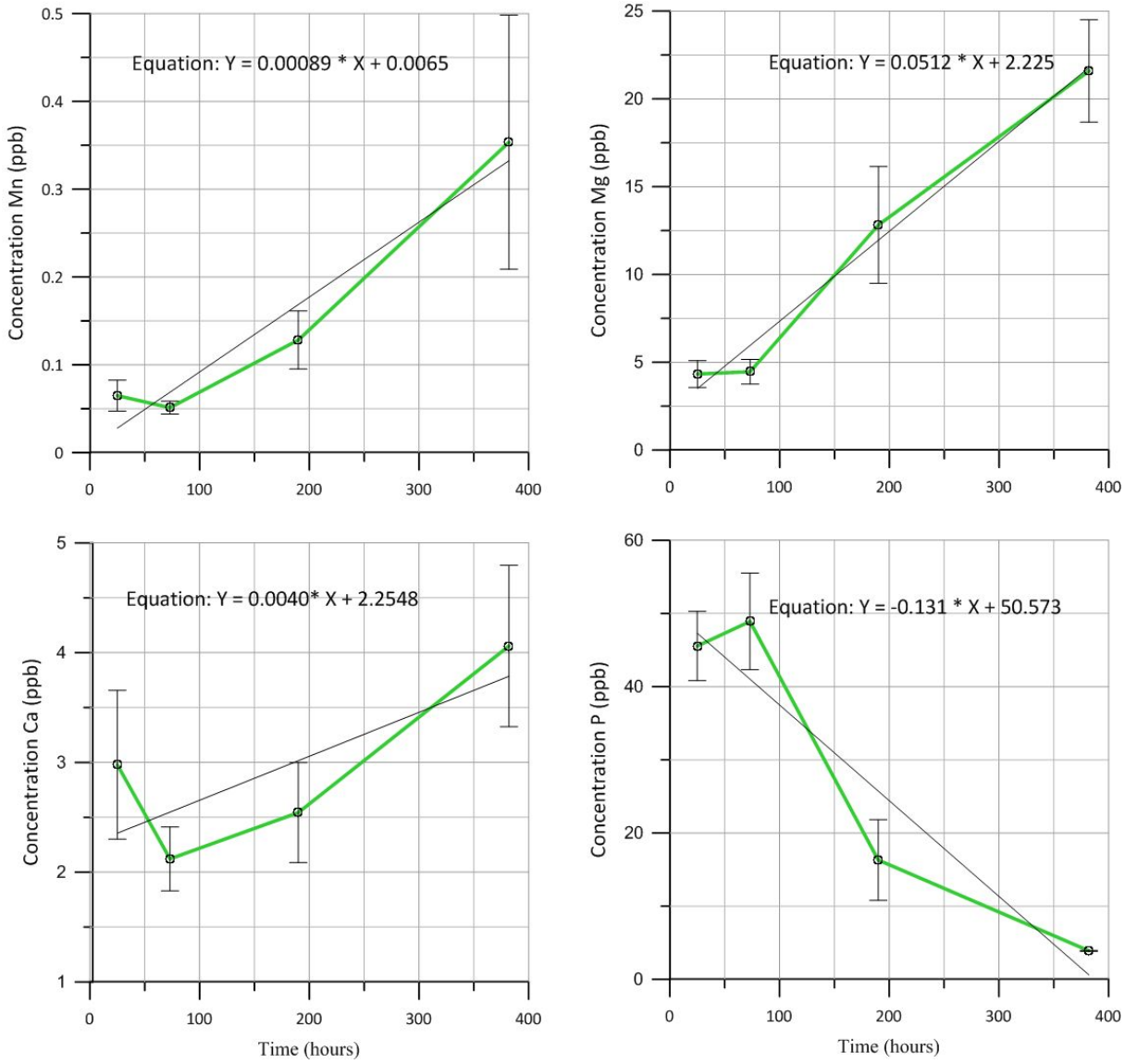

Figure 38 – Dissolution of Mn, Mg, Ca and P from 0.378 g of glaucony over 383 hours. Black lines are the line of best fit, green is the absolute values

Experiment 2 - with and without birnessite at pH 4.6 and 8

Table 21 and Figures 39 and 38 show elemental concentrations dissolved from glaucony over 103 hours in solutions of pH 4.6 and 8, both in the presence and absence of birnessite. Potassium concentration released from glaucony increased with decreasing pH and with the addition of birnessite. A maximum value of 63,113 ppb was released from a solution containing birnessite at pH 4.6 over 103 hours. This was 9.3 times more K than the same sample at pH 4.6 without birnessite and 13 times more than the same sample dissolving at pH 8 with no birnessite. This relationship between K release is true for WP04 and EQ01, which measure 8.8 and 8.7 weight % K_2O respectively.

Birnessite deccelerates Ca release in both samples at either pH. Glaucony released an average of 1.14 times more Ca without birnessite in the system from samples EQ01 (either pH) and WP04 (pH 4.6) and 8.3 times more Ca from WP04 at pH 8. Birnessite also increased the rate of Cr released from glaucony. No Cr was present in samples that contained no birnessite and 1.1 to 1.3 ppm was released from samples containing birnessite. Manganese concentrations were also higher in samples containing birnessite. Birnessite does not effect the release of Al into solution.

Acidic conditions accelerated the release of K, Mg and Ca. In solutions of pH 4.6 Ca concentrations averaged 29,589 ppm, whereas in pH 8 solutions Ca averaged 4,968 ppm. Potassium concentration was 1.6 times higher in the acidic solution compared to the basic solution when birnessite was present, and 1.5 times higher in acidic conditions when birnessite was absent. Magnesium concentration increased by 8 times in the acidic solution compared with the basic solution in the presence of birnessite and 4.7 times in the absence of birnessite.

Basic conditions accelerates Fe release. In the pH 4.6 solution no Fe was detected, despite it being the most abundant element in the solid phase (averaging 25.7 and 23.8 weight % in WP04 and EQ01 respectively). In the basic solution Fe concentration averaged 198 ppm. Neither basic or acidic conditions had an effect on the release of Al into solution.

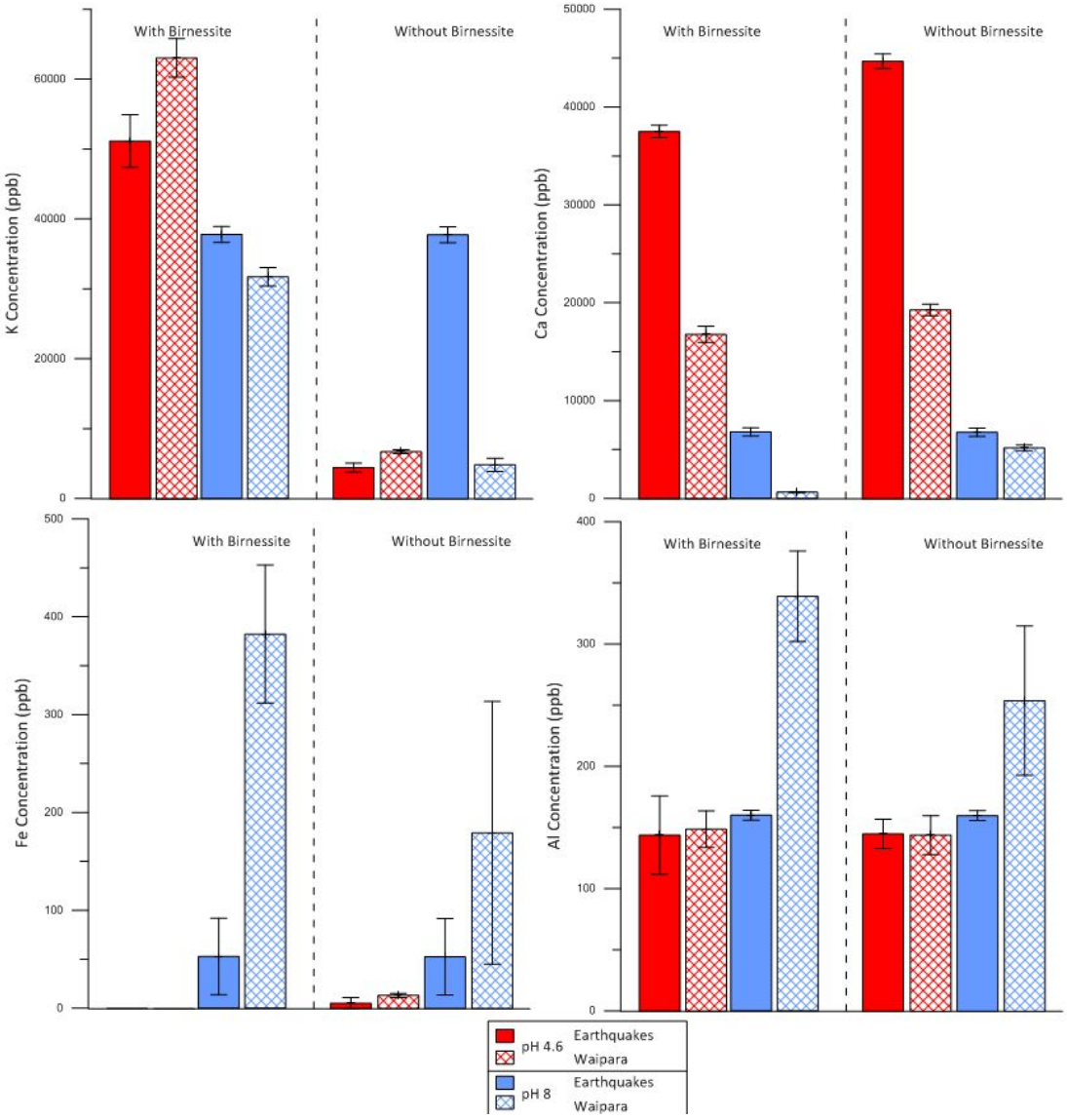

Figure 39 – Elemental concentrations of K, Fe, Al and Ca from solubility analysis with and without birnessite conducted at pH 4.6 and 8. Red bars are pH 4.6, blue bars are pH 8. Solid fill represents samples from Earthquakes and hatched fill are from the Waipara Greensand

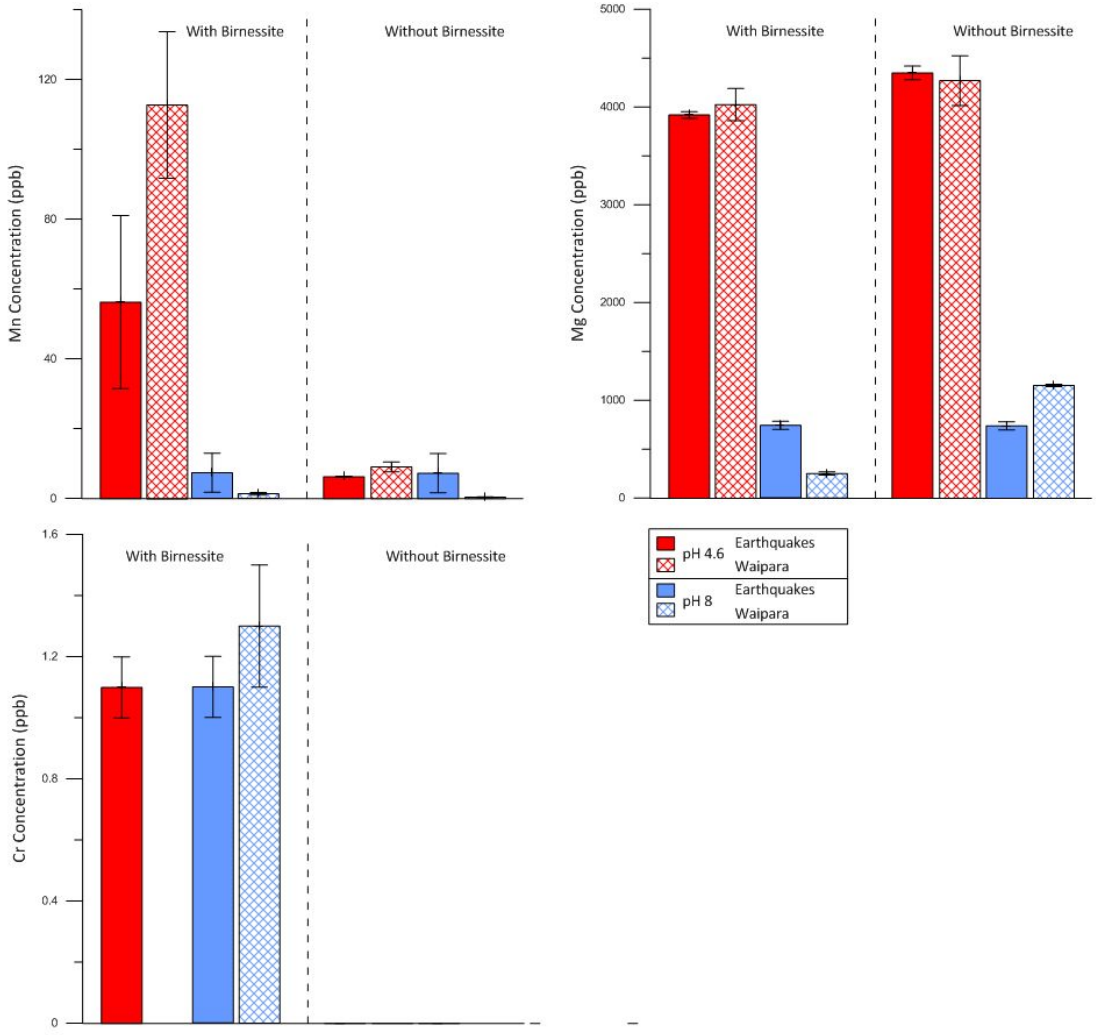

Figure 40 – Elemental concentrations of Cr, Mn and Mg from solubility analysis with and without birnessite conducted at pH 4.6 and 8. Red bars are pH 4.6, blue bars are pH 8. Solid fill represents samples from Earthquakes and hatched fill are from the Waipara Greensand

6 Discussion

This section discusses the geochemical evolution of glauconitic minerals, the influence that host materials have on the maturity of glaucony and the interpreted palaeoredox conditions for different deposits before evaluating the geochemical variations of glaucony analysed in this research. An assessment of glaucony as a K fertiliser resource is provided with predictions on the mass of elements released form glaucony over time.

Several trace elements of concern for soil contamination were present in glaucony including Cr, Zn, Ni, Cu and U. From these elements it was found that only Cr was present in elevated concentrations (averaging 268 ppm from all grains). For this reason Cr is selected as an element for further discussion, specifically with respect to the mobility and toxicity of Cr in marine and soil environments.

6.1 Quality of data collection

Geochemical variations in glauconitic minerals were measured on a grain by grain basis using spatially resolved geochemical analytical techniques (LA-ICP-MS and SEM+EDS). The data allowed comparisons between grains to be determined without being influenced by accessory phases which are often present in bulk sediment analysis. Figure 27 (section 4.5.6) shows that the REE concentrations measured by LA-ICP-MS in this research are consistently depleted, by almost an order of magnitude, relative to the geostandard for glaucony (which was measured using bulk analytical methods (XRF)) (Govindaraju, 1994).

Apatite (Ca-phosphate) has a high affinity for incorporating REE and trace elements, and is a common accessory mineral found with glaucony. Therefore, to avoid overprinting of the true chemical signature of marine clays it is important to use spatially resolved analytical techniques on separated, polished grain surfaces, where micron scale spot sampling can be achieved. This corroborates the findings of Toth et al. (2010) who suggested that the co-precipitation of sub-microscopic authigenic phosphorites as accessory phases within glauconitic grains overprinted the true REE signature of glaucony. The precision of this data has allowed interpretations to be made on the influence of host grain material on glaucony's geochemical signature, the geochemical evolution of glauconitic minerals and the palaeoredox conditions of the environment where glaucony precipitated.

6.1.1 Raman spectroscopy as a tool for determining glaucony maturity

The statistical analysis presented in section 4.3.2 suggests that Raman analysis does not detect variations in the level of maturation in glauconitic minerals. No distinctive clusters on the PCA scores plot (Figure 34, Section 5.4) and low explained variance for the principal components (Figure 36) shows that the spectra are all similar. No correlation between the major element concentrations and the position of the prominent wavelength peaks shows that the variations in major element chemical signatures are not reflected in variations in wavelength position (Figure 33). Therefore, Raman spectroscopy has no applications as a tool for discriminating the maturity state of glauconitic minerals, however it does consistently display the same prominent peaks (549, 693 and 1013 cm^{-1}) and can be used to identify glaucony as a mineral.

6.2 The geochemistry and mineralogy of glauconitic minerals

Given the range of depositional environments and the different grain types which were sampled it was expected that the major element geochemistry would vary significantly. However, all of the glaucony analysed in this research falls into the evolved (>6.5 wt% K) to highly evolved (>8 wt% K) maturity parameters established by Odin and Matter (1981). Iron, Al, Mg, Si and K are all present in concentrations comparable to published chemical data and the minerals analysed in this research all fall into the true field of glaucony described by Odin and Matter (1981) (Figure 41). X-ray diffraction peaks matched the expected peaks for glauconitic minerals, therefore the crystalline structure of the minerals analysed are of true glaucony and no unusual results were observed.

6.2.1 Substrate control on geochemical signatures

The two main host materials identified in all deposits were faecal pellets and bioclasts. Of these it was the pelletal variety which were present in the greatest abundance. Pellets were enriched in K and Fe relative to bioclast hosted glaucony (Figure 24, Section 4.2.4). This corroborates the findings of Banerjee et al. (2012a) who found that the maturity of authigenic glaucony was controlled by parent material characteristics and that in Western Kutch, India, pelletal glaucony was of the evolved type (5-7 weight% K_2O), whereas bioclast hosted glaucony at the same stratigraphic level was only slightly evolved (<5 weight% K_2O).

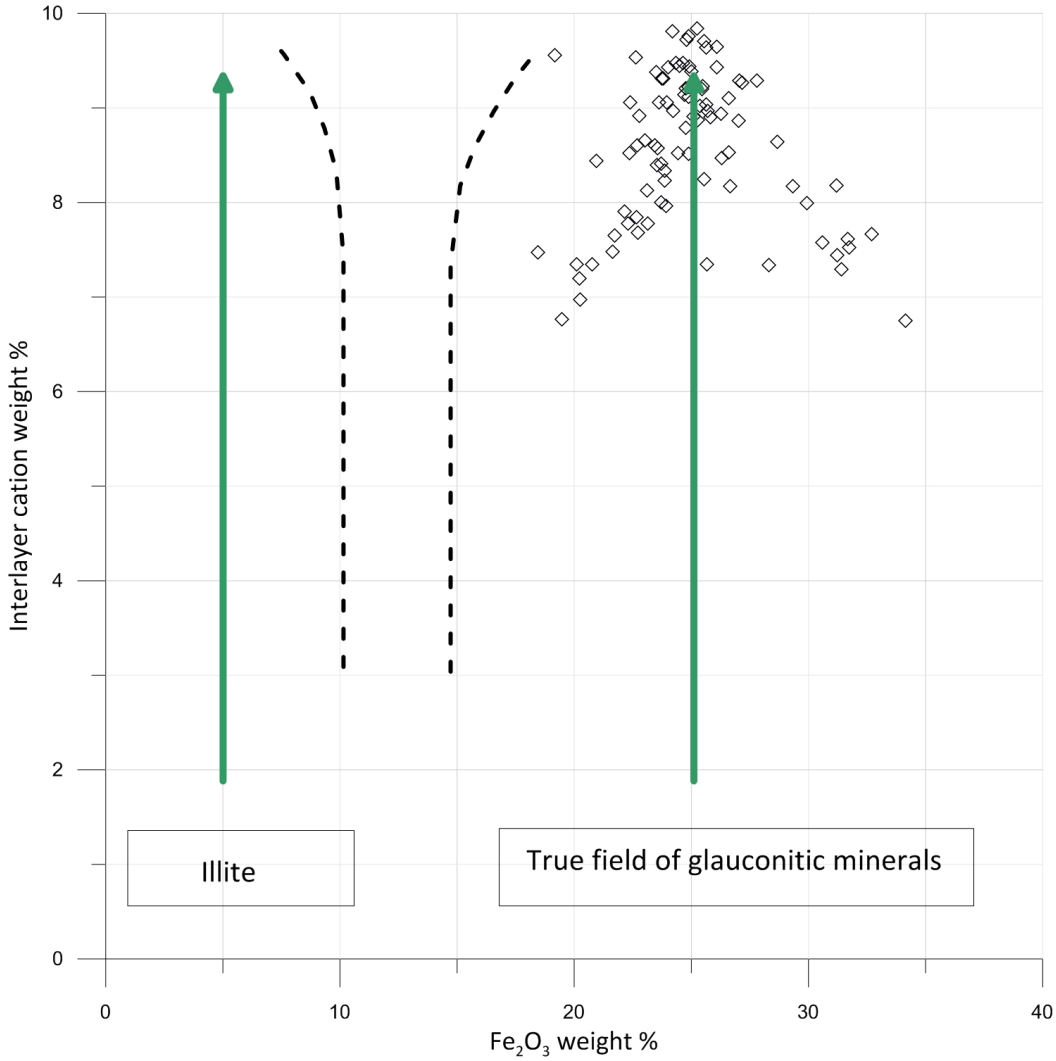

Figure 41 – Diagram showing the true field of glauconitic minerals and illite (Odin and Matter, 1981). Data collected in this research all falls within the true field of glauconitic minerals

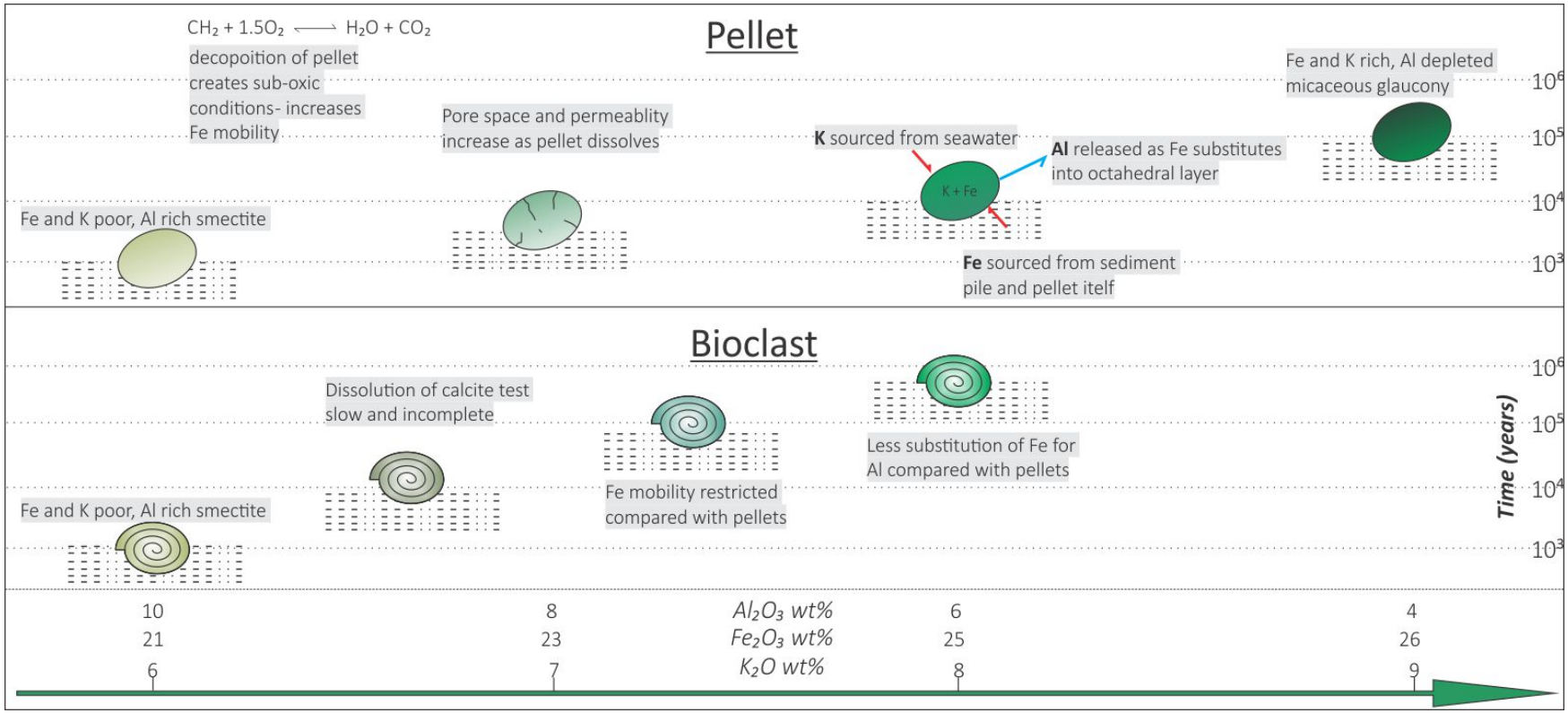

Figure 42 – Schematic diagram showing the different geochemical evolutionary pathways of pelletal and bioclast hosted glaucony. Maturation is faster in the pellets due to sub-oxic conditions created through decomposition of inherent organic matter, contribution of ions from the host itself and faster dissolution of the host grain creating pore space and permeability. The time scale is arbitrary and used as an example to show different rates of maturation

The *'verdissement of grains'* theory of Odin and Matter (1981) describes the growth of glaucony as a process of progressive dissolution of the host material with concurrent precipitation of glaucony inside the intra-particle pore spaces of parent grains. The creation of pore space and the resulting increase in permeability are important factors influencing the growth of crystallites. Bioclasts are more resistant to dissolution than faecal pellets because the intra-particle pore spaces of the calcite tests are slightly alkaline (Banerjee et al., 2012a). Therefore, as faecal pellets dissolve and become replaced with glaucony the continued creation of pore space allows the percolation of seawater into the semi-confined micro-environment of the grain, fueling precipitation and maturation. This process is hindered in grains where permeability is restricted and maturation occurs at a slower rate, as is the case in bioclasts. Faecal pellets are also more likely to directly contribute ions (mainly Fe and K) which are incorporated into the newly forming minerals, whereas bioclasts lack these ions and rely on Fe diffusing through the seafloor sediments, as Fe is present in very low concentrations in seawater.

Aluminium depletion in pellets relative to bioclasts is due to lesser amounts of Fe substituting for Al in the octahedral layer during maturation (Banerjee et al., 2012a). The mobility of Fe was increased in localised sub-oxic conditions created from the decomposition of organic material in pellets. This allowed Fe to diffuse through the grain more easily in pellets than bioclasts which had relatively restricted diffusion of Fe, resulting in less substitution of Fe for Al in the latter.

6.2.2 Geochemical evolution of glauconitic minerals

Despite generally homogenous major element chemical signatures, subtle variations do occur and can provide insight into the geochemical evolution of glauconitic minerals. The well established role of K content as an indicator for glaucony maturation allows reconstruction of the precipitation mechanisms at different stages of maturity (McRae, 1972; Odin and Matter, 1981; Amorosi et al., 2007). Positive correlations between the concentration of an element and the concentration of K represent incorporation into the newly formed crystal. Negative correlations between an element and K are interpreted as dissolution of the host material or as ionic substitutions in the crystal lattice (Amorosi et al., 2007).

Different trends in elemental relationships between outcrops suggest that the geochemical evolution of glaucony is influenced by the environment of deposition and the host grain

material. The cross plots presented in Figure 23 (Section 4.5.3) contain significant scatter, however when the data is analysed as a series of separate outcrops, trends become evident.

Iron, Mg and Al are the 3 co-ordinating cations in the octahedral layer. Iron concentration correlates positively with K indicating that it was incorporated into the mineral structure with increasing maturation. Aluminium shows the opposite trend to Fe and becomes depleted from glaucony with increasing maturation. The decrease in Al at the expense of Fe is due to Fe substituting for Al in the octahedral sheets (Odin and Matter, 1981; Amorosi et al., 2007). Magnesium becomes enriched with increasing maturation for all samples suggesting it is incorporated throughout the maturation process regardless of host grain composition or the seafloor environment.

Silica dominates the tetrahedral layer and generally comprises >3.80 atoms per formula unit, with subordinate Al filling the remaining tetrahedral sites (Tables 11 and 12, Appendix A). Silica correlates negatively with K in all samples apart from those collected from Gee's Beach and Campbell's Beach (the Gee Greensand) (Figure 23, Section 5.3.3). Both of these outcrops contain glaucony which was deposited in a sediment starved environment on the volcanic high to the east of the Waitaki Basin. In all other outcrops silica was present as detrital quartz grains in the seafloor sediments. The negative correlations with K suggest that when Si was readily available it became saturated in the crystal lattice before subsequent maturation and incorporation of K, at which point Si became progressively depleted with increasing maturation. When Si is not immediately available it will not become saturated before maturation and will concomitantly be incorporated with K, resulting in positive R^2 values.

Based on the major element relationships presented above, the geochemical evolution of a grain of glaucony is as follows:

- Silica and Al rich smectite crystallites precipitate inside the host grain. Dissolution of the host grain proceeds and may contribute elements to the local chemical environment (pellets are likely to contribute Fe and K; bioclasts contribute no elements as Ca is not a structural component of glaucony and is only present as relicts of host grains (Amorosi et al., 2007)).
- Iron and K are progressively incorporated into the mineral as the dominant octahedral cation and the interlayer cation, respectively. Aluminium becomes depleted and Si may become depleted or enriched depending on the concentration of Si in the early stages of precipitation. The increasing K content leads to neutralisation of

the negative surface charges, decreasing the expandability of the crystal lattice and producing illite - micaceous structures.

- Magnesium is incorporated into the crystal lattice throughout the maturation process.

6.2.3 Palaeoredox interpretations

The REE group have similar ionic radii and are present as trivalent ions making them a coherent suite of elements. The exception to this is Ce which exists as Ce^{3+} or may become oxidised to Ce^{4+}. As Ce^{3+} becomes oxidised it is removed from solution by adsorption onto Fe-oxides. This results in *seawater* with a depleted Ce concentration relative to its REE neighbours. Under anoxic to sub-oxic conditions Ce will remain in solution as Ce^{3+} and Ce^{4+} will desorb from Fe-oxide surfaces, resulting in seawater which is enriched in Ce relative to other REE (Elderfield and Greaves, 1982; Wright et al., 1987). The authigenic precipitation of glauconitic minerals on the seafloor will reflect the REE signature of seawater at a given point in time. Therefore, Ce anomolies in glaucony provide a tracer for changes in ocean redox potential.

The precipitation of glaucony occurs near the redox boundary (Odin and Matter, 1981). Cerium anomolies calculated in this study corroborate this, however there is evidence of variations in redox potentials between outcrops. The Waipara Greensand contains distinctly enriched Ce concentrations relative to all other outcrops sampled (see Figure 29, Section 5.3). This suggests that Ce remained soluble in seawater and was available for incorporation into the precipitating glauconitic minerals. In contrast, Ce is depleted in samples from Oamaru and Oparara, suggesting Ce was removed from seawater via the oxidation of Ce^{3+} to Ce^{4+} and subsequent adsorption onto Fe-oxide phases. The Waipara Greensand was therefore precipitated on a relatively reducing seafloor environment compared with all other samples. Figure 43 shows this process schematically using the Waipara Greensand and Earthquakes Marl as examples.

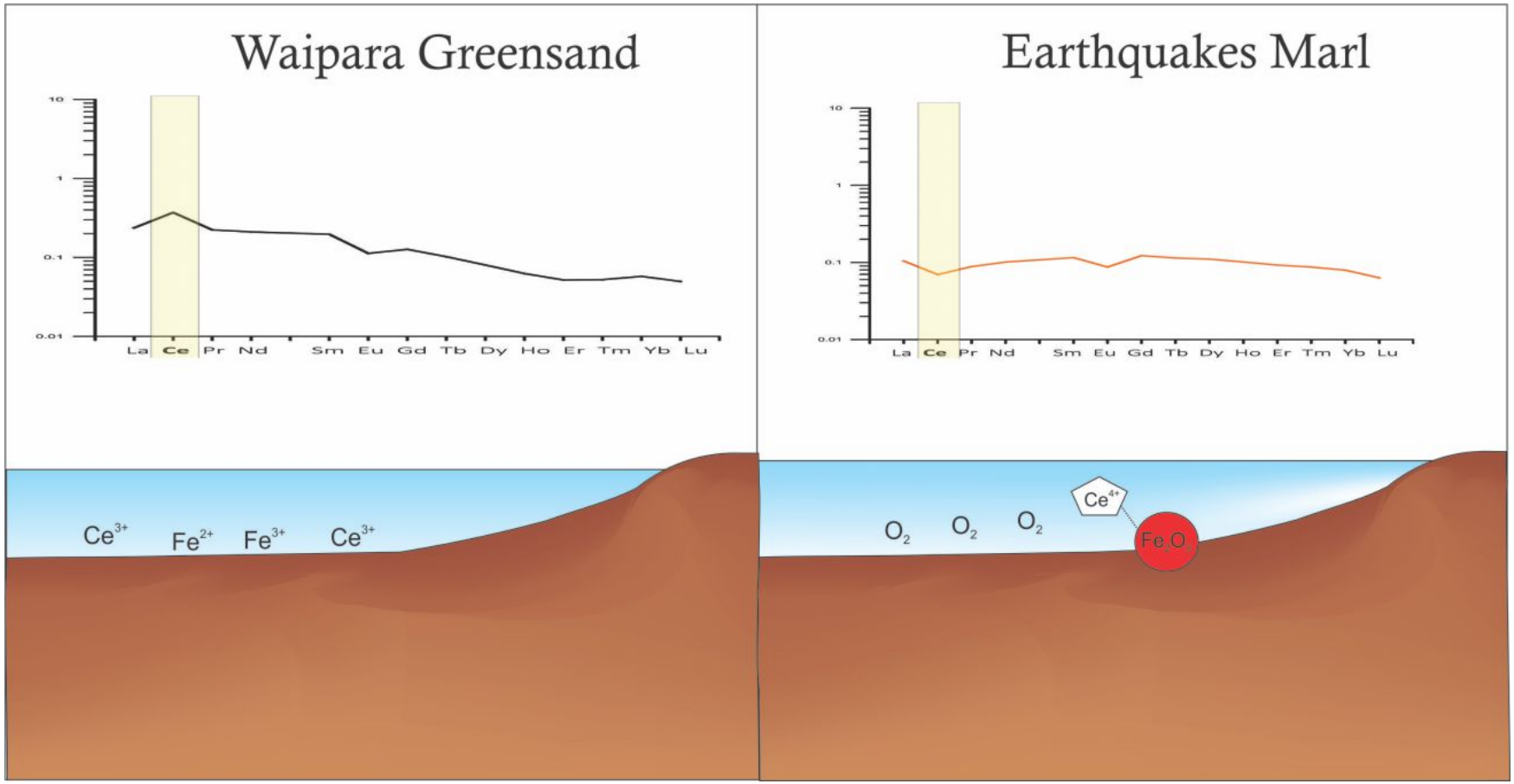

Figure 43 – Schematic diagram displaying the fractionation of Ce in seawater. The Waipara Greensand represents precipitation in more reducing conditions relative to the Earthquakes Marl

Sub-oxic conditions on the seafloor were most likely created by the decomposition of organic matter and decreased ocean circulation. The Waipara Greensand was deposited during the Mid-Late Paleocene; a 'greenhouse' climatic period where increased atmospheric CO_2 levels warmed the earth and global latitudinal heat gradients were low (Zachos et al., 1994; Crouch and Brinkhuis, 2005). Increased rates of continental weathering boosted primary production resulting in productive surface water bioactivity. The resulting decomposition of organic matter on the seafloor produced sub-oxic pore waters. Oceanic circulation was suppressed by subdued heat gradients which limited the circulation of cold oxygenated water. In contrast, the Oligocene aged rocks sampled from the Oamaru region and the Oparara Quarry were deposited during cooler climatic conditions (Cooper and Cooper, 1995). Biological activity was still high, as shown by the fossiliferous and bioturbated nature of the rocks, however the glaciated poles created latitudinal heat gradients which in turn increased oceanic circulation, delivering cold oxygenated water to the seafloor.

6.2.4 Variations between outcrops

The concentration of **major elements** generally shows only minor variation between outcrops. The exceptions are the Stoney Creek Limestone (Oparara Quarry) which is enriched in Al and depleted in Fe and K, and Gee's Beach which has a high average Fe content. Both of these exceptions can be explained by the above discussion on the geochemical evolution of glaucony and the influence of host grain on glaucony maturation. The sample from Oparara contained bioclastic hosted glaucony. These grains had less substitution of Fe for Al and the calcitic tests took longer to dissolve and lacked porosity and permeability, resulting in inhibited maturation and lower K content than pelletal hosted glaucony which was prevalent in other outcrops.

The Gee Greensand, as sampled at Gee's Beach and Campbell's Beach, contains 30-40% phosphorite in the bulk rock and was heavily bioturbated, indicating deposition in an organic-rich environment. The high organic content would have created a relatively oxygen depleted seafloor sediment pile which increased the mobility of Fe, allowing diffusion through the seafloor sediments and creating increased Fe concentrations in the zone of glauconitisation. The Waipara Greensand and Campbell's Beach contain the next highest Fe concentrations and this is likely also due to the mobilisation of Fe in sub-oxic conditions.

In contrast to the major elements, **trace elements** do show significant variations between outcrops. Glaucony from the Waitaki Basin is depleted in total trace elements (average of

1360 ppm from all four outcrops) compared to both the Waipara Greensand (2244 ppm) and the Oparara Quarry, which contained the highest total trace element content (2398 ppm). The trace element distributions are influenced by the proximity of the precipitation zone of glaucony relative to terrestrial source rocks and the chemical environment of the seafloor.

The Stoney Creek Limestone (Oparara) was deposited on a wave cut platform composed of Karamea Granite (German, 1976). Glauconitic minerals from this outcrop are enriched in Ti, V, Ni, Cu, Zn, Rb, Sr, Zr, Cs, Ba and Pb compared with the geostandard for glaucony and the other rocks sampled for this research. There is nothing exceptional about the palaeoredox conditions interpreted for the Oparara samples (most grains have Ce anomalies placing it near the redox boundary, Figure 29, section 4.2.6). Thin section analysis showed that glaucony precipitated in the presence of detrital quartz and biotite grains which were derived from the underlying granite. The Karamea Granite is of the 's-type' (Kutsukake, 1988) and can be expected to contain enrichments of incompatible trace elements. Thus, the best explanation for the trace element enrichments measured in glaucony from the Oparara Quarry is simply that they precipitated in an environment which was proximal to a source of trace element enriched minerals which were degrading in the seafloor sediment pile. The enrichment in trace elements observed in the Waipara Greensand are likely due to the high proportion of detrital quartz and terrestrial silts, introducing a source of trace elements to the seafloor sediment pile. The Waitaki Basin was starved of detrital material relative to the Waipara Greensand and this could explain the depleted trace element totals measured in these samples.

6.2.5 Chromium in glauconitic minerals

Chromium is a potentially carcinogenic trace metal for humans (Tang et al., 2014) and is toxic for plants at elevated concentrations (Shanker et al., 2005). The valence state of Cr controls its mobility and toxicity. Chromium exists in two stable oxidation states, trivalent Cr (III) and hexavalent Cr (VI). Of these, Cr (VI) is mobile and toxic whereas Cr (III) is less mobile and is a micronutrient (Richard and Bourg, 1991; Kotas and Stasicka, 2000; Shanker et al., 2005; Tang et al., 2014).

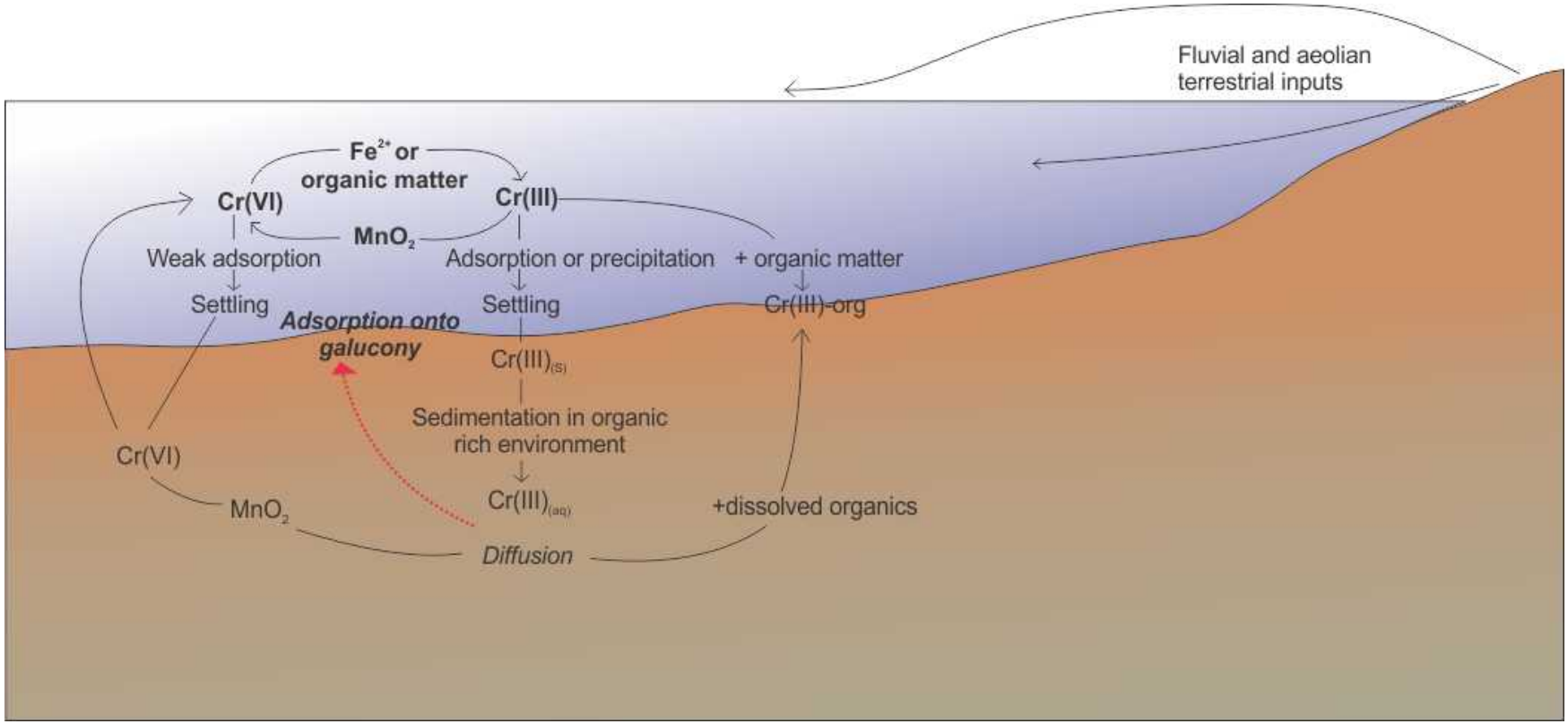

Figure 44 – Schematic representation of Cr speciation in aquatic environments and possible association with glauconitic mineral precipitation, modified from Richard and Bourg (1991)

Chromium occurs in marine water in both trivalent and hexavalent oxidation states. Chromium (VI) is reduced to Cr(III) in the presence of organic matter, Fe(II) and reduced sulphur species (Rai et al., 1989). Once reduced, Cr(III) is insoluble and precipitates as Cr-Fe-oxyhydroxides, adsorbs to the surfaces of Fe/Al oxides or becomes complexed with organic material before settling to the seafloor (Richard and Bourg, 1991). Chromium (VI) is a strong oxidant and is unstable in the presence of electron donors (Kotas and Stasicka, 2000). The oxidation of Cr(III) to Cr(VI) is mediated by Mn oxides, and these are considered the only oxidant capable of oxidising Cr in natural environmental conditions (Fendorf, 1995; Richard and Bourg, 1991; Tang et al., 2014). Chromium (VI) forms anionic species such as $HCrO_4^-$ and CrO_4^{2-} which are mobile in marine environments and soil systems.

The decomposition of labile organics in marine sediments remobilises Cr resulting in bottom water enrichment. The fate of the Cr following remobilisation depends on the chemical environment of the seafloor sediments and interstitial pore fluids. In the absence of MnO_2 Cr will be present as Cr(III) and will most likely be complexed with organic material or adsorbed onto Fe/Al oxides or hydroxyl groups of marine clays. In the presence of MnO_2 Cr will become oxidised and will be mobile in the marine environment. Given that glauconitic minerals precipitate in organic-rich environments in sub-oxic to near neutral redox conditions it is likely that Cr(III) is the prevalent valency present in glaucony. Furthermore, due to the negative surface charge of the clay structure it is unlikely that the anionic species of Cr(VI) would be attracted to the surface of glaucony. Figure 44 shows a schematic explanation of the speciation of Cr in the marine environment and the relationship between Cr and glauconitic minerals.

There is no correlation between Cr and the evolutionary stage of glaucony (as indicated by K concentration), suggesting that Cr is adsorbed to the surface of glaucony rather than being incorporated as a structural component (see Figure 26 section 4.5.5). If Cr were a true structural component its concentration would be expected to increase or decrease as a function of K content, as do the major elements which are proven structural components of glaucony.

Chromium concentrations are highest in grains from the Waipara Greensand (334 ppm). This is likely due to high amounts of dissolved organic matter on the seafloor which complexes with Cr and increases its' mobility, enhancing diffusion through the sediment pile and adsorption onto the surface of glaucony.

6.3 Applications of glaucony as a K fertiliser

6.3.1 The K budget

Solubility analysis of glaucony from the Waipara Greensand in H_2O (pH∼4) over 16 days showed that K was released into solution and the straight line equation $y = 2.69x+696.16$ was produced (Figure 37, section 4.7). This equation predicts that over one year 2.53 g of K^+ will be released from one kg of glaucony. This equates to ∼6.94 mg of K^+ per kg of glaucony per day. The results obtained from this research are lower than concentrations measured by Karimi et al. (2012), where 23 mg K^+ per kg of glaucony per day was measured from a crushed glauconitic sandstone containing 2.24 weight % K_2O dissolved in H_2O and Rao and Rao (2008) who measured 13 to 20 mg K^+ per kg of glaucony. Plants require 50-100 kg of K^+ per hectare per year (Karimi et al., 2012), therefore ∼20 t per ha of glaucony at 8.66 weight % K_2O (the concentration of K_2O in the Waipara Greensand) would be required to satisfy the minimum plant requirement of K. Sample calculations are presented in Appendix A.

The specific gravity of glaucony ranges between 2.3-2.9 (McRae, 1972) and is most likely influenced by Fe content, where mature Fe rich grains are denser than immature Fe depleted grains. Taking the Waipara Greensand as an example; the bulk rock contains 40-65% glaucony which averages 25 weight % FeO*: to produce 20 t of glaucony from an assay of 40% and a specific gravity of 2.70 g/cm^3, 50 t or ∼18.50 m^3 of bulk rock would need to be excavated to satisfy the requirements outlined above (assuming bulk rock density = 2700 kg/m^3 (the composition is dominantly quartz and glaucony)). Magnetic separation would be required to concentrate the glauconitic fraction.

The average representative stoichiometric mineral formula for glaucony from the Waipara Greensand was $K_{0.75}(Fe_{1.29}Al_{0.27}Mg_{0.37})_{1.94}(Si_{3.82}Al_{0.18})_4$. From this it was calculated that K comprised 47.66 mg of the 0.37 g of glaucony in the sample which equates to 130 g of K per 1 kg of glaucony. Thus, in 24 hours the proportion of K released into solution was 0.006% of the total K in the sample, and if dissolution rates remain constant ∼2% of the total K will dissolve from the mineral over one year. Rao and Rao (2008) and Mazumder et al. (1993) showed that the rate of K released into solution depends on the grain size and that finer grain sizes release more K than coarser grains. It would therefore be expected that over time the rate of K release would increase as the minerals undergo physical and chemical weathering and decrease in size (increase in surface area). Considering that the analysis conducted in this research used whole grains with no crushing, the K^+

Table 7 – Predicted mass of elements dissolved from glaucony over one year and percentage of total element mass dissolved from the solid phase

	K	Mn	Mg	Fe	Al	U	Na	Ca
Concentration after one year (mg/kg)	24.259	0.007	0.451	0.528	0.012	0.002	3.684	0.037
Mass (mg)	0.970	0.000	0.018	0.021	0.000	0.000	0.147	0.001
Mass dissolved per kg of glaucony (mg)	2533.606	0.781	47.095	55.185	1.282	0.260	384.733	3.900
Mass of element in one kg of glaucony (g)	126.073	0.041	38.664	309.728	52.203	0.650	1.977	5.500
Percent dissolved in one year	2.010	1.905	0.122	0.018	0.002	0.040	19.462	0.071
Mass from a 20 t fertiliser application (kg)	50	0.015	0.93	1.09	0.026	0.005	7.59	0.08

*Equations are derived from Figures 37 and 38 (section 4.7) . Mass from a 20 t application is based on the required amount of glaucony which would be distributed over one ha to satisfy plant demands of K for one year. Example calculations are shown in Appendix A

concentrations in solution reported above can be taken to represent minimum values. The release of K will be greater following crushing and subsequent increase of specific surface area where dissolution reactions occur.

Solubility analysis showed that the mass of K released into solution increased by up to 13 times when high valent Mn-oxides (birnessite) were present in the system. This shows that birnissite is affecting the dissolution of glaucony by altering the mineralogy in some way. One possible explanation is that Mn is oxidising a component of the glaucony structure to modify the surface charge and fixing capacity of the clay structure (i.e, electrons are being lost from an element in glaucony and the overall negative charge is becoming less negative). Iron is the most likely element to become oxidised, as Mg, Al and Si would have to precipitate as native metals following oxidation which is thermodynamically unlikely. Therefore, it is proposed that the presence of Mn-oxides promote oxidation of Fe(II) to Fe(III) in the octahedral layer of glaucony, and this increases the release of K^+ from the interlayer cation position. Figure 45 schematically displays this reaction pathway.

Assuming that this rate increase remains constant over time, the amount of glaucony required to satisfy plant demands would decrease from 20 t to 1.5 t ($\sim$1.4 m^3 of bulk sediment) per ha per year if birnessite is present in the soil system. Furthermore, Tang et al. (2014) showed that during the oxidation of Cr(III), Mn-oxides were recycled in the presence of light and organic matter. In other words, after Mn(IV) has been reduced to Mn(II) it is regenerated by organic- and/or oxygen-radicals. The implication of this is that only a small amount of Mn-oxides will facilitate enhanced K^+ release from glaucony and this reaction pathway will be sustained as long as light and organic matter are present

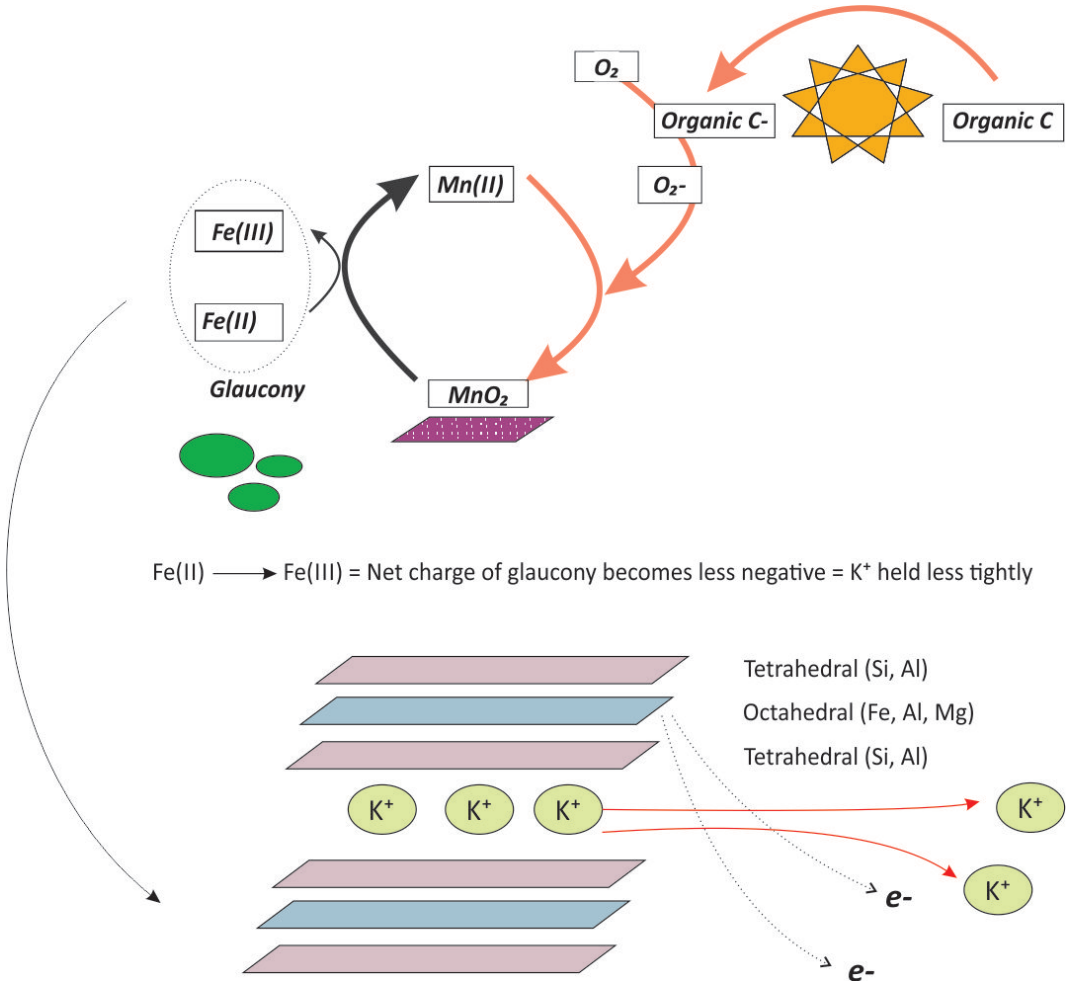

Figure 45 – Schematic showing the proposed interactions between glaucony and birnissite. Manganese is reduced from Mn(IV) in MnO_2 to Mn(II) as it takes electrons from Fe(II), resulting in the oxidation of Fe(II). This makes the overall charge of glaucony less negative, decreasing the attraction of K^+ to the interlayer cation position and increasing the release of K^+ from glaucony. The re(cycling) of Mn (orange arrows) in the presence of light and organic matter was proven by Tang et al. (2014) using changes in Cr oxidation in the presence of birnissite

in the system. Therefore, given the ubiquitous presence of Mn-oxides in soil environments it is likely that the release of K^+ from glaucony will have a naturally occurring catalyst present before the product is even applied to the soil.

This is obviously a simplified model of the K budget and adsorption onto soil colloids, excretion of plant enzymes for K release catalysis and additional sources/sinks of K will influence the total amount of K available. However, based on the solubility kinetics presented here, glaucony can provide a source of slow releasing K and one bulk application of mature glaucony may provide a base load which satisfies the minimum end of the plant requirements of K for up to fifty years. Additional inputs of imported potash would be used as a supplement according to soil characteristics and crop demands for K. It is recommended that applications are restricted to naturally acidic soils and soils that contain Mn-oxides as these factors will increase K release.

6.3.2 Other elements of interest

Sodium is released into solution very quickly compared with all other elements. Over one year it is predicted that 384 mg of Na will be dissolved from one kg of glaucony. This represents 20% of the total Na content present in one kg of glaucony. For ions of the same valency it is the size of the hydrated radius which determines the affinity for adsorption onto negative surfaces; ions with a smaller hydrated radii are held more tightly than ions with larger hydrated radii (McLaren and Cameron, 1990). Sodium has a larger hydrated radius (0.79 nm) than K (0.53 nm) and is therefore held less tightly than K in the interlayer cation position. This may explain why Na^+ is present in relatively high concentrations; however, 20% seems like a lot of the total mass of an element to be released in one year, especially given that the analysis included uncrushed grains with a low surface area. The dissolution analysis was conducted using a magnetically separated *bulk sediment* of concentrated glaucony and it is likely that there were salts (NaCl) and other minor accessory phases which may have contributed to the high Na^+ concentrations.

Predicted masses of other elements of interest are listed in Table 7. Magnesium and Fe will both release ~1 kg over the course of a year from an application of 20 t of glaucony. Calcium release was increased in acidic conditions, however the overall concentrations are low. The fact that Ca concentrations were twice as high in solutions that dissolved samples from Earthquakes (carbonate hosted glaucony) compared with the Waipara Greensand suggests that Ca is present as grains of carbonate aggregated to the glaucony grain surfaces

or relicts of the host material itself. The mass of Al and P is negligible. Manganese is present in low amounts and will not significantly increase the MnO_2 content of soil.

6.3.3 Other benefits

In addition to providing a source of K to soil, glauconitic minerals have an inherent CEC associated with the net negative charges on the crystal surface. Increasing the cation exchange capacity of soil can increase the adsorption of trace metals, retaining them in the soil profile and decreasing the risk of leaching unwanted contaminants into the groundwater and connected surface water ecosystems. Tedrow (2002) found that the CEC of a glauconitic sandstone was between 19 and 31 milli-equivalents/100 g soil and that the highest values were measured in the finest grain sizes. McRae (1972) reported ranges between 5-39 milli-equivalents/100 g and suggested that the CEC varied inversely with the concentration of the interlayer cation. This is to be expected as the increase in interlayer cation will neutralise the net negative charge on the surface of glaucony. Therefore, the more mature and K rich the glaucony in question is, the less it will contribute to the overall CEC of the soil to which it is added. Whilst increasing the soils CEC is a desirable side effect of using glaucony as a fertiliser, there are better alternatives for increasing the CEC. Humic matter is one example which contains 100-300+ milli-equivalents/100 g soil.

The slow release of K avoids the possibility of upsetting the nutrient budget in downstream ecosystems. Leaching through soil profiles into groundwater systems and the interconnected surface water bodies can unintentionally transfer nutrients from the intended place of deposition (i.e a farm) to sensitive ecosystems. When high concentrations of nutrients are suddenly introduced into environments the naturally established ecological diversity may become disrupted. In New Zealand P is usually the limiting nutrient and additions of P will often trigger algal blooms (McLaren and Cameron, 1990; Moore et al., 2005), therefore increases in K content are not likely to disrupt the established ecology. However, in areas where it is determined that K is a limiting nutrient the slow release of K from glaucony could make it a desirable product to use in terms of avoiding ecosystem disruption whilst providing plants with a minimum long-term baseload of K.

6.3.4 Potential issues

Despite measuring high concentrations in the solid phase analysis, Cr was negligible or undetectable in solution, indicating that it is held tightly to the surface of glaucony. Over

long time scales the total amount of Cr would eventually be released from glauconitic minerals into the soil, however, given that Cr(VI) is unstable in the presence of organic matter and Fe(II) species, it would be expected that the Cr that is eventually released will be present in the reduced form as Cr(III). This would then imply that Cr is present as a micronutrient and will be beneficial to soil and plants. The presence of Mn oxides did increase the Cr released into solution (Figure 40, section 4.4) and this was probably in the Cr(VI) form (1.1 ppb was not enough to determine the oxidation state), however the rate of release was so minimal and the ubiquitous presence of Cr reducing agents (organic material and Fe) in soil means that Cr toxicity is not an issue relevant to the application of glauconitic minerals to soil environments.

The slow release of K from glaucony means that to meet K^+ demands significant amounts of bulk material would need to be excavated ($\sim$ 18.5 m^3 in the case of the Waipara Greensand). This should restrict the use of glaucony to farms within close proximity of the deposit. Furthermore, glaucony would need to be concentrated through magnetic separation and this would only be effective in loosely consolidated rock. To avoid a high proportion of gangue mineral waste product and unnecessary amounts of bulk rock excavation, only deposits with high proportions of mature glaucony should be considered as a K resource.

7 Conclusions

Glaucony from the Waitaki Basin, the Waipara Greensand and the Stoney Creek Limestone contain similar geochemical signatures and are highly evolved (K_2O >6.5 weight %). Subtle variations in major element concentrations reflect the host grain influencing the maturation process, resulting in K and Fe enrichments in faecal pellet hosted glaucony compared with bioclast hosted grains. These enrichments are due to the pellets' tendency to dissolve and create new pore space, the oxidation of organic matter creating localised sub-oxic conditions and a greater contribution of the ions involved in the precipitation process from pellets than bioclasts. Trace element concentrations are enriched in the Stoney Creek Limestone and this potentially reflects the proximity of the zone of glaucony precipitation to a source of trace element enriched granite.

Cerium anomalies demonstrate that glaucony precipitated near the oxic to sub-oxic boundary. The only location which is distinctive in terms of palaeoredox conditions was the Waipara Greensand. Here, Ce enrichments indicate that glaucony formed in a relatively oxygen depleted environment. Oxygen depletion occurred as a result of the increased decomposition of organic matter on the sea-floor during the Palaeocene 'greenhouse' period, in which increased rates of continental weathering enhanced primary productivity and the flux of organic matter to the sea-floor.

In dissolution experiments, K was released from glaucony at faster rates than any other element (2.5 g K^+ released from 1 kg of glaucony per $year^{-1}$). Sodium was the next highest (0.38 g Na^+/kg glaucony/$year^{-1}$) followed by Fe and Mg (both$\sim$ 0.05 g/kg glaucony/$year^{-1}$). The predicted mass of elements released over time suggests that large amounts of bulk rock would be required to meet plant requirements for K. However, the presence of naturally occurring oxidising agents (birnessite) and increased acidity enhanced the release of K from glaucony 13-fold, and this is considered a likely scenario to occur in natural soil environments. Increased K release in the presence of birnessite was potentially due to oxidation of ferrous Fe in the octahedral layer of glaucony, creating a less negative overall charge and decreasing the attraction of K to the interlayer cation space. Additionally, the release of K could be accelerated by crushing grains to increase the surface area exposed to dissolution reactions.

Several trace metals were present in glaucony, in order of decreasing concentration these include Cr, Zn, Cu, Ni, Co and Pb. Of these, Cr was the only element present in elevated concentrations (averaging 268 ppm from all samples). Dissolution experiments revealed

that trace metal concentrations in were generally < 1 ppb and there are no concerns over soil contamination from glauconitic minerals. Furthermore, the organic-rich nature of glaucony precipitation and the inherent organic matter in soil environments would result in Cr occurring in its reduced state, in which it is a micro-nutrient for plants.

The hypothesis proposed at the start of this research was that glaucony will release sufficient K^+ into solution and provide a feasible alternative fertiliser resource. This hypothesis is accepted, but more importantly it has been shown that interactions between glaucony with naturally occurring soil components such as birnessite provide a catalyst for K release. The slower rate of K release compared to KCl is attractive as it provides a long lasting base-load for plants and will not interrupt the nutrient budget of sensitive downstream ecosystems. Overall, given the abundance of glaucony, the ease at which it can be obtained and the benefits it may bring to soil systems, glauconitic minerals are a feasible K fertiliser resource which can assist the agricultural industry, both in New Zealand and on the global stage.

Table 8 – Summary of conclusions obtained for the research aims of this thesis

Research question/aim	Results obtained during this research
Evaluate variations in major, trace and REE between outcrops	Major and REE show only subtle variations between outcrops. Trace elements are enriched in the Stoney Creek Limestone compared to other outcrops
Assess the influence of host grain material on glaucony maturation	Pellet hosted glaucony is enriched in K and Fe, and is depleted in Al. Bioclastic hosted glaucony displays the opposite trends
Ascertain the mass of elements released from glaucony over time	Potassium is the only element released in significant quantities. To satisfy plant demands for K, $\sim$ 20 t of glaucony (50 t of bulk rock) would be required from a typical South Island deposit
Assess the influence that strong oxidising agents and pH have on the solubility of glaucony	Potassium release increased with the addition of strong oxidising agents and in acidic conditions
Determine whether different deposits of glaucony have distinct release characteristics	Deposits with higher K_2O concentrations in the solid phase release more K^+ into solution
Estimate the palaeoredox conditions at the time of glaucony precipitation for different outcrops	Cerium anomalies revealed that the Palaeocene aged Waipara Greensand precipitated in more reducing conditions than rocks from the Oligocene
Evaluate the application of Raman analysis for determining glaucony maturity and use XRD to determine compare glaucony to published data	Raman microscopy is not a useful tool for determining glaucony maturity, although it does display consistent spectra for and can be used to identify glauconitic minerals. Peaks on X-Ray diffractograms match those expected for evolved glaucony

References

Amorosi, A. (1997). Detecting compositional, spatial, and temporal attributes of glaucony: a tool for provenance research. *Sedimentary Geology*, 109(1-2):135–153.

Amorosi, A., Sammartino, I., and Tateo, F. (2007). Evolution patterns of glaucony maturity: A mineralogical and geochemical approach. *Deep Sea Research Part II: Topical Studies in Oceanography*, 54(11-13):1364–1374.

Baldermann, a., Grathoff, G. H., and Nickel, C. (2012). Micromilieu-controlled glauconitization in fecal pellets at Oker (Central Germany). *Clay Minerals*, 47(4):513–538.

Banerjee, S., Chattoraj, S. L., Saraswati, P., Dasgupta, S., and Sarkar, U. (2012a). Substrate control on formation and maturation of glauconites in the Middle Eocene Harudi Formation, western Kutch, India. *Marine and Petroleum Geology*, 30(1):144–160.

Banerjee, S., Chattoraj, S. L., Saraswati, P. K., Dasgupta, S., Sarkar, U., and Bumby, A. (2012b). The origin and maturation of lagoonal glauconites: a case study from the Oligocene Maniyara Fort Formation, western Kutch, India. *Geological Journal*, 47(4):357–371.

Barringer, J. L., Reilly, P. a., Eberl, D. D., Blum, A. E., Bonin, J. L., Rosman, R., Hirst, B., Alebus, M., Cenno, K., and Gorska, M. (2011). Arsenic in sediments, groundwater, and streamwater of a glauconitic Coastal Plain terrain, New Jersey, USA - Chemical fingerprints for geogenic and anthropogenic sources. *Applied Geochemistry*, 26(5):763–776.

Browne, G. H. and Field, B. D. (1985). The lithostratigraphy of Late Cretaceous to early Pleistocene rocks of northern Canterbury, New Zealand. *Department of Scientific and Industrial Research*.

Burst, J. F. (1958). Glauconite pellets: their mineral nature and applications to stratigraphic interpretations. *Bulletin of the American Association of Petroleum Geologists*, 42.

Carter, R. and Landis, C. (1972). Correlative unconformities in southern Australasia. *Nature*.

Cas, R., Landis, C., and Fordyce, R. (1989). A monogenetic, Surtla-type, Surtseyan volcano from the Eocene-Oligocene Waiareka-Deborah volcanics, Otago, New Zealand: a model. *Bulletin of Volcanology*, 51:281–298.

Chafetz, H. S. (2007). Paragenesis of the Morgan Creek Limestone, Late Cambrian, central Texas: Constraints on the formation of glauconite. *Deep Sea Research Part II: Topical Studies in Oceanography*, 54(11-13):1350–1363.

Cook, G. H. (1868). Geology of New Jersey. *The Daily Advertiser*, page 899.

Cooper, A. and Cooper, R. a. (1995). The Oligocene Bottleneck and New Zealand Biota: Record of a Past Environmental Crisis. *Proceedings. Biological sciences / The Royal Society*, 261(1362):293–302.

Cooper, R. A. (2004). The New Zealand geological timescale. *Institute of Geological and Nuclear Science Monograph 22*, page 284.

Creech, J. B., Baker, J. a., Hollis, C. J., Morgans, H. E., and Smith, E. G. (2010). Eocene sea temperatures for the mid-latitude southwest Pacific from Mg/Ca ratios in planktonic and benthic foraminifera. *Earth and Planetary Science Letters*, 299(3-4):483–495.

Crouch, E. M. and Brinkhuis, H. (2005). Environmental change across the Paleocene - Eocene transition from eastern New Zealand: A marine palynological approach. *Marine Micropaleontology*, 56(3-4):138–160.

Doepel, J. J. G. (2013). Exploration target report, Dinner Hill potash deposit, Dandaragan project, Western Australia. *Potash West technical reports*.

Dooley, J. H. (1998). Comprehensive chemistry of select greensand from the New Jersey coastal plain. *N.J Geol. Surv. Tech. Memo. 98-1. Trenton 20pp*.

Elderfield, H. and Greaves, M. J. (1982). The rare earth elements in seawater. *Nature*, 296.

Fendorf, S. E. (1995). Surface reactions of chromium in soils and waters. *Geoderma*, 67:55–71.

Fixen, P. E. and Johnston, A. M. (2011). World fertilser nutrient reserves: a view to the future. *J Sci Food Agric*, 92:1001–1005.

Fordyce, R., Jones, C., and Field, B. (1986). The Worlds Oldest Penguin? *Geological Society of New Zealand newsletter*, 74:56–57.

Forsyth, P. (2001). Geology of the Waitaki area. *Institue of Geological and Nuclear Sciences 1:250000 Geological Map 19*.

Franzosi, C., Castro, L. N., and Celeda, A. M. (2014). Technical Evaluation of Glauconies as Alternative Potassium Fertilizer from the Salamanca Formation, Patagonia, Southwest Argentina. *Natural Resources Research*, 23(3):311–320.

Gage, M. (1957). The Geology of Waitaki Subdivision. *New Zealand Geological Survey*, 55.

German, R. C. (1976). Stratigraphy and sedimentology of the Nile group (Oligocene) southwest Nelson.

Govindaraju, K. (1994). Compilation of working values and sample description for 383 geostandards. *Geostandards Newsletter*, 18.

Gromet, L. P., Dymek, R. F., Haskin, L. A., and Korotev, R. L. (1984). The North American shale composite: Its compilation, major and trace element characteristics. *Geochemica el cosmochemica acia*, 48:2469–2482.

Haast, J. (1871). On the Geology of the Waipara District, Canterbury; with geological map and sections. *New Zealand Geological Survey Report*, 6:5–19.

Heffer, P. and Prud, M. (2014). Fertilizer Outlook 2014-2018. *International Fertiliser Industry Association*, (May):26–28.

Hollis, C., Crampton, J., Morgans, H., and Reid, C. (2013). Cretaceous-Paleogene Stratigraphy of North-Eastern South Island. *Geosciences 2013 Annual Conference of the Geoscience Society of New Zealand*, 4487(November).

Hollis, C. J., Beu, A., Crampton, J., Jones, C. M., Crundwell, M., Morgans, H., and Boyes, A. (2010). Calibration of the New Zealand Cretaceous- Cenozoic Timescale to GTS2004. *GNS Science report 2010/43*, (August):20.

Hollis, C. J. and Strong, C. P. (2003). Biostratigraphic review of the Cretaceous/Tertiary boundary transition, mid Waipara River section, North Canterbury, New Zealand. *New Zealand Journal of Geology and Geophysics*, 46(2):243–253.

Hollis, C. J., Tayler, M. J., Andrew, B., Taylor, K. W., Lurcock, P., Bijl, P. K., Kulhanek, D. K., Crouch, E. M., Nelson, C. S., Pancost, R. D., Huber, M., Wilson, G. S., Ventura, G. T., Crampton, J. S., Schiø ler, P., and Phillips, A. (2014). Organic-rich sedimentation in the South Pacific Ocean associated with Late Paleocene climatic cooling. *Earth-Science Reviews*, 134:81–97.

Huggett, J. M. (2005). Glauconites. *Elsevier*, 20(Minerals/glauconites):542–548.

Hutton, F. (1894). On a new Plesiosaur from the Waipara River. *Transactions of the New Zealand Institute*, 6:333–358.

ICDD (2015). Traces Database. *International Center for Diiffraction Data*.

Kapoutsos, D. (2005). Provenance changes and glauconite formation in the Broken River to Iron Creek/Waipara Greensand Formations marks the late Cretaceous - Eocene Transgression. *A thesis submitted in partial fulfilment for the degree of MSc. University of Canterbury.*

Karimi, E., Abdolzadeh, A., Sadeghipour, H. R., and Aminei, A. (2012). The potential of glauconitic sandstone as a potassium fertilizer for olive plants. *Archives of Agronomy and Soil Science*, 58(9):983–993.

Kotas, J. and Stasicka, Z. (2000). Chromium occurrence in the environment and methods of its speciation. *Environmental Pollution*, 107:263–283.

Kutsukake, T. (1988). The Britannia Granite pluton in the Karamea Batholith, South Island, New Zealand. *New Zealand Journal of Geology and Geophysics*, 31(3):275–286.

Mazumder, A., Sharma, T., and Rao, T. (1993). Extraction of potassium from glauconitic sandstone by the roast-leach method. *International journal of mineral processing*, 38:111–123.

McConchie, D. M. and Lewis, D. W. (1980). Varieties of glauconite in late Cretaceous and early Tertiary rocks of the South Island of New Zealand, and new proposals for classification. *New Zealand Journal of Geology and Geophysics*, 23:413–437.

McLaren, R. G. and Cameron, K. C. (1990). *Soil Science - An introduction to the properties and management of New Zealand soils*. Oxford University Press.

McRae, S. (1972). Glauconite. *Earth-Science Reviews*, 8(4):397–440.

Merchant, R. J. (2012). Glauconite - the future potash for fertilisers in New Zealand. *AusIMM bulletin*, 2(December):78–81.

Moore, T. A., Black, A., Centeno, J. A., Harding, J. S., and Trumm, D. A. (2005). *Metal Contaminants in New Zealand: Sources, Treatments, and Effects on Ecology and Human Health*. Resolutionz Press, Christchurch.

Morgans, H. E. (2005). Upper Cretaceous to Eocene stratigraphy and sample colletions, mid-Waipara River section, North Canterbury. *Institue of Geological and Nuclear Sciences science report; 2003/08*.

Mortimer, N. (2004). New Zealand ' s Geological Foundations. *Gondwana Research*, 7(I):261–272.

Muir, R. J., Weaver, S. D., Bradshaw, J. D., Eby, G. N., Evans, J. A., and Ireland, T. R. (1996). Geochemistry of the Karamea Batholith , New Zealand and comparisons with the Lachlan Fold Belt granites of SE Australia. 39(96).

Nathan, S. (1973). Stratigraphic nomenclature for the Cretaceous-Lower Quaternary rocks of Buller and North Westland, West Coast, South Island, New Zealand. *New Zealand Journal of Geology and Geophysics*, 17(2):423–445.

Neef, G. (1981). Cenozoic stratigraphy and structure of Karamea-Little Wanganui district, Buller, South Island, New Zealand. *New Zealand Journal of Geology and Geophysics*, 24(2):177–208.

Odin, G. S. and Fullagar, P. D. (1988). Geological significance of the glucony facies. In: Green Marine Clays: Developments in Sedimentology. *Elsevier*, pages 295–332.

Odin, G. S. and Matter, A. (1981). De Glauconiarum Origine.

Pearce, N., Perkins, W., Westgate, J., Gorton, M., Jackson, S., Neal, C., and Chenery, S. (1997). A compilation of new and published major and trace element data for NIST SRM 610 and NIST SRM 612 glass reference materials. *Geostandards Newsletter 21*, pages 115–144.

Pufahl, P. K. (2010). Bioelemental Sediments. *Facies Models 4*, pages 477–504.

Rai, D., Eary, L., and Zachara, J. (1989). Environmental chemistry of chromium. *The Science of the Total Environment*, 86:15–23.

Rao, C. S. and Rao, a. S. (2008). Characterization of indigenous glauconitic sandstone for its potassium supplying potential by chemical, biological, and electroultrafiltration methods. *Communications in Soil Science and Plant Analysis*, 30(7-8):1105–1117.

Richard, F. C. and Bourg, A. C. M. (1991). Aqueous geochemistry of chromium: a review. *Water Research*, 25:807–816.

Roncaglia, L., Field, B. D., Raine, J. I., Schiø ler, P., and Wilson, G. J. (1999). Dinoflagellate biostratigraphy of Piripauan-Haumurian (Upper Cretaceous) sections from northeast South Island , New Zealand. pages 271–314.

Seed, D. (1964). Studies of the Solid State - The mineralogy and Environments of some New Zealand Galuconites. *A thesis presented for the degree of Doctor of Philosophy*, University.

Shanker, A. K., Cervantes, C., Loza-Tavera, H., and Avudainayagam, S. (2005). Chromium toxicity in plants. *Environment International*, 31:739–753.

Stille, P. and Clauer, N. (1994). The process of glauconitization : chemical and isotopic evidence. (October 1993):253–262.

Tang, Y., Webb, S. M., Estes, E. R., and Hansel, C. M. (2014). Chromium oxidation by biogenic manganese oxides of varying structural ripening. *Environmental Science: Processes and Impacts*.

Tedrow, J. C. F. (2002). Greensand and Greensand Soils of New Jersey : A Review. *New Jersey Agricultural Experimental Section*.

Thompson, N., Bassett, K., and Reid, C. (2014a). The effect of volcanism on cool-water carbonate facies during maximum inundation of Zealandia in the Waitaki-Oamaru region. *New Zealand Journal of Geology and Geophysics*, 57(2):149–169.

Thompson, N. K. (2013). Cool-Water Carbonate Sedimentology abd Sequence Stratigraphy of the Waitaki Region, South Island, New Zealand. *A thesis presented for the degree of Doctor of Philosophy*.

Thompson, N. K., Reid, C. M., Bassett, K. N., and Pufahl, P. K. (2014b). Authigenic Mineral Production in an Oligocene Cool-Water Carbonate Sequence Stratigraphic Framework, Waitaki Basin, New Zealand. *In Press*.

Thomson, J. A. (1920). The Notocene geology of the Middle Waipara and Weka Pass district, North Canterbury, New Zealand. *M F Marks*.

TIFAC (2009). Technologies for agricultural applications of glauconite - a potash mineral.

Toth, E., Weiszburg, T. G., Jeffries, T., Williams, C. T., Bartha, A., Bertalan, E., and Cora, I. (2010). Submicroscopic accessory minerals overprinting clay mineral REE patterns (celadonite - glauconite group examples). *Chemical Geology*, 269(3-4):312–328.

Triplehorn, D. (1966). Morphology, Internal Structure, and Origin of Glauconite Pellets. *Sedimentology*, 6(4):247–266.

Vajda, V. and Raine, J. I. (2003). Pollen and spores in marine Cretaceous/Tertiary boundary sediments at mid Waipara River, North Canterbury, New Zealand. *New Zealand Journal of Geology and Geophysics*, 46(2):255–273.

Wilson, D. (1963). Geology of the Waipara Subdivision (Amberley and Motunau Sheets, S68 and S69). *New Zealand Geological Survey bulletin*, 64:124.

Wright, J., Der, H. H., Iamt, W. I., Er, H. O., Geology, Q., and Trom, L. (1987). Paleoredox variations in ancient oceans recorded by rare earth elements in fossil apatite. 5.

Zachos, J. C., Stott, L. D., and Lohmann, K. C. (1994). Evolution of early Cenozoic marine temperatures. *Paleoceanography*, 9(2):353–387.

Zorb, C., Senbayram, M., and Peiter, E. (2014). Potassium in agriculture - status and perspectives.

8 Appendices

A Chemical Data

Solid phase analysis

	GL-O	All outcrops	Oparara	Earthquakes	Ross Farm	Campbell's Beach	Gee's Beach	Waipara
Sc	8.0	11.3	8.0	8.4	9.2	6.6	6.2	18.3
V	65.0	207.1	418.0	121.3	101.6	73.6	153.0	251.4
Cr	140.0	268.2	263.1	201.4	281.5	304.8	174.2	334.2
Co	14.0	7.1	21.6	2.5	3.0	3.2	10.5	4.1
Ni	36.0	37.6	78.7	29.3	29.4	31.6	61.2	18.6
Cu	3.5	27.4	53.4	19.7	27.1	17.5	30.6	21.4
Zn	38.0	170.2	196.7	129.6	145.3	129.6	200.2	188.5
Ga	13.0	21.8	29.2	20.6	19.7	17.0	12.3	25.0
Rb	238.0	333.7	579.5	249.7	280.1	273.1	253.3	335.4
Sr	19.3	14.9	48.4	10.9	10.0	8.2	11.2	7.0
Y	13.2	3.2	3.6	3.2	4.3	6.6	5.4	1.2
Zr	36.0	24.7	41.1	13.8	18.8	21.2	24.2	26.4
Nb	3.7	2.5	1.0	1.0	2.0	1.6	2.2	4.6
Cs	3.3	9.9	39.5	3.8	3.5	2.2	6.2	5.8
Ba	6.0	18.9	43.2	6.6	7.0	3.6	15.3	24.1

Table 9 – Average trace element concentrations for all samples measured by LA-ICP-MS

	Oparara	Earthquakes	Ross Farm	Campbell's Beach	Gee's Beach	Waipara
Sc	1.0	1.1	1.2	0.8	0.8	2.3
V	6.4	1.9	1.6	1.1	2.4	3.9
Cr	1.9	1.4	2.0	2.2	1.2	2.4
Co	1.5	0.2	0.2	0.2	0.8	0.3
Ni	2.2	0.8	0.8	0.9	1.7	0.5
Cu	15.3	5.6	7.7	5.0	8.8	6.1
Zn	5.2	3.4	3.8	3.4	5.3	5.0
Ga	2.2	1.6	1.5	1.3	0.9	1.9
Rb	2.4	1.0	1.2	1.1	1.1	1.4
Sr	2.5	0.6	0.5	0.4	0.6	0.4
Y	0.3	0.2	0.3	0.5	0.4	0.1
Zr	1.1	0.4	0.5	0.6	0.7	0.7
Nb	0.3	0.3	0.5	0.4	0.6	1.2
Cs	12.0	1.2	1.1	0.7	1.9	1.7
Ba	7.2	1.1	1.2	0.6	2.6	4.0
Pb	4.0	1.1	1.7	0.9	3.8	1.7
U	0.8	0.8	0.8	0.8	0.5	1.0

Table 10 – Trace elements normalised to GLO measured by LA-ICP-MS (Govindaraju, 1994)

Grain Number	Sample	Colour	Parent material	Structural formula
01	EQ06	Medium-dark green	Pellet	$K_{0.80}\ (Fe_{1.21}Al_{0.34}Mg_{0.39})_{1.94}\ (Si_{3.77}Al_{0.23})_4\ (O_{10})(OH)_2$
02	EQ06	Medium green	Pellet	$K_{0.73}\ (Fe_{1.14}Al_{0.44}Mg_{0.36})_{1.94}\ (Si_{3.81}Al_{0.19})_4\ (O_{10})(OH)_2$
03	EQ06	Medium green	Vermicular	$K_{0.74}\ (Fe_{1.18}Al_{0.35}Mg_{0.41})_{1.94}\ (Si_{3.86}Al_{0.14})_4\ (O_{10})(OH)_2$
04	EQ02	Medium-pale green	Planktic foram	$K_{0.66}\ (Fe_{1.13}Al_{0.48}Mg_{0.32})_{1.93}\ (Si_{3.87}Al_{0.13})_4\ (O_{10})(OH)_2$
22	WP07	Medium green	Amorphous	$K_{0.66}\ (Fe_{1.15}Al_{0.42}Mg_{0.36})_{1.94}\ (Si_{3.90}Al_{0.10})_4\ (O_{10})(OH)_2$
23	WP07	Medium green	Pellet	$K_{0.72}\ (Fe_{1.19}Al_{0.39}Mg_{0.35})_{1.93}\ (Si_{3.84}Al_{0.16})_4\ (O_{10})(OH)_2$
25	WP04	Medium-dark green	Pellet	$K_{0.74}\ (Fe_{1.36}Al_{0.23}Mg_{0.33})_{1.92}\ (Si_{3.83}Al_{0.17})_4\ (O_{10})(OH)_2$
26	WP04	Medium green	Pellet	$K_{0.69}\ (Fe_{1.15}Al_{0.40}Mg_{0.34})_{1.90}\ (Si_{3.95}Al_{0.15})_4\ (O_{10})(OH)_2$
27	WP04	Medium-dark green	Pellet	$K_{0.76}\ (Fe_{1.28}Al_{0.26}Mg_{0.35})_{1.90}\ (Si_{3.90}Al_{0.10})_4\ (O_{10})(OH)_2$
28	WP10	Medium-dark green	Pellet	$K_{0.71}\ (Fe_{1.04}Al_{0.52}Mg_{0.37})_{1.93}\ (Si_{3.87}Al_{0.13})_4\ (O_{10})(OH)_2$
32	RF01	Medium green	Vermicular	$K_{0.62}\ (Fe_{0.90}Al_{0.58}Mg_{0.52})_{2.00}\ (Si_{3.90}Al_{0.10})_4\ (O_{10})(OH)_2$
33	RF01	Medium-pale green	Pellet	$K_{0.58}\ (Fe_{0.99}Al_{0.62}Mg_{0.36})_{1.97}\ (Si_{3.90}Al_{0.10})_4\ (O_{10})(OH)_2$
34	EQ06	Medium-dark green	Pellet	$K_{0.73}\ (Fe_{1.19}Al_{0.38}Mg_{0.38})_{1.95}\ (Si_{3.81}Al_{0.19})_4\ (O_{10})(OH)_2$
35	EQ06	Medium-dark green	Foram	$K_{0.68}\ (Fe_{1.19}Al_{0.38}Mg_{0.38})_{1.96}\ (Si_{3.82}Al_{0.18})_4\ (O_{10})(OH)_2$
36	EQ06	Medium green	Vermicular	$K_{0.73}\ (Fe_{1.24}Al_{0.31}Mg_{0.40})_{1.95}\ (Si_{3.83}Al_{0.17})_4\ (O_{10})(OH)_2$
37	EQ02	Medium green	Pellet	$K_{0.80}\ (Fe_{1.26}Al_{0.26}Mg_{0.42})_{1.94}\ (Si_{3.81}Al_{0.19})_4\ (O_{10})(OH)_2$
38	EQ02	Medium green	Pellet	$K_{0.84}\ (Fe_{1.34}Al_{0.18}Mg_{0.43})_{1.95}\ (Si_{3.74}Al_{0.26})_4\ (O_{10})(OH)_2$
39	EQ02	Medium-dark green	Vermicular	$K_{0.81}\ (Fe_{1.22}Al_{0.30}Mg_{0.42})_{1.94}\ (Si_{3.74}Al_{0.22})_4\ (O_{10})(OH)_2$
40	EQ08	Medium-pale green	Amorphous	$K_{0.68}\ (Fe_{1.21}Al_{0.36}Mg_{0.44})_{2.01}\ (Si_{3.74}Al_{0.26})_4\ (O_{10})(OH)_2$
41	EQ08	Medium-dark green	Pellet	$K_{0.73}\ (Fe_{1.12}Al_{0.38}Mg_{0.49})_{1.99}\ (Si_{3.79}Al_{0.21})_4\ (O_{10})(OH)_2$
42	EQ08	Medium-dark green	Foram	$K_{0.77}\ (Fe_{1.13}Al_{0.40}Mg_{0.42})_{1.95}\ (Si_{3.81}Al_{0.19})_4\ (O_{10})(OH)_2$
43	RF03	Medium-dark green	Pellet	$K_{0.85}\ (Fe_{1.31}Al_{0.20}Mg_{0.42})_{1.94}\ (Si_{3.76}Al_{0.24})_4\ (O_{10})(OH)_2$
44	RF03	Medium green	Foram	$K_{0.77}\ (Fe_{1.23}Al_{0.30}Mg_{0.42})_{1.94}\ (Si_{3.81}Al_{0.19})_4\ (O_{10})(OH)_2$
45	RF03	Medium-pale green	Pellet	$K_{0.72}\ (Fe_{1.18}Al_{0.36}Mg_{0.42})_{1.96}\ (Si_{3.81}Al_{0.19})_4\ (O_{10})(OH)_2$
46	CB01	Medium-dark green	Pellet	$K_{0.80}\ (Fe_{1.27}Al_{0.24}Mg_{0.45})_{1.96}\ (Si_{3.77}Al_{0.23})_4\ (O_{10})(OH)_2$
47	CB01	Medium-dark green	vermicular	$K_{0.82}\ (Fe_{1.15}Al_{0.35}Mg_{0.45})_{1.94}\ (Si_{3.79}Al_{0.21})_4\ (O_{10})(OH)_2$
48	CB01	Medium green	Foram	$K_{0.77}\ (Fe_{1.28}Al_{0.26}Mg_{0.41})_{1.95}\ (Si_{3.80}Al_{0.20})_4\ (O_{10})(OH)_2$
49	GB07	Medium green	Benthic foram	$K_{0.70}\ (Fe_{1.55}Al_{0.08}Mg_{0.36})_{1.99}\ (Si_{3.68}Al_{0.32})_4\ (O_{10})(OH)_2$
50	GB07	Medium green	Benthic foram	$K_{0.67}\ (Fe_{1.65}Al_{0.05}Mg_{0.33})_{2.03}\ (Si_{3.57}Al_{0.43})_4\ (O_{10})(OH)_2$
51	GB07	Medium green	Pellet	$K_{0.68}\ (Fe_{1.71}Al_{0.00}Mg_{0.34})_{2.05}\ (Si_{3.60}Al_{0.40})_4\ (O_{10})(OH)_2$
52	GB04	Medium-pale green	Benthic foram	$K_{0.66}\ (Fe_{1.58}Al_{0.06}Mg_{0.35})_{1.99}\ (Si_{3.71}Al_{0.29})_4\ (O_{10})(OH)_2$
53	GB04	Medium green	Pellet	$K_{0.64}\ (Fe_{1.63}Al_{0.09}Mg_{0.32})_{2.04}\ (Si_{3.57}Al_{0.43})_4\ (O_{10})(OH)_2$
55	WP07	Medium green	Pellet	$K_{0.75}\ (Fe_{1.48}Al_{0.12}Mg_{0.33})_{1.93}\ (Si_{3.79}Al_{0.21})_4\ (O_{10})(OH)_2$
56	WP07	Medium-dark green	Pellet	$K_{0.77}\ (Fe_{1.39}Al_{0.20}Mg_{0.35})_{2.03}\ (Si_{3.77}Al_{0.23})_4\ (O_{10})(OH)_2$
57	WP07	Dark green	Vermicular	$K_{0.71}\ (Fe_{1.36}Al_{0.24}Mg_{0.35})_{1.94}\ (Si_{3.81}Al_{0.19})_4\ (O_{10})(OH)_2$
58	WP04	Dark green	Pellet	$K_{0.76}\ (Fe_{1.26}Al_{0.28}Mg_{0.39})_{1.92}\ (Si_{3.86}Al_{0.14})_4\ (O_{10})(OH)_2$
59	WP04	Medium-dark green	Pellet	$K_{0.81}\ (Fe_{1.43}Al_{0.09}Mg_{0.40})_{1.92}\ (Si_{3.81}Al_{0.19})_4\ (O_{10})(OH)_2$
60	WP04	Medium-dark green	Amorphous	$K_{0.79}\ (Fe_{1.36}Al_{0.17}Mg_{0.40})_{1.93}\ (Si_{3.82}Al_{0.18})_4\ (O_{10})(OH)_2$
61	WP10	Medium-dark green	pellet	$K_{0.74}\ (Fe_{1.16}Al_{0.38}Mg_{0.39})_{1.92}\ (Si_{3.88}Al_{0.12})_4\ (O_{10})(OH)_2$
62	WP10	Medium-dark green	Pellet	$K_{0.82}\ (Fe_{1.34}Al_{0.20}Mg_{0.39})_{1.92}\ (Si_{3.80}Al_{0.20})_4\ (O_{10})(OH)_2$
63	WP10	Medium-dark green	Amorphous	$K_{0.84}\ (Fe_{1.31}Al_{0.21}Mg_{0.39})_{1.91}\ (Si_{3.82}Al_{0.18})_4\ (O_{10})(OH)_2$
64	RF01	Medium green	Planktic foram	$K_{0.78}\ (Fe_{1.22}Al_{0.30}Mg_{0.44})_{1.95}\ (Si_{3.80}Al_{0.20})_4\ (O_{10})(OH)_2$
65	RF01	Medium-dark green	Pellet	$K_{0.82}\ (Fe_{1.25}Al_{0.26}Mg_{0.43})_{1.94}\ (Si_{3.79}Al_{0.21})_4\ (O_{10})(OH)_2$
66	RF01	Medium-dark green	Vermicular	$K_{0.76}\ (Fe_{1.15}Al_{0.38}Mg_{0.41})_{1.94}\ (Si_{3.82}Al_{0.18})_4\ (O_{10})(OH)_2$

Table 11 – Structural formula, host grain and colour for grains 1-66 as analysed with SEM+EDS. Stoichiometric formulas were calculated based on general formula of glaucony K $(Si_{4-x}, Al_x)_{\sim 4}$ (Fe, Mg, Al)$_{\sim 2}$ $O_{10}(OH)_2$(Huggett, 2005). All Fe is expressed as Fe_2O_3

Grain Number	Sample	Colour	Host material	Structural formula
67	EQ06	Dark green	Pellet	$K_{0.63}\ (Fe_{1.07}Al_{0.54}Mg_{0.36})_{1.96}\ (Si_{3.84}Al_{0.16})_4\ (O_{10})(OH)_2$
68	EQ06	Dark green	Pellet	$K_{0.78}\ (Fe_{1.29}Al_{0.25}Mg_{0.39})_{1.93}\ (Si_{3.81}Al_{0.19})_4\ (O_{10})(OH)_2$
69	EQ06	Dark green	Pellet	$K_{0.66}\ (Fe_{1.11}Al_{0.49}Mg_{0.35})_{1.95}\ (Si_{3.84}Al_{0.16})_4\ (O_{10})(OH)_2$
70	EQ02	Medium-dark green	Amorphous	$K_{0.82}\ (Fe_{1.24}Al_{0.23}Mg_{0.47})_{1.94}\ (Si_{3.84}Al_{0.16})_4\ (O_{10})(OH)_2$
71	EQ02	Medium-dark green	Amorphous	$K_{0.82}\ (Fe_{1.26}Al_{0.26}Mg_{0.43})_{1.94}\ (Si_{3.77}Al_{0.23})_4\ (O_{10})(OH)_2$
72	EQ02	Medium-dark green	Pellet	$K_{0.80}\ (Fe_{1.30}Al_{0.17}Mg_{0.47})_{1.95}\ (Si_{3.84}Al_{0.16})_4\ (O_{10})(OH)_2$
73	RF03	Medium-dark green	Pellet	$K_{0.86}\ (Fe_{1.30}Al_{0.17}Mg_{0.46})_{1.93}\ (Si_{3.82}Al_{0.18})_4\ (O_{10})(OH)_2$
74	RF03	Medium green	Amorphous	$K_{0.79}\ (Fe_{1.26}Al_{0.26}Mg_{0.43})_{1.95}\ (Si_{3.79}Al_{0.21})_4\ (O_{10})(OH)_2$
75	RF03	Medium-dark green	Amorphous	$K_{0.81}\ (Fe_{1.28}Al_{0.25}Mg_{0.42})_{1.95}\ (Si_{3.76}Al_{0.24})_4\ (O_{10})(OH)_2$
76	CB01	Medium-dark green	Pellet	$K_{0.85}\ (Fe_{1.27}Al_{0.20}Mg_{0.46})_{1.93}\ (Si_{3.81}Al_{0.19})_4\ (O_{10})(OH)_2$
77	CB01	Medium green	Amorphous	$K_{0.80}\ (Fe_{1.21}Al_{0.31}Mg_{0.43})_{1.95}\ (Si_{3.79}Al_{0.21})_4\ (O_{10})(OH)_2$
78	CB01	Dark green	Vermicular	$K_{0.85}\ (Fe_{1.24}Al_{0.24}Mg_{0.46})_{1.93}\ (Si_{3.82}Al_{0.18})_4\ (O_{10})(OH)_2$
79	CB01	Medium-dark green	Amorphous	$K_{0.80}\ (Fe_{1.30}Al_{0.22}Mg_{0.42})_{1.95}\ (Si_{3.77}Al_{0.23})_4\ (O_{10})(OH)_2$
80	GB07	Medium-pale green	Amorphous	$K_{0.71}\ (Fe_{1.20}Al_{0.34}Mg_{0.42})_{1.96}\ (Si_{3.82}Al_{0.18})_4\ (O_{10})(OH)_2$
81	GB07	Medium-dark green	Pellet	$K_{0.82}\ (Fe_{1.27}Al_{0.22}Mg_{0.45})_{1.94}\ (Si_{3.81}Al_{0.19})_4\ (O_{10})(OH)_2$
82	GB07	Medium-dark green	Amorphous	$K_{0.85}\ (Fe_{1.27}Al_{0.23}Mg_{0.45})_{1.95}\ (Si_{3.75}Al_{0.25})_4\ (O_{10})(OH)_2$
83	GB07	Medium-pale green	Benthic foram	$K_{0.60}\ (Fe_{1.79}Al_{0.00}Mg_{0.32})_{2.11}\ (Si_{3.44}Al_{0.56})_4\ (O_{10})(OH)_2$
84	GB04	Medium-pale green	Bryozoan	$K_{0.64}\ (Fe_{1.45}Al_{0.23}Mg_{0.34})_{2.02}\ (Si_{3.66}Al_{0.44})_4\ (O_{10})(OH)_2$
85	GB04	Medium green	Amorphous	$K_{0.72}\ (Fe_{1.62}Al_{0.02}Mg_{0.35})_{1.99}\ (Si_{3.65}Al_{0.35})_4\ (O_{10})(OH)_2$
86	GB04	Medium-pale green	Benthic foram	$K_{0.65}\ (Fe_{1.62}Al_{0.10}Mg_{0.31})_{2.02}\ (Si_{3.58}Al_{0.42})_4\ (O_{10})(OH)_2$
87	WP07	Medium green	Amorphous	$K_{0.71}\ (Fe_{1.51}Al_{0.10}Mg_{0.37})_{1.98}\ (Si_{3.71}Al_{0.29})_4\ (O_{10})(OH)_2$
88	WP07	Pale green	Bryozoan	$K_{0.63}\ (Fe_{1.30}Al_{0.35}Mg_{0.35})_{2.00}\ (Si_{3.73}Al_{0.27})_4\ (O_{10})(OH)_2$
89	WP07	Medium green	Amorphous	$K_{0.66}\ (Fe_{1.65}Al_{0.01}Mg_{0.38})_{2.05}\ (Si_{3.55}Al_{0.45})_4\ (O_{10})(OH)_2$
90	WP07	Medium green	Pellet	$K_{0.81}\ (Fe_{0.96}Al_{0.71}Mg_{0.27})_{1.94}\ (Si_{3.64}Al_{0.36})_4\ (O_{10})(OH)_2$
91	WP04	Medium-dark green	Amorphous	$K_{0.77}\ (Fe_{1.32}Al_{0.21}Mg_{0.41})_{1.93}\ (Si_{3.84}Al_{0.16})_4\ (O_{10})(OH)_2$
92	WP04	Medium-dark green	Amorphous	$K_{0.78}\ (Fe_{1.31}Al_{0.20}Mg_{0.43})_{1.94}\ (Si_{3.84}Al_{0.16})_4\ (O_{10})(OH)_2$
93	WP04	Medium-dark green	Amorphous	$K_{0.77}\ (Fe_{1.34}Al_{0.19}Mg_{0.40})_{1.93}\ (Si_{3.84}Al_{0.16})_4\ (O_{10})(OH)_2$
94	WP04	Medium-dark green	Amorphous	$K_{0.79}\ (Fe_{1.27}Al_{0.23}Mg_{0.44})_{1.94}\ (Si_{3.84}Al_{0.16})_4\ (O_{10})(OH)_2$
95	WP10	Dark green	Amorphous	$K_{0.78}\ (Fe_{1.31}Al_{0.23}Mg_{0.39})_{1.93}\ (Si_{3.82}Al_{0.18})_4\ (O_{10})(OH)_2$
96	WP10	Dark green	Amorphous	$K_{0.78}\ (Fe_{1.20}Al_{0.30}Mg_{0.43})_{1.93}\ (Si_{3.87}Al_{0.13})_4\ (O_{10})(OH)_2$
97	WP10	Medium green	Amorphous	$K_{0.73}\ (Fe_{1.34}Al_{0.21}Mg_{0.39})_{1.93}\ (Si_{3.86}Al_{0.14})_4\ (O_{10})(OH)_2$
98	RF01	Dark green	Pellet	$K_{0.81}\ (Fe_{1.39}Al_{0.17}Mg_{0.36})_{1.92}\ (Si_{3.78}Al_{0.22})_4\ (O_{10})(OH)_2$
99	RF01	Dark green	Amorphous	$K_{0.81}\ (Fe_{1.40}Al_{0.16}Mg_{0.37})_{1.92}\ (Si_{3.79}Al_{0.21})_4\ (O_{10})(OH)_2$
100	RF01	Medium green	Amorphous	$K_{0.81}\ (Fe_{1.19}Al_{0.30}Mg_{0.45})_{1.94}\ (Si_{3.83}Al_{0.17})_4\ (O_{10})(OH)_2$
101	OP01	Pale green	Bioclast	$K_{0.71}\ (Fe_{1.30}Al_{0.36}Mg_{0.37})_{2.04}\ (Si_{3.54}Al_{0.46})_4\ (O_{10})(OH)_2$
102	OP01	Pale green	Bioclast	$K_{0.71}\ (Fe_{1.21}Al_{0.44}Mg_{0.39})_{2.04}\ (Si_{3.57}Al_{0.43})_4\ (O_{10})(OH)_2$
103	OP01	Pale green	Bioclast	$K_{0.74}\ (Fe_{1.27}Al_{0.36}Mg_{0.41})_{2.04}\ (Si_{3.55}Al_{0.45})_4\ (O_{10})(OH)_2$
104	OP01	Pale green	Bioclast	$K_{0.56}\ (Fe_{0.96}Al_{0.79}Mg_{0.29})_{2.04}\ (Si_{3.60}Al_{0.40})_4\ (O_{10})(OH)_2$
105	OP01	Pale green	Bioclast	$K_{0.62}\ (Fe_{1.03}Al_{0.64}Mg_{0.37})_{2.04}\ (Si_{3.62}Al_{0.38})_4\ (O_{10})(OH)_2$
107	OP01	Pale green	Bioclast	$K_{0.62}\ (Fe_{0.99}Al_{0.69}Mg_{0.36})_{2.05}\ (Si_{3.61}Al_{0.39})_4\ (O_{10})(OH)_2$
108	OP01	Pale green	Bioclast	$K_{0.65}\ (Fe_{1.08}Al_{0.57}Mg_{0.38})_{2.04}\ (Si_{3.61}Al_{0.39})_4\ (O_{10})(OH)_2$
109	OP01	Pale green	Bioclast	$K_{0.65}\ (Fe_{1.14}Al_{0.53}Mg_{0.38})_{2.05}\ (Si_{3.58}Al_{0.42})_4\ (O_{10})(OH)_2$
110	OP01	Pale green	Bioclast	$K_{0.60}\ (Fe_{1.00}Al_{0.67}Mg_{0.37})_{2.03}\ (Si_{3.67}Al_{0.33})_4\ (O_{10})(OH)_2$

Table 12 – Structural formula, host grain and colour for grains 67-110 as analysed with SEM+EDS. Stoichiometric formulas were calculated based on general formula of glaucony K $(Si_{4-x}, Al_x)_{\sim 4}$ (Fe, Mg, Al)$_{\sim 2}$ $O_{10}(OH)_2$(Huggett, 2005). All Fe is expressed as Fe_2O_3

Grain number	Outcrop	MgO	Al_2O_3	SiO_2	K_2O	Fe_2O_3
		Weight %				
101	OP01-01.	3.70	10.22	52.29	8.24	25.55
102	OP01-02.	3.86	10.93	53.10	8.23	23.87
103	OP01-03.	4.09	10.07	52.44	8.51	24.89
104	OP01-04.	3.03	15.55	55.19	6.77	19.47
105	OP01-05.	3.81	13.09	55.00	7.35	20.75
107	OP01-07.	3.70	13.90	54.94	7.35	20.11
108	OP01-08.	3.86	12.29	54.48	7.65	21.72
109	OP01-09.	3.81	12.13	53.65	7.68	22.73
110	OP01-10.	3.75	12.87	55.94	7.20	20.23
70	EQ02	4.63	4.89	56.65	9.47	24.36
71	EQ02	4.21	6.11	55.56	9.48	24.64
37	EQ02	4.19	5.62	56.21	9.21	24.77
38	EQ02	4.19	5.42	54.66	9.65	26.08
72	EQ02	4.68	4.19	56.48	9.20	25.46
39	EQ02	4.13	6.53	55.90	9.43	24.00
35	EQ06	3.85	7.12	57.30	8.00	23.73
1	EQ06	3.84	7.14	55.91	9.31	23.79
2	EQ06	3.66	7.92	57.12	8.61	22.69
34	EQ06	3.80	7.26	56.81	8.58	23.56
67	EQ06	3.62	8.97	58.29	7.48	21.64
68	EQ06	3.86	5.51	56.24	9.02	25.37
69	EQ06	3.57	8.34	57.99	7.78	22.31
36	EQ06	3.96	6.14	56.96	8.52	24.42
3	EQ06	4.13	6.17	57.66	8.61	23.43
40	EQ08	4.37	7.90	55.84	7.97	23.92
42	EQ08	4.19	7.48	56.89	9.06	22.39
41	EQ08	4.90	7.55	56.68	8.52	22.34
100	RF01	4.43	5.86	56.84	9.38	23.49
64	RF01	4.34	6.26	56.38	9.06	23.97
99	RF01	3.60	4.57	55.39	9.27	27.17
33	RF01	3.68	9.59	59.51	6.97	20.26
65	RF01	4.24	5.94	55.89	9.45	24.49
98	RF01	3.51	4.86	55.27	9.29	27.06
32	RF01	5.38	8.87	59.83	7.47	18.45
66	RF01	4.11	7.17	57.01	8.92	22.79
74	RF03	4.22	5.96	55.96	9.14	24.71
75	RF03	4.14	6.06	55.40	9.39	25.00
44	RF03	4.19	6.06	56.58	8.97	24.21
43	RF03	4.14	5.46	55.14	9.71	25.55
45	RF03	4.23	6.93	56.92	8.40	23.52
73	RF03	4.56	4.41	55.93	9.84	25.26
77	CB01	4.28	6.48	56.20	9.31	23.74
79	CB01	4.16	5.65	55.47	9.23	25.48
48	CB01	4.10	5.82	56.09	8.91	25.09

Grain number	Outcrop	MgO	Al_2O_3	SiO_2	K_2O	Fe_2O_3
		Weight %				
46	CB01	4.43	5.85	55.62	9.22	24.87
76	CB01	4.49	4.88	55.98	9.76	24.89
47	CB01	4.45	7.04	56.35	9.54	22.62
78	CB01	4.54	5.20	56.26	9.81	24.19
52	GB04	3.43	4.37	54.03	7.57	30.60
86	GB04	3.00	6.31	52.02	7.44	31.23
85	GB04	3.37	4.54	52.72	8.18	31.20
84	GB04	3.33	7.18	53.83	7.34	28.33
53	GB04	3.14	6.36	51.81	7.29	31.40
82	GB07	4.41	6.08	54.98	9.73	24.80
49	GB07	3.54	4.92	53.62	7.99	29.92
50	GB07	3.17	5.98	51.55	7.61	31.69
83	GB07	3.11	6.65	49.35	6.75	34.15
80	GB07	4.24	6.56	57.02	8.34	23.85
51	GB07	3.24	4.59	51.80	7.67	32.70
81	GB07	4.40	5.17	56.08	9.44	24.92
60	WP04	3.91	4.40	55.99	9.10	26.60
91	WP04	4.03	4.65	56.61	8.91	25.81
92	WP04	4.27	4.49	56.57	8.97	25.71
93	WP04	3.92	4.34	56.53	8.94	26.27
94	WP04	4.33	4.97	56.71	9.12	24.88
25	WP04	3.31	5.00	56.56	8.53	26.60
26	WP04	3.48	5.72	59.58	8.13	23.10
27	WP04	3.50	4.59	57.76	8.87	25.29
58	WP04	3.88	5.23	57.33	8.79	24.76
59	WP04	3.89	3.45	55.57	9.29	27.79
22	WP07	3.68	6.69	58.73	7.78	23.13
89	WP07	3.67	5.73	51.35	7.52	31.73
87	WP07	3.61	4.84	54.05	8.17	29.33
88	WP07	3.50	7.90	55.58	7.34	25.68
23	WP07	3.48	6.97	57.44	8.41	23.70
55	WP07	3.26	4.10	55.33	8.64	28.67
56	WP07	3.47	5.29	55.37	8.87	27.01
90	WP07	2.72	13.76	54.80	9.56	19.16
57	WP07	3.49	5.32	56.36	8.17	26.66
63	WP10	3.85	4.87	55.99	9.64	25.64
95	WP10	3.86	5.14	56.32	9.04	25.65
96	WP10	4.32	5.40	57.59	9.06	23.63
97	WP10	3.82	4.28	57.13	8.47	26.29
28	WP10	3.73	8.38	58.51	8.44	20.93
29	WP10	3.61	6.99	59.34	7.90	22.15
61	WP10	3.88	6.40	58.04	8.66	23.03
62	WP10	3.79	5.03	55.67	9.43	26.07

Table 13 – Major element concentrations for all grains measured by SEM+EDS

	Sc	Ti	V	Cr	Mn	Co	Ni	Cu	Zn	Ga	Rb	Sr	Y	Zr	Nb	Cs	Ba
								ppm									
OP01-01.	5.72	281.93	341.42	193.52	31.44	18.09	66.22	74.11	186.96	29.54	573.85	29.43	0.77	35.26	0.52	23.57	32.03
OP01-02.	7.80	453.15	350.02	249.84	53.44	20.05	78.59	73.95	187.07	29.00	568.46	29.60	1.00	40.96	1.02	37.39	37.43
OP01-03.	7.83	476.21	390.82	271.75	69.96	21.85	86.26	70.61	205.28	27.99	606.91	44.91	21.77	38.87	1.20	52.87	25.90
OP01-04.	4.63	636.96	534.37	268.52	32.70	18.12	74.19	29.50	192.86	38.50	646.66	31.02	0.58	48.52	1.00	30.45	52.60
OP01-05.	6.43	537.96	484.18	236.41	33.22	19.34	78.30	36.64	241.53	32.43	632.91	31.77	0.64	45.95	0.85	40.95	48.20
OP01-06.	0.76	84.44	0.86	1.74	20.79	0.18	1.74	11.44	5.37	0.91	26.17	26.75	1.00	85.60	0.24	0.35	165.16
OP01-07.	12.78	588.58	426.23	272.29	113.76	24.07	72.67	55.76	202.30	25.19	567.68	62.48	2.14	40.68	1.16	54.35	55.50
OP01-08.	8.85	525.39	407.44	315.66	52.12	24.74	103.09	28.23	178.80	24.37	488.33	109.27	3.71	39.30	1.04	35.64	52.86
OP01-09.	8.66	562.60	410.42	257.73	81.41	25.10	73.95	53.29	180.15	27.78	552.05	51.10	0.94	40.30	1.09	35.42	42.64
OP01-10.	9.26	454.47	416.83	302.02	54.42	22.62	74.95	58.67	195.67	27.81	579.00	46.17	0.96	40.23	1.09	44.61	41.96
JS03-67-EQ06	10.25	360.25	109.95	172.25	67.21	3.55	28.25	11.34	96.24	22.88	245.48	10.94	0.29	14.85	1.00	4.01	6.11
JS03-69-EQ06	9.25	279.89	112.62	140.35	54.19	3.43	26.67	9.36	94.86	25.20	264.83	10.04	0.36	14.67	1.15	3.04	7.30
JS02-34-EQ06	9.67	330.10	121.15	151.20	48.20	3.69	27.06	13.87	115.61	23.34	248.49	11.09	2.98	15.37	0.94	4.89	5.98
JS01-01-EQ06	7.17	377.02	72.93	179.12	20.63	1.17	24.29	12.24	113.57	18.02	250.29	11.99	4.95	10.31	1.11	1.49	1.66
JS01-02-EQ06	6.47	289.73	86.60	238.86	15.45	1.32	26.31	15.11	117.83	16.56	247.83	13.52	7.02	8.04	0.77	2.15	1.95
JS01-03-EQ06	6.24	322.41	79.42	351.12	22.39	1.51	29.11	15.72	128.28	16.23	264.12	14.89	6.28	6.83	1.07	4.20	1.98
JS03-71-EQ02	7.23	238.62	81.83	193.38	11.39	1.17	27.10	12.67	100.88	15.38	287.25	5.92	3.92	10.49	0.90	3.19	1.73
JS01-04-EQ02	11.81	834.62	121.11	191.19	31.78	3.93	27.82	16.50	125.20	21.48	218.99	11.07	1.12	27.27	1.37	7.52	18.95
JS01-05-EQ02	10.85	542.63	125.33	210.31	23.12	3.37	25.91	16.09	113.31	22.81	228.07	9.94	0.41	16.03	0.86	5.75	9.10
JS02-40-EQ08	6.32	534.87	302.65	191.07	12.48	1.96	44.36	55.61	266.89	19.71	226.92	12.32	4.82	13.46	0.91	3.27	3.59
JS02-42-EQ08	7.30	259.71	120.24	196.46	13.36	2.79	35.20	37.65	152.86	24.81	264.63	7.83	2.71	13.94	1.29	2.58	14.07
JS03-73-RF03	5.45	193.72	96.99	194.34	5.08	2.25	29.04	14.80	94.03	16.07	293.02	3.09	0.12	18.12	1.92	1.26	2.21
JS03-75-RF03	6.58	286.53	70.99	314.10	7.91	4.20	31.40	13.48	130.54	17.51	266.30	3.77	0.13	20.52	1.76	1.57	3.00
JS02-44-RF03	9.23	540.10	119.95	348.25	8.49	2.94	31.72	27.61	166.12	19.00	264.78	23.65	10.71	20.15	1.74	5.06	5.19
JS02-45-RF03	8.30	358.49	106.89	362.05	6.47	2.66	31.71	40.49	147.34	16.44	256.02	13.63	9.94	22.14	1.84	3.41	5.28
JS03-98-RF01	20.73	917.08	151.32	294.91	45.22	1.13	21.74	19.79	125.83	25.72	344.01	7.74	0.68	17.55	2.84	5.02	22.57
JS02-64-RF01	8.83	489.86	85.47	266.80	13.34	3.21	30.83	33.10	171.32	19.33	247.89	8.87	5.66	21.37	1.92	3.15	4.07
JS02-66-RF01	5.61	351.26	79.26	190.00	27.02	4.92	29.67	40.26	182.01	24.05	288.43	9.17	2.89	11.69	1.83	5.03	7.00
JS03-76-CB01	6.54	246.86	69.61	314.62	6.02	2.87	32.20	18.87	118.47	16.99	280.89	7.72	3.12	20.23	1.75	1.51	3.49
JS03-79-CB01	6.52	191.67	75.83	231.13	6.76	3.48	29.44	11.49	117.29	16.68	266.54	7.38	8.11	22.77	1.52	1.77	3.34
JS02-47-CB01	6.86	377.93	75.26	368.69	7.32	3.27	33.19	22.23	153.15	17.26	272.01	9.44	8.56	20.49	1.68	3.31	4.07
JS03-80-GB07	8.43	375.80	123.56	384.20	12.40	3.98	32.34	21.84	128.94	15.34	251.43	11.21	14.27	24.26	1.91	3.77	5.10
JS03-81_GB07	7.42	318.29	84.40	301.51	7.76	3.03	33.98	19.13	133.83	18.93	272.18	6.90	9.41	23.38	2.12	2.65	3.71
JS03-83-GB07	6.41	1625.16	453.72	138.91	105.23	16.05	97.35	35.49	233.22	12.41	270.44	16.99	2.82	39.66	5.83	13.85	46.53
JS02-50-GB07	5.84	402.46	121.53	90.57	41.64	12.96	54.46	30.37	267.98	11.82	260.01	12.12	3.64	26.48	1.97	7.16	13.42
JS02-51_GB07	3.85	332.33	116.43	81.40	49.82	12.30	58.16	29.23	216.64	10.63	247.30	9.96	10.17	17.82	1.62	5.39	8.78
JS03-85-GB04	3.81	155.69	86.13	84.16	45.80	9.36	45.47	14.72	141.36	9.78	238.57	7.58	0.85	15.56	0.89	4.17	9.37
JS02-53-GB04	7.04	833.35	159.60	145.91	63.16	15.22	118.20	43.98	280.70	10.53	237.33	15.56	1.48	25.74	2.22	5.76	25.88
JS02-54-GB04	6.66	517.07	79.02	167.16	31.19	11.12	49.31	50.34	199.10	9.34	249.21	9.60	0.65	20.68	1.22	6.50	9.63
JS03-87-WP07	3.36	176.96	71.91	117.28	19.48	7.39	50.23	12.58	144.06	9.15	244.38	5.81	0.19	13.59	0.65	3.24	6.64
JS03-89-WP07	4.79	785.03	244.52	193.76	42.11	8.98	94.61	13.59	163.22	8.82	226.85	7.36	0.76	20.21	3.42	3.81	4.72
JS02-55-WP07	12.43	667.43	221.20	395.82	27.08	1.56	8.31	29.01	173.64	21.01	377.99	5.76	0.90	22.78	4.22	6.26	7.44
JS02-56-WP07	15.24	837.95	225.49	345.33	40.07	1.84	7.88	22.46	183.14	23.78	365.67	6.40	0.73	21.74	4.26	6.14	17.43
JS02-57-WP07	13.80	755.71	246.76	393.02	56.83	3.61	9.51	36.39	215.59	23.45	356.69	7.94	1.07	30.76	4.11	6.79	8.33
JS01-22-WP07	25.75	1354.16	299.56	482.07	83.96	4.24	10.03	40.10	210.59	27.91	313.37	8.17	2.90	24.25	3.01	6.72	14.25
JS01-23-WP07	11.56	565.03	222.21	357.50	157.08	5.07	14.40	36.99	209.68	20.86	367.82	6.41	2.15	20.85	3.01	8.44	4.76
JS01-24-WP07	23.00	2050.23	359.71	457.32	67.36	3.62	9.82	41.82	206.26	39.16	335.49	7.30	1.63	52.18	10.71	4.46	122.78
JS03-91-WP04	15.15	745.24	258.28	306.02	29.80	2.36	9.40	20.11	147.70	22.02	363.11	7.53	2.22	23.25	4.32	6.44	3.86
JS03-94-WP04	20.84	770.80	318.17	252.81	55.41	3.72	11.99	10.18	194.20	33.15	362.25	5.37	0.45	30.74	7.76	2.97	33.54
JS02-58-WP04	22.55	949.30	226.92	236.18	43.04	3.49	11.20	11.60	209.01	23.19	370.56	7.04	0.73	27.73	4.23	8.88	33.67
JS02-59-WP04	17.34	568.83	221.63	274.26	45.44	4.39	12.40	13.05	188.62	21.97	361.36	6.29	0.53	23.66	4.68	6.75	37.51
JS02-60-WP04	33.63	1552.15	293.14	285.41	59.11	4.50	13.68	15.48	229.40	35.58	360.65	6.29	0.32	35.28	5.79	4.22	16.01
JS01-25-WP04	32.99	1687.16	300.26	504.69	124.11	6.57	14.31	13.73	236.97	31.02	342.63	4.33	0.53	36.47	4.60	5.79	6.61
JS01-26-WP04	19.09	848.91	200.54	343.65	57.38	4.74	11.87	18.07	169.45	20.85	315.80	8.26	0.22	23.68	4.32	7.50	18.06
JS01-27-WP04	22.18	1264.80	216.45	489.81	27.00	1.85	10.02	36.19	167.19	26.06	301.02	12.97	1.30	17.82	1.59	10.92	37.22
JS03-95-WP10	22.42	795.27	345.48	263.99	95.49	4.25	12.95	8.42	183.78	30.73	375.67	7.54	0.67	33.21	7.26	2.82	30.12
JS03-96-WP10	29.14	1046.27	363.20	320.63	54.08	3.59	11.53	9.29	204.34	32.26	360.86	4.73	0.53	37.19	8.53	3.22	24.51
JS02-61-WP10	11.68	328.81	270.26	294.99	17.46	1.59	10.35	17.27	166.58	30.30	365.71	4.39	3.01	13.42	4.06	3.17	44.27
JS01-28-WP10	9.31	546.73	123.08	369.78	12.42	4.97	36.91	21.51	165.80	18.76	239.18	10.15	2.31	18.74	1.49	6.48	9.36

Table 14 – Trace element concentrations for all grains as measured by LA-ICP-MS

	La	Ce	Pr	Nd	Sm	Eu	Gd	Tb	Dy	Ho	Er	Tm	Yb	Lu	Hf	Ta	Pb	Th	U
	ppm																		
OP01-01.	0.52	1.07	0.18	0.84	0.21	0.04	0.21	0.02	0.13	0.03	0.05	0.01	0.04	0.01	2.41	0.03	7.13	0.29	0.37
OP01-02.	0.82	1.47	0.28	1.16	0.30	0.07	0.25	0.03	0.19	0.03	0.08	0.01	0.05	0.01	2.94	0.06	6.81	0.58	0.40
OP01-03.	17.22	32.33	5.71	27.27	6.31	1.33	5.57	0.71	3.73	0.66	1.54	0.14	0.80	0.09	2.42	0.11	11.70	1.58	1.55
OP01-04.	0.81	0.61	0.14	0.55	0.11	0.15	0.10	0.01	0.09	0.02	0.04	0.01	0.07	0.01	3.07	0.08	8.34	0.16	0.40
OP01-05.	0.47	1.00	0.10	0.43	0.14	0.03	0.10	0.02	0.12	0.02	0.07	0.01	0.06	0.01	3.35	0.07	11.16	0.33	0.39
OP01-06.	1.20	2.83	0.22	0.85	0.13	0.11	0.10	0.02	0.13	0.03	0.10	0.01	0.15	0.02	2.05	0.02	6.94	0.28	0.20
OP01-07.	1.07	3.64	0.74	3.52	1.06	0.17	0.80	bdl	0.49	0.07	0.22	0.04	0.24	0.03	2.87	0.11	20.12	0.85	0.57
OP01-08.	3.20	5.07	1.05	5.15	1.07	0.22	0.88	0.14	0.71	0.14	0.28	0.04	0.23	0.03	2.42	0.07	17.71	1.12	0.97
OP01-09.	0.79	2.00	0.22	0.83	0.19	0.03	0.21	0.03	0.15	0.04	0.09	0.01	0.07	0.01	2.50	0.11	18.88	0.28	0.46
OP01-10.	0.95	1.58	0.26	1.38	0.29	0.05	0.22	0.03	0.22	0.04	0.08	0.01	0.05	0.01	2.85	0.06	7.48	0.39	0.37
JS03-67-EQ06	0.23	0.54	0.06	0.25	0.05	0.02	0.03	0.01	0.04	0.01	0.02	bdl	0.02	0.00	0.63	0.05	2.35	0.05	0.46
JS03-69-EQ06	0.23	0.50	0.06	0.28	0.06	0.01	0.06	0.01	0.05	0.00	0.02	0.00	0.02	0.00	0.51	0.05	2.96	0.06	0.46
JS02-34-EQ06	1.29	3.53	0.42	2.00	0.55	0.13	0.52	0.08	0.40	0.08	0.23	0.04	0.19	0.03	0.52	0.05	3.38	0.11	0.51
JS01-01-EQ06	1.90	3.01	0.49	2.31	0.57	0.14	0.60	0.09	0.55	0.11	0.29	0.03	0.22	0.03	0.33	0.04	2.50	0.15	0.76
JS01-02-EQ06	4.26	5.46	0.91	4.18	0.86	0.21	0.93	0.13	0.81	0.16	0.41	0.05	0.29	0.04	0.32	0.04	2.86	0.12	0.54
JS01-03-EQ06	4.78	6.11	0.98	4.48	0.79	0.20	0.83	0.11	0.67	0.14	0.36	0.04	0.25	0.03	0.25	0.04	3.46	0.16	0.49
JS03-71-EQ02	1.87	2.24	0.43	2.02	0.50	0.10	0.48	0.07	0.44	0.09	0.27	0.03	0.18	0.02	0.42	0.04	1.27	0.09	0.45
JS01-04-EQ02	2.44	4.65	0.37	1.40	0.24	0.05	0.24	0.04	0.19	0.04	0.10	0.02	0.14	0.02	1.01	0.11	4.10	0.31	0.82
JS01-05-EQ02	0.35	0.73	0.08	0.47	0.10	0.01	0.04	0.01	0.06	0.02	0.04	0.00	0.04	0.01	0.67	0.06	2.81	0.07	0.47
JS02-40-EQ08	1.70	2.96	0.60	2.78	0.74	0.19	0.67	0.11	0.72	0.13	0.34	0.04	0.24	0.03	0.61	0.05	6.53	0.31	0.91
JS02-42-EQ08	1.64	2.38	0.46	2.07	0.47	0.10	0.44	0.06	0.33	0.06	0.17	0.02	0.14	0.01	0.39	0.04	5.62	0.23	0.75
JS03-73-RF03	0.08	0.06	0.01	0.06	0.01	0.00	0.02	0.00	0.02	bdl	0.01	0.00	bdl	bdl	0.58	0.05	1.34	0.02	0.59
JS03-75-RF03	0.06	0.08	0.02	0.07	0.01	0.00	0.01	0.00	0.01	0.00	0.01	bdl	bdl	bdl	0.70	0.07	1.71	0.02	0.63
JS02-44-RF03	8.14	8.05	1.59	7.62	1.50	0.33	1.43	0.20	1.13	0.26	0.64	0.07	0.42	0.05	0.93	0.10	5.30	0.52	0.62
JS02-45-RF03	6.48	6.96	1.35	6.43	1.37	0.30	1.41	0.19	1.09	0.23	0.56	0.07	0.37	0.05	0.94	0.07	5.01	0.46	0.52
JS03-98-RF01	1.00	3.13	0.26	1.15	0.22	0.05	0.14	0.02	0.10	0.03	0.06	0.01	0.08	0.01	0.81	0.11	5.56	0.77	0.50
JS02-64-RF01	3.52	3.84	0.82	3.48	0.74	0.18	0.78	0.10	0.61	0.13	0.34	0.04	0.27	0.03	0.93	0.11	6.30	0.16	0.73
JS02-66-RF01	1.35	1.65	0.36	1.63	0.33	0.09	0.40	0.06	0.34	0.08	0.19	0.02	0.10	0.02	0.64	0.15	9.83	0.14	0.69
JS03-76-CB01	1.34	1.67	0.33	1.58	0.38	0.08	0.38	0.06	0.37	0.07	0.20	0.02	0.12	0.02	0.81	0.06	1.63	0.12	0.48
JS03-79-CB01	4.28	4.94	1.05	4.79	1.10	0.25	1.16	0.16	1.06	0.21	0.50	0.05	0.28	0.04	0.87	0.05	1.74	0.15	0.62
JS02-47-CB01	5.42	5.71	1.15	5.63	1.16	0.27	1.26	0.17	1.06	0.21	0.53	0.06	0.32	0.05	0.86	0.08	4.86	0.66	0.78
JS03-80-GB07	7.34	9.13	1.74	8.34	1.80	0.44	1.99	0.27	1.57	0.33	0.83	0.08	0.54	0.07	1.19	0.08	2.28	0.18	0.45
JS03-81_GB07	4.30	5.39	1.11	5.24	1.18	0.25	1.32	0.19	1.19	0.25	0.59	0.07	0.41	0.06	0.93	0.08	2.44	0.20	0.67
JS03-83-GB07	1.85	2.46	0.32	1.52	0.36	0.09	0.37	0.05	0.43	0.09	0.31	0.04	0.40	0.05	1.10	0.20	25.93	1.24	0.52
JS02-50-GB07	1.54	3.77	0.53	2.35	0.55	0.12	0.65	0.09	0.52	0.10	0.24	0.03	0.15	0.02	1.01	0.05	9.25	0.37	0.20
JS02-51_GB07	4.97	8.85	1.31	6.39	1.37	0.33	1.54	0.20	1.17	0.25	0.55	0.06	0.33	0.04	0.58	0.05	9.74	0.36	0.28
JS03-85-GB04	0.42	0.82	0.10	0.40	0.10	0.02	0.11	0.01	0.10	0.02	0.08	0.01	0.04	0.01	0.58	0.02	4.59	0.24	0.31
JS02-53-GB04	1.18	1.79	0.27	1.04	0.24	0.07	0.21	0.03	0.18	0.04	0.11	0.02	0.09	0.02	1.04	0.12	30.30	0.36	0.35
JS02-54-GB04	0.42	0.80	0.10	0.44	0.11	0.02	0.08	0.01	0.10	0.02	0.05	0.01	0.05	0.00	0.79	0.06	7.61	0.17	0.33
JS03-87-WP07	0.07	0.14	0.02	0.05	0.02	0.01	0.02	0.01	0.02	0.01	0.02	bdl	0.02	0.00	0.43	0.03	3.94	0.07	0.32
JS03-89-WP07	0.33	0.44	0.06	0.22	0.10	0.02	0.09	0.01	0.09	0.02	0.07	0.01	0.08	0.01	0.64	0.09	11.75	0.17	0.40
JS02-55-WP07	3.57	12.13	0.89	3.38	0.66	0.12	0.39	0.05	0.27	0.04	0.09	0.01	0.08	0.01	0.71	0.07	5.41	2.01	1.20
JS02-56-WP07	4.02	14.87	1.04	3.83	0.70	0.10	0.36	0.05	0.19	0.04	0.07	0.01	0.09	0.01	0.82	0.08	6.55	1.76	0.81
JS02-57-WP07	5.87	20.88	1.46	5.78	1.00	0.17	0.58	0.07	0.31	0.05	0.13	0.02	0.10	0.02	1.10	0.09	6.69	2.20	0.85
JS01-22-WP07	16.38	61.23	4.30	15.80	2.66	0.47	1.46	0.17	0.82	0.12	0.30	0.04	0.19	0.03	1.00	0.10	5.78	3.41	1.34
JS01-23-WP07	11.83	44.56	3.05	11.44	1.88	0.35	1.07	0.12	0.57	0.08	0.20	0.02	0.15	0.02	0.57	0.07	5.38	2.46	1.12
JS01-24-WP07	5.78	22.69	1.52	5.86	0.89	0.16	0.47	0.07	0.32	0.07	0.20	0.04	0.32	0.05	1.48	0.24	7.37	3.39	2.00
JS03-91-WP04	7.92	30.83	2.37	9.13	1.70	0.27	1.06	0.14	0.63	0.10	0.26	0.03	0.20	0.02	0.66	0.06	2.10	0.79	0.41
JS03-94-WP04	0.79	3.29	0.26	1.04	0.22	0.04	0.13	0.02	0.09	0.02	0.04	0.01	0.08	0.02	0.86	0.06	2.20	0.16	0.28
JS02-58-WP04	2.48	9.41	0.69	2.51	0.52	0.09	0.33	0.04	0.23	0.03	0.07	0.01	0.08	0.01	0.95	0.07	4.68	0.25	0.34
JS02-59-WP04	1.70	6.73	0.47	1.77	0.32	0.06	0.24	0.03	0.14	0.02	0.06	0.01	0.07	0.01	0.67	0.04	6.33	0.18	0.33
JS02-60-WP04	0.31	1.14	0.09	0.39	0.08	0.02	0.08	0.01	0.06	0.01	0.04	0.01	0.07	0.01	1.24	0.09	5.16	0.16	0.27
JS01-25-WP04	5.09	17.01	1.12	3.93	0.59	0.10	0.33	0.03	0.16	0.03	0.06	0.01	0.06	0.01	1.33	0.11	4.07	2.16	0.78
JS01-26-WP04	0.47	1.34	0.10	0.37	0.05	0.01	0.04	0.01	0.02	0.02	0.01	bdl	0.04	0.01	0.65	0.06	2.79	0.10	0.41
JS01-27-WP04	6.73	19.27	1.46	5.36	0.90	0.14	0.49	0.05	0.33	0.04	0.12	0.02	0.11	0.02	0.86	0.12	6.04	2.29	2.31
JS03-95-WP10	2.12	7.76	0.54	2.07	0.42	0.08	0.26	0.04	0.19	0.03	0.06	0.02	0.11	0.02	0.97	0.08	2.88	0.76	0.50
JS03-96-WP10	0.70	2.89	0.24	0.94	0.21	0.04	0.15	0.02	0.12	0.02	0.06	0.01	0.08	0.01	1.04	0.07	2.35	0.18	0.33
JS02-61-WP10	7.31	32.00	2.29	8.64	2.02	0.37	1.29	0.17	0.78	0.15	0.27	0.03	0.24	0.04	0.40	0.05	5.45	1.96	1.81
JS01-28-WP10	1.79	2.26	0.36	1.76	0.36	0.08	0.31	0.05	0.26	0.05	0.14	0.01	0.11	0.01	0.93	0.11	3.41	0.30	0.70

Table 15 – Rare earth element concentrations for all grains measured with LA-ICP-MS

	Oparara	Earthquakes	Ross Farm	Campbell's Beach	Gee's Beach	Waipara	All
Average	0.180	0.091	0.127	0.172	0.149	0.134	0.142
Maximum	0.438	0.122	0.166	0.259	0.217	0.370	0.192
Minimum	0.069	0.046	0.081	0.057	0.075	0.050	0.068
Range	0.369	0.076	0.085	0.203	0.142	0.320	0.124

Table 16 – Rare earth elements for all sampled outcrops normalised to NASC Gromet et al. (1984)

Table 17 – R^2 values showing correlation between SiO_2, MgO and Fe_2O_3 with K_2O

	$\mathbf{SiO_2}$	$\mathbf{Fe_2O_3}$	**MgO**	$\mathbf{Al_2O_3}$
Waipara	-0.53	0.24	0.25	-0.37
Gee's Beach	0.55	-0.65	0.82	-0.05
Campbell's Beach	0.14	0.13	0.76	-0.11
Ross Farm	-0.85	0.7	0.64	-0.86
Earthquakes	-0.6	0.47	0.61	-0.57
Oparara	-0.84	0.91	0.53	-0.93
All grains	0.04	0	0.47	-0.25

Table 18 – R^2 values showing correlation between K with V, Cr, Rb and Ti.

	Cr	V	Rb	Ti
Waipara (N=20)	0.06	0.37	0.52	0.00
Gee's Beach (N=8)	0.19	0.76	0.00	0.73
Campbell's Beach (N=3)	0.86	0.30	0.60	0.55
Ross Farm (N=7)	0.67	0.21	0.86	0.42
Earthquakes (N=11)	0.08	0.06	0.47	0.64
Oparara (N=10)	0.13	0.48	0.00	0.54

Solubility results

Sample number	Mass of solid (g)	Volume of water (ml)	Time (hours)	pH
WP07A	0.370	40	25	3.66
WP07B	0.398	40	25	3.6
WP07C	0.367	40	25	3.65
WP07D	0.369	40	73	3.67
WP07E	0.373	40	73	3.66
WP07F	0.344	40	73	3.69
WP07G	0.375	40	190	3.64
WP07H	0.367	40	190	3.52
WP07I	0.377	40	190	3.48
WP07J	0.365	40	382	3.47
WP07K	0.371	40	382	3.48
WP07L	0.383	40	382	3.48
WP07M (distilled water sample)	0.000	40	25	5.25
WP07N (distilled water sample)	0.000	40	382	7.26

Table 19 – Solubility testing set up

Table 20 – Concentration of elements dissolved from glaucony as measured by ICP-MS. All concentrations are measured in ppb

Time (hours)	25			73			190			382			Water sample
Sample	WP07A	WP07B	WP07C	WP07D	WP07E	WP07F	WP07G	WP07H	WP07I	WP07J	WP07K	WP07L	WP07M
23 Na	320.52	362.99	286.64	307.36	320.17	340.11	345.09	449.90	541.55	384.05	472.85	480.55	4.48
24 Mg	5.53	4.56	2.91	5.86	3.59	3.94	6.78	13.46	18.23	16.29	22.12	26.37	0.85
27 Al	1.22	1.01	0.78	8.46	0.94	1.00	1.25	0.98	1.17	1.25	1.35	1.70	0.99
31 P	37.51	45.19	53.94	53.93	56.97	35.82	26.35	15.24	7.31	3.83	4.02	3.84	0.22
39 K	711.75	794.97	649.13	826.78	773.80	844.71	1116.85	1502.18	1626.35	1518.35	1697.44	1698.25	28.02
43 Ca	3.98	3.27	1.69	3.28	1.77	2.48	2.46	1.80	3.37	3.33	4.80	31.84	1.01
44 Ca	3.24	3.50	1.86	5.83	2.31	2.89	2.66	4.56	5.42	7.57	6.80	43.19	1.74
51 V	<0.000	<0.000	<0.000	<0.000	<0.000	<0.000	<0.000	<0.000	<0.000	<0.000	<0.000	<0.000	<0.000
53 Cr	0.13	0.09	<0.000	<0.000	<0.000	<0.000	<0.000	<0.000	<0.000	<0.000	<0.000	<0.000	<0.000
55 Mn	0.10	0.06	0.04	0.07	0.05	0.04	0.07	0.12	0.19	0.17	0.25	0.64	0.01
57 Fe	5.39	3.02	2.07	25.73	3.92	3.69	11.35	10.30	14.13	22.96	22.13	26.97	0.41
59 Co	0.07	0.07	0.05	0.05	0.05	0.05	0.04	0.04	0.05	0.07	0.06	0.07	0.03
60 Ni	<0.000	<0.000	<0.000	<0.000	<0.000	<0.000	<0.000	<0.000	0.00	0.02	0.05	0.04	<0.000
63 Cu	3.81	5.33	3.99	3.48	3.13	3.58	3.18	3.23	3.91	3.56	3.94	3.78	2.96
66 Zn	0.51	0.77	0.21	0.41	0.19	0.54	0.09	0.46	0.58	0.81	0.88	1.28	0.15
75 As	1.01	1.39	1.28	1.15	1.38	0.81	0.84	0.61	0.48	0.56	0.42	0.51	<0.000
88 Sr	0.11	0.09	0.05	0.12	0.05	0.06	0.11	0.19	0.27	0.25	0.34	0.46	0.01
90 Zr	0.53	0.38	0.28	0.23	0.20	0.17	0.13	0.12	0.11	0.10	0.09	0.08	0.08
101 Ru	0.02	0.01	0.01	0.00	0.00	0.00	0.00	0.00	<0.000	<0.000	0.00	0.00	0.00
111 Cd	0.03	0.02	0.01	0.01	0.01	0.00	0.00	0.00	0.00	0.00	0.00	0.00	0.00
118 Sn	<0.000	<0.000	<0.000	<0.000	<0.000	<0.000	<0.000	<0.000	<0.000	<0.000	<0.000	<0.000	<0.000
121 Sb	0.11	0.10	0.08	0.09	0.07	0.06	0.02	0.02	0.02	0.01	0.00	<0.000	<0.000
133 Cs	0.03	0.02	0.01	0.02	0.00	0.00	0.00	0.00	0.01	0.01	0.01	0.01	0.00
140 Ce	0.03	0.02	0.01	0.19	0.00	0.00	0.00	0.00	0.00	0.00	0.01	0.01	0.00
205 Tl	0.03	0.02	0.01	0.01	0.01	0.01	0.01	0.01	0.01	0.01	0.01	0.01	0.00
206 Pb	0.05	0.07	<0.000	0.06	0.01	<0.000	0.00	0.11	0.02	0.01	0.04	0.04	0.01
207 Pb	0.03	0.06	0.00	0.06	0.01	0.00	0.00	0.10	0.03	0.01	0.03	0.05	<0.000
208 Pb	0.04	0.06	<0.000	0.06	0.00	<0.000	<0.000	0.10	0.02	0.01	0.03	0.04	<0.000
232 Th	0.03	0.01	0.01	0.01	0.00	0.00	<0.000	<0.000	<0.000	<0.000	<0.000	<0.000	<0.000
238 U	0.05	0.05	0.03	0.03	0.02	0.03	0.06	0.09	0.11	0.10	0.14	0.15	0.00
103 Rh (ISTD) [1]	104.83	104.18	104.77	103.40	102.69	104.73	105.06	102.31	100.67	102.07	103.26	102.08	102.03

Table 21 – Solubility analysis with and without birnessite at pH 4.6 and 8

Sample	pH	Solution	Glaucony	Birnessite	Time	Mg	Al	K	Ca	Cr	Mn	Fe
		(mL)	g		(hours)	ppb						
EQO1	4.6	10	0.25	0.015	103.25	3,921 ±34	144 ±32	51,193 ±3754	37,540 ±632	1.1±0.1	56.3 ±24.8	bd
EQO1	4.6	10	0.25	0	103.25	4,351 ±70	145 ±12	4,465 ±646	44,703 ±749	bd	6.3 ±0.1	5.3 ±5.9
EQO1	8	10	0.25	0.015	103.25	741 ±42	160 ±4	37,780 ±1130	6,789 ±433	1.1±0.1	7.3 ±5.6	52.8 ±39.1
EQO1	8	10	0.25	0	103.25	689 ±12	211 ±20	2,558 ±458	7,265 ±119	bd	0.3 ±0.2	176.6 ±23.9
WPO4	4.6	10	0.25	0.015	103.25	4,029 ±164	149 ±15	63,113 ±2744	16,817 ±822	bd	112.8 ±21.0	bd
WPO4	4.6	10	0.25	0	103.25	4,272 ±254	144 ±16	6,733 ±279	19,297 ±589	bd	9.1 ±1.4	13.3 ±2.2
WPO4	8	10	0.25	0.015	103.25	250 ±17	339 ±36	31720 ±1337	628 ±28	1.3±0.2	1.3 ±0.4	382.3 ±70.5
WPO4	8	10	0.25	0	103.25	1,154 ±12	254 ±61	4,855 ±939	5,188 ±294	bd	0.4 ±0.1	179.6 ±134.2

B Grain Images

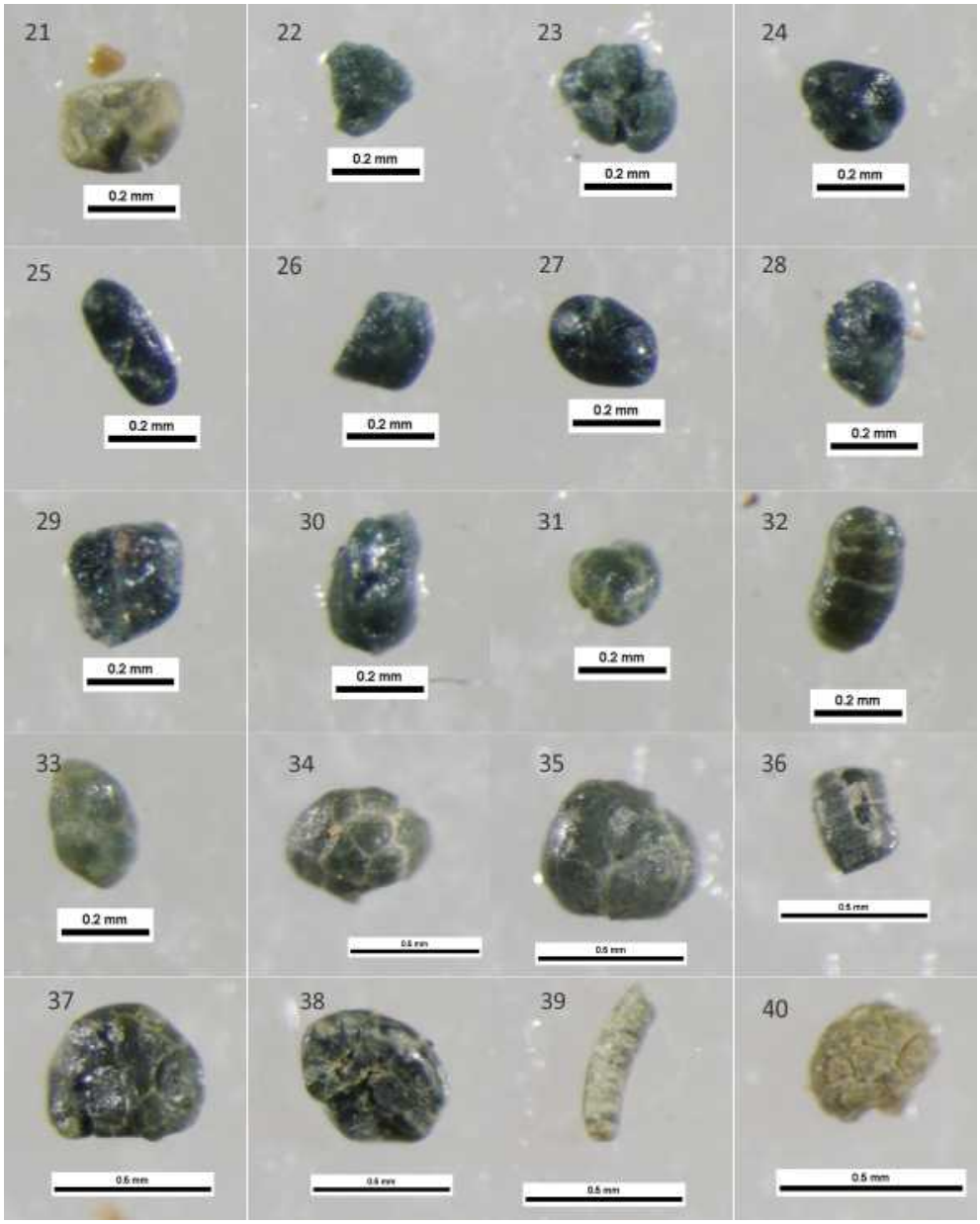

Figure 46 – Binocular images for grains 1-20

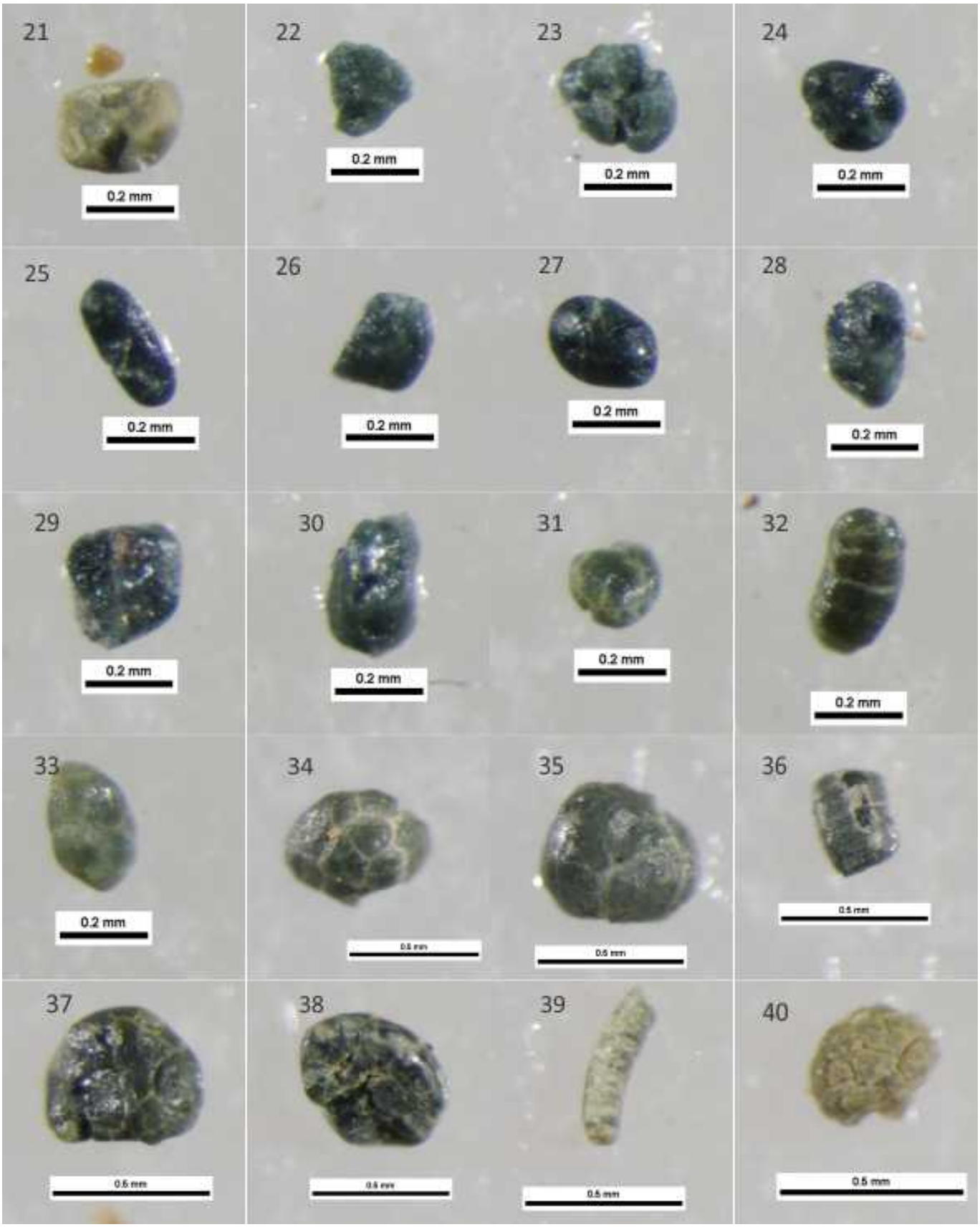

Figure 47 – Binocular images for grains 21-40

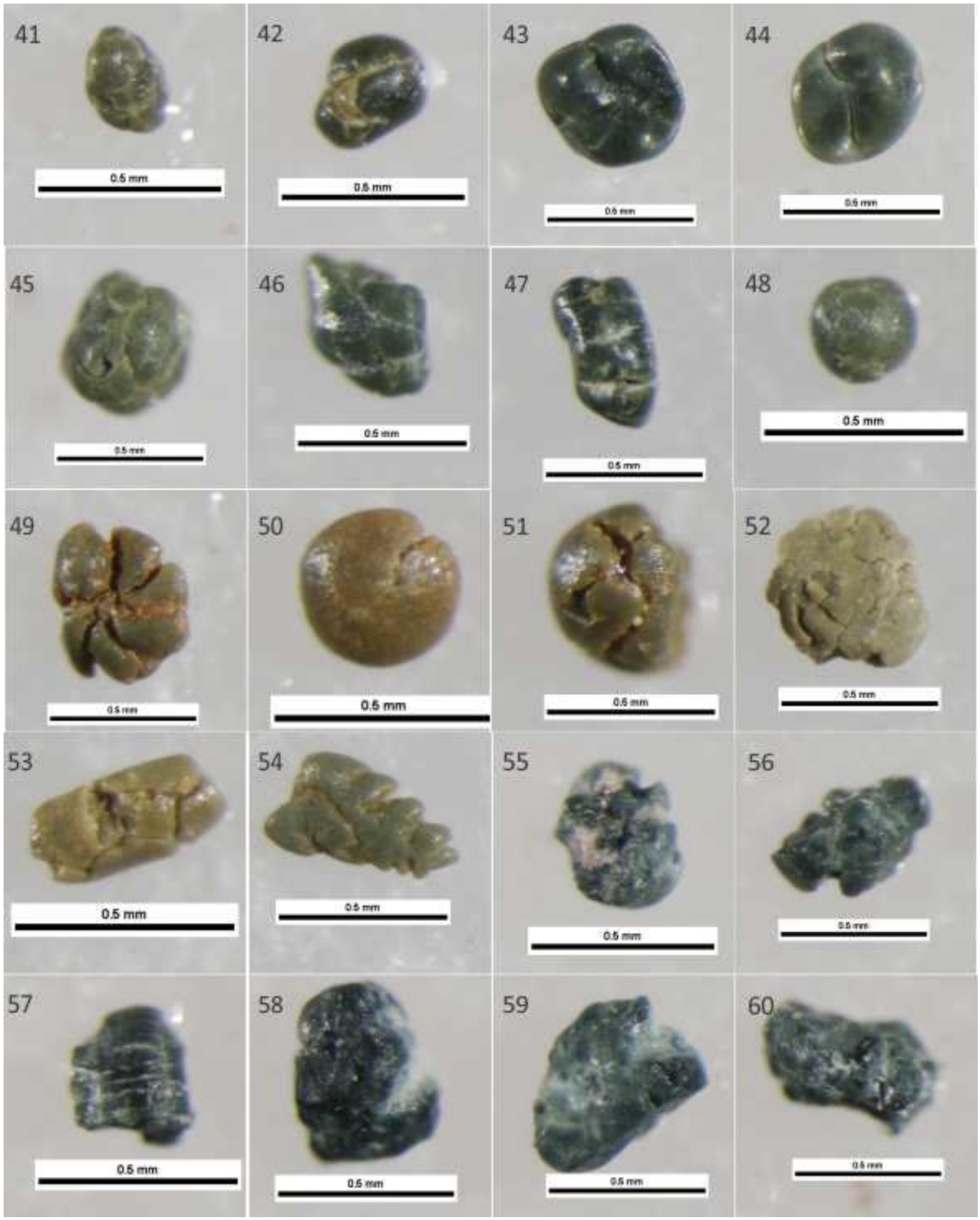

Figure 48 – Binocular images for grains 41-60

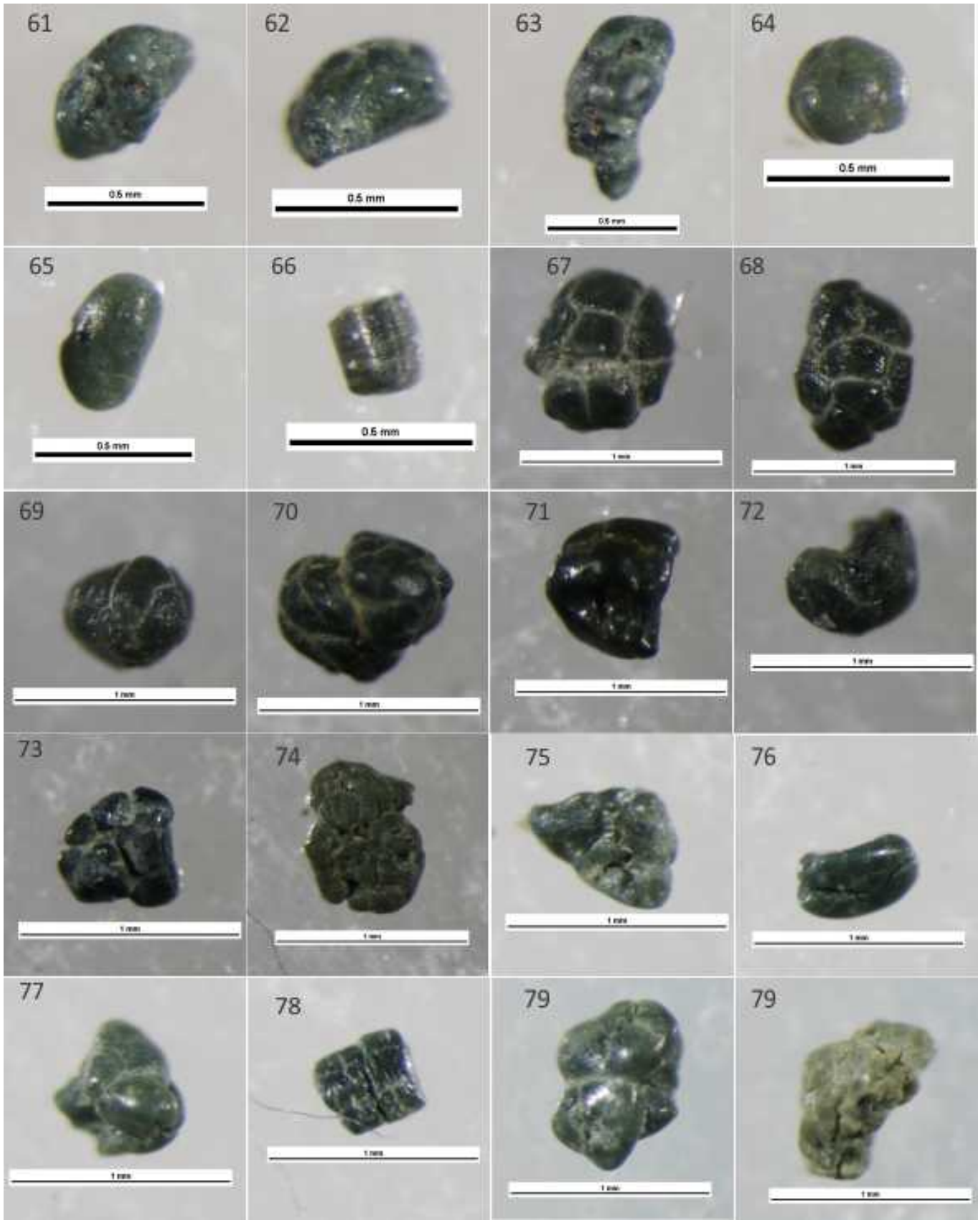

Figure 49 – Binocular images for grains 61-80

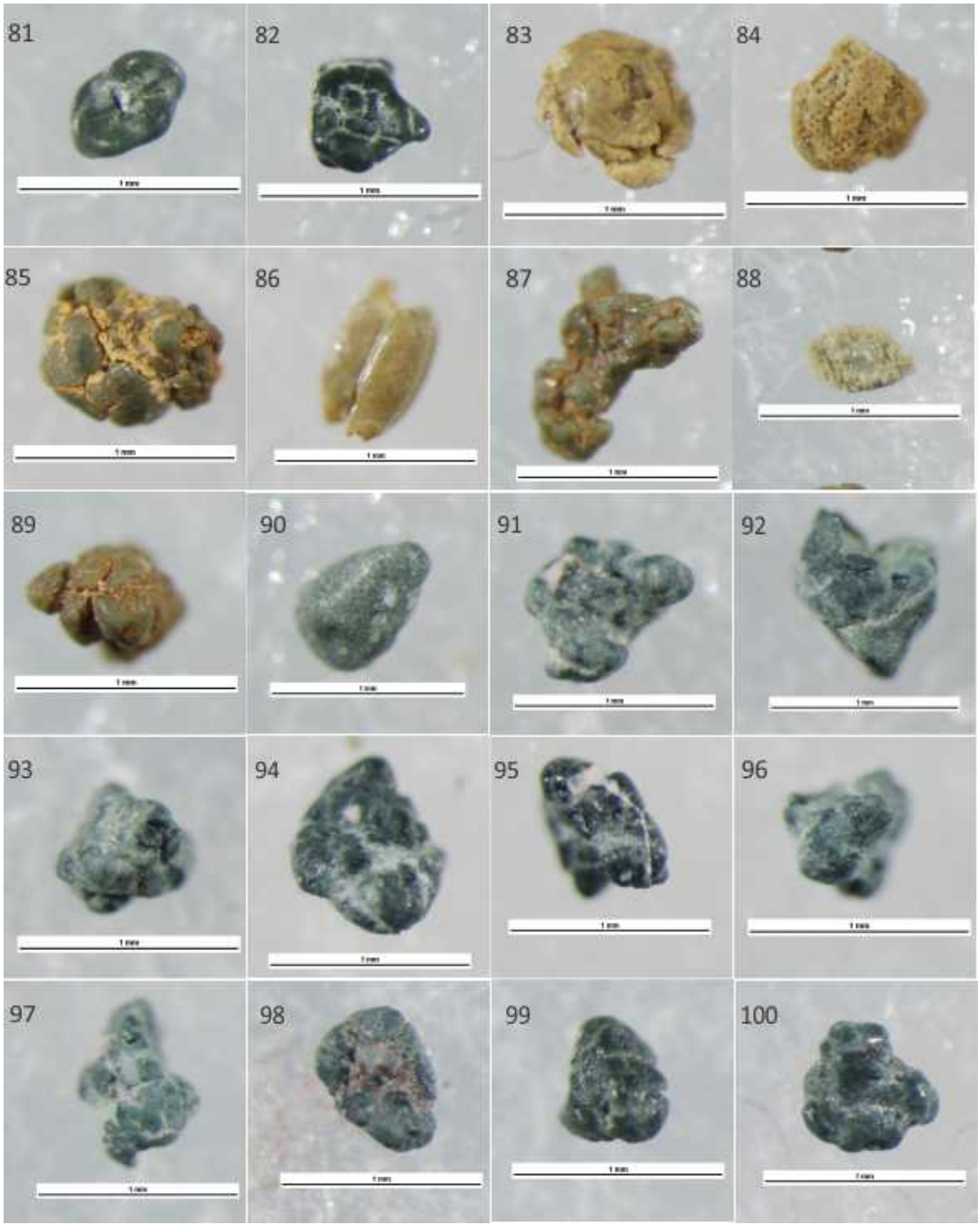

Figure 50 – Binocular images for grains 81-100

C Sample Calculations for Elements Released into Solution

The predicted quantity of K released was calculated using the straight line equation generated in Figure 37.

$$y = (2.69 * 8760hours + 696.16)/1000 \tag{1}$$

$$\frac{(24.26^{mg}/_{L}/1000)}{39.098^{g}/_{mol)}} = 0.00062^{mol}/_{L}/year^{-1} \tag{2}$$

$$0.04L * 0.00062^{mol}/_{L} = 2.48E10^{-5}moles/year^{-1} \tag{3}$$

$$(2.48E10^{-5}mol * 39.098^{g}/_{mol}) * 1000 = 0.970mg/year^{-1} \tag{4}$$

To convert to mass per kg of glaucony:

$$1000g/0.383g = 2611 \tag{5}$$

$$2611 * 0.970mg = 2533.6mg \tag{6}$$

The mass of glaucony required to satisfy K^+ demands for plants of 50 kg per ha per year:

$$(50kg/0.0025kg)/1000 = 19.7t \tag{7}$$

The volume of bulk sediment required to be excavated to satisfy the above demands:

$$(20,000kg/0.4)/2700^{kg}/_{m^3} = 18.519m^3 \tag{8}$$

The mass of K in the solubility analysis using the average structural formula:

$K_{0.75}(Fe_{1.29}Al_{0.27}Mg_{0.37})_{1.94}(Si_{3.82}Al_{0.18})_4$:

- Molar mass of glaucony = 232.5915 g/mol
- Mass of glaucony in solubility analysis = 0.378 g

$$\frac{(0.378g * 0.75mol)}{232.59^{g}/_{mol}} = 0.012mol \tag{9}$$

$$0.012mol * 39.0398^{g}/_{mol} = 0.0477g \tag{10}$$